NRL Report 7986

Non-Rayleigh Sea Clutter: Properties and Detection of Targets

GERARD V. TRUNK

Radar Analysis Staff
Radar Division

June 25, 1976

NAVAL RESEARCH LABORATORY
Washington, D.C.

SECURITY CLASSIFICATION OF THIS PAGE (When Data Entered)

REPORT DOCUMENTATION PAGE		READ INSTRUCTIONS BEFORE COMPLETING FORM
1. REPORT NUMBER NRL Report 7986	2. GOVT ACCESSION NO.	3. RECIPIENT'S CATALOG NUMBER
4. TITLE (and Subtitle) NON-RAYLEIGH SEA CLUTTER: PROPERTIES AND DETECTION OF TARGETS		5. TYPE OF REPORT & PERIOD COVERED Interim report on one phase of a continuing NRL Problem. 6. PERFORMING ORG. REPORT NUMBER
7. AUTHOR(s) Gerard V. Trunk		8. CONTRACT OR GRANT NUMBER(s)
9. PERFORMING ORGANIZATION NAME AND ADDRESS Naval Research Laboratory Washington, D.C. 20375		10. PROGRAM ELEMENT, PROJECT, TASK AREA & WORK UNIT NUMBERS R02-54.101 and R02-97.101 62712N and 611533N RF12-151-402-4010/RR021-41-5703
11. CONTROLLING OFFICE NAME AND ADDRESS Department of the Navy Office of Naval Research Washington, D.C. 20375		12. REPORT DATE June 25, 1976 13. NUMBER OF PAGES 86
14. MONITORING AGENCY NAME & ADDRESS(if different from Controlling Office)		15. SECURITY CLASS. (of this report) Unclassified 15a. DECLASSIFICATION/DOWNGRADING SCHEDULE

16. DISTRIBUTION STATEMENT (of this Report)

Approved for public release; distribution unlimited.

17. DISTRIBUTION STATEMENT (of the abstract entered in Block 20, if different from Report)

18. SUPPLEMENTARY NOTES

19. KEY WORDS (Continue on reverse side if necessary and identify by block number)

Detectors
High-resolution radar
Log-normal density
Non-Rayleigh density
Sea clutter
Sea surface simulation
Spatial variation

20. ABSTRACT (Continue on reverse side if necessary and identify by block number)

Sea clutter has a non-Rayleigh probability density when examined with a radar that has high resolution. This report discusses the properties of non-Rayleigh sea clutter and the detection of targets in non-Rayleigh sea clutter. The spatially varying clutter model is presented and is used to explain the non-Rayleigh nature of sea clutter. The variation of clutter distributions with various radar parameters such as frequency, pulse width, and polarization was determined,

(Continued)

DD FORM 1 JAN 73 1473 EDITION OF 1 NOV 65 IS OBSOLETE
S/N 0102-014-6601

and the correlation properties of clutter were established. A way was developed of constructing a realistic realization of the sea surface on a computer, and the surface was used to predict non-Rayleigh clutter densities for various conditions and to indicate some finer points associated with the detection of small targets on the ocean's surface. Finally, various detectors were compared and the problems of pulse-to-pulse and scan-to-scan processing were analyzed.

CONTENTS

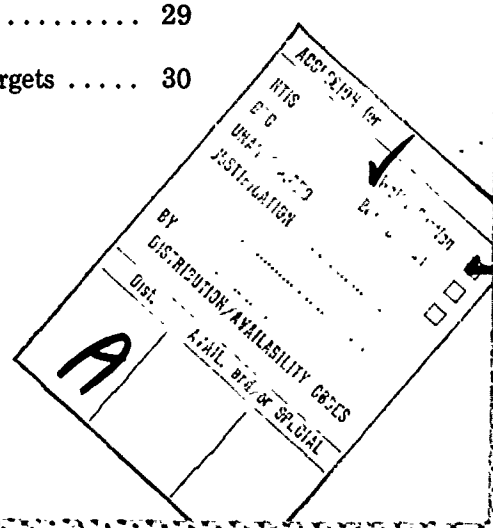

BACKGROUND

During the last decade many articles and reports have been published on the properties of sea clutter echoes obtained with a high-resolution radar and the detection of targets in non-Rayleigh sea clutter. The purpose of this report is to present a unified summary on the status of this work.

FUTURE WORK

While much work has been accomplished, there remain several outstanding problems:

- What should be the polarization of a high-resolution radar?
- What is the physical cause of the "spikes"; and more importantly, are there any techniques for suppressing the "spikes"?
- A better understanding is needed of the non-Rayleigh nature of sea clutter obtained at shallow grazing angles with large pulsewidths. Is this phenomenon simply due to shadowing causing an apparent large water wavelength?

NON-RAYLEIGH SEA CLUTTER: PROPERTIES AND DETECTION OF TARGETS

I. INTRODUCTION

In the last several years, many investigators have studied the scattering mechanisms that produce radar sea clutter. With results for scattering from slightly rough surfaces and composite surfaces obtained by Rice [1], Wright [2,3], Valenzuela [4-6], Guinard and Daley [7], and others, the properties of average radar backscatter can be modeled fairly well.

The original work on the probability density $p(x)$ of sea clutter is that of Goldstein [8]. Goldstein states that if many scatterers are uniformly distributed in an illuminated patch (the area defined by the pulsewidth and the radar beamwidth, $c\tau/2$ by $R\theta$), the relative phases of the individual echoes will be random. He adds that the central limit theorem yields the Rayleigh density for envelope-detected sea clutter.

He notes, however, that if the pulsewidth is small, the assumption of uniformly distributed scatterers does not hold. As an example, he shows a photograph of an A-scope (Fig. 1) and notes the "spiky" appearance. Furthermore, he infers that the radar is in fact resolving the individual waves.

This work was published in 1951. During the next 15 years, very little research was done on the density of sea clutter, and that which was done was either classified or appeared in reports of limited circulation. In 1969, Nathanson [9] reported some results obtained by the Naval Research Laboratory (NRL) and the Applied Physics Laboratory of the Johns Hopkins University (APL). Specifically, he gave standard-deviation-to-mean ratios for various pulsewidths and showed a deviation from the Rayleigh density for small pulsewidths. Furthermore, he stated that for short pulses, the density function for horizontal polarization had a longer tail than the density function for vertical polarization.

In 1970, Trunk and George [10] considered the log-normal and contaminated-normal descriptions of sea clutter and calculated detection probabilities for targets in these densities. With that, the detailed description of the clutter density will begin. In Sec. II, measurements of the average backscatter σ_0 are given, and the results of slightly rough scattering and the composite surface-scattering model are introduced so that they may be used later in this report. In Sec. III, a spatially varying conditional density $p(x|\sigma_0)$ is introduced. This conditional density is a natural consequence of the composite surface-scattering model and is used to explain the non-Rayleigh nature of sea clutter. The variation of the clutter densities, $p(x)$ and $p(x|\sigma_0)$, with various radar parameters such as frequency, pulsewidth, and polarization are found using analysis of variance techniques. In Sec. IV, a way of constructing a realistic computer model of the sea surface is given. The surface is used to predict non-Rayleigh clutter densities for various conditions and to indicate some finer points associated with the detection of small targets on the surface of the

Manuscript submitted February 10, 1976.

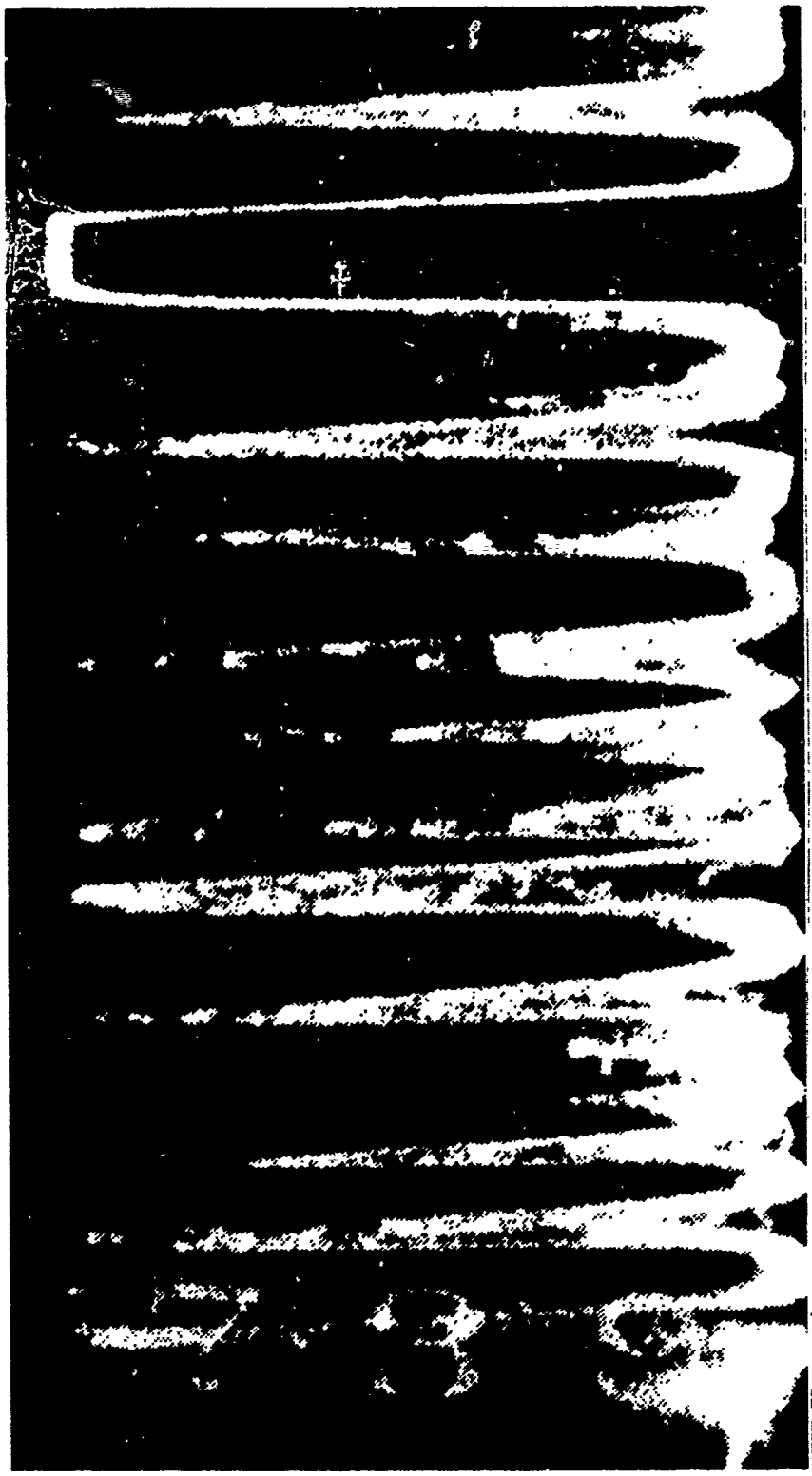

Fig. 1—A-scope trace showing "spiky" appearance of sea echo. The sweep length was 2,000 yd (1,829 m), the pulsewidth was 0.15 μs, and the beamwidth was 0.8°. The square-topped pulse is an artificial echo from a signal generator [8]

ocean. In Sec. V, various detectors such as integrators, rank detectors, and the Neyman-Pearson detector are compared. The major results of the report are summarized in Sec. VI.

II. AVERAGE RADAR CROSS SECTION

Important developments in understanding the nature of sea clutter have been made by studying the interaction of electromagnetic waves with the surface of the ocean. These studies [2-6] are based on Rice's work [1] on slightly rough surfaces (surfaces whose height variations are small in relationship to the incident wavelength and whose slopes are $<<1$). Using perturbation techniques, they found that the reflected energy was directly proportional to the energy density spectrum of the surface height variation evaluated at the Bragg scattering condition. Specifically, the radar cross section for direct polarization is

$$\sigma_{HH} = 4\pi k^4 \sin^4\theta \, \alpha_{HH} W(2k\cos\theta) \tag{1}$$

$$\sigma_{VV} = 4\pi k^4 \sin^4\theta \, \alpha_{VV} W(2k\cos\theta)\,, \tag{2}$$

where $k = 2\pi/\lambda$ is the wavenumber of the incident wave, θ is the grazing angle, $W(K)$ is the energy density spectrum, and $K = 2k\cos\theta$ is the Bragg resonant condition. (Valenzuela [4] found the cross-polarization cross section by considering the second-order perturbation terms.) The α terms are

$$\alpha_{HH} = \left| \frac{(\epsilon - 1)}{[\sin\theta + (\epsilon - \cos^2\theta)^{1/2}]^2} \right|^2 \tag{3}$$

and

$$\alpha_{VV} = \left| \frac{(\epsilon - 1)[(\epsilon - 1)\cos^2\theta + \epsilon]}{[\epsilon \sin\theta + (\epsilon - \cos^2\theta)^{1/2}]^2} \right|^2, \tag{4}$$

where ϵ is the complex dielectric constant of the ocean. Now, if the wave spectrum $S(\omega)$ is available, $W(K)$ can be calculated since

$$KW(K)\,dK = S(\omega)\,d\omega \tag{5}$$

where $\omega^2 = gk$. However, a more useful approach is to use a result of Phillips [11] who investigated the growth of water waves and concluded that there exists an upper bound for the height of gravity and capillary waves. Using a dimensional argument, he concluded that in the range where waveheight is limited, the energy spectrum was of the form

$$W(K) = BK^{-4}\,. \tag{6}$$

There is uncertainty about the value of B; however, Phillips gives $B \approx 6 \times 10^{-3}$ for gravity waves and $B \approx 1.5 \times 10^{-2}$ for capillary waves. Substituting Eq. (6) into Eqs. (1) and (2), one obtains the following limiting values for the cross sections:

$$\sigma_{HH} = 1.5\pi \times 10^{-3} \alpha_{HH} \tan^4\theta \tag{7}$$

and

$$\sigma_{VV} = 1.5\pi \times 10^{-3} \alpha_{VV} \tan^4\theta \,, \tag{8}$$

where the α's are defined by Eqs. (3) and (4).

Guinard and Daley [7] have compared sea clutter data with the theoretical model. Their data were taken with the four-frequency radar (4FR) system, which is an airborne, coherent, pulsed radar capable of transmitting a sequence of four frequencies, *X* band (8910 MHz), *C* band (4455 MHz), *L* band (1228 MHz), and *P* band (428 MHz), alternatively on horizontal and vertical polarizations. The basic radar parameters of the 4FR system are given in Table 1. A basic description of the 4FR system can be found in Ref. 7 and a detailed description in Guinard [12].

The data used in Guinard and Daley's study [7] came from two major experiments. In July 1965, a measurement program was conducted off Puerto Rico. Radar echoes were recorded for all frequencies, both polarizations, and a variety of grazing angles and sea states. Sea conditions were measured by a team from the Applied Physics Laboratory, Johns Hopkins University. During the measurements the sea state varied between 0 and 2 and the maximum wind was 20 knots with 9-ft seas. The second measurement program was conducted in February 1969 in the North Atlantic to study rougher sea conditions. Ground truth was provided by ocean stations India (59°N, 19°W) and Juliet (52.5°N, 20°W). Sea states varied between 0 and 8, a maximum wind of 45 knots was recorded, and a significant wave height of 26 ft was observed. The *L*-band data are shown in Figs. 2 and 3 for vertical and horizontal polarizations, respectively. Each data point

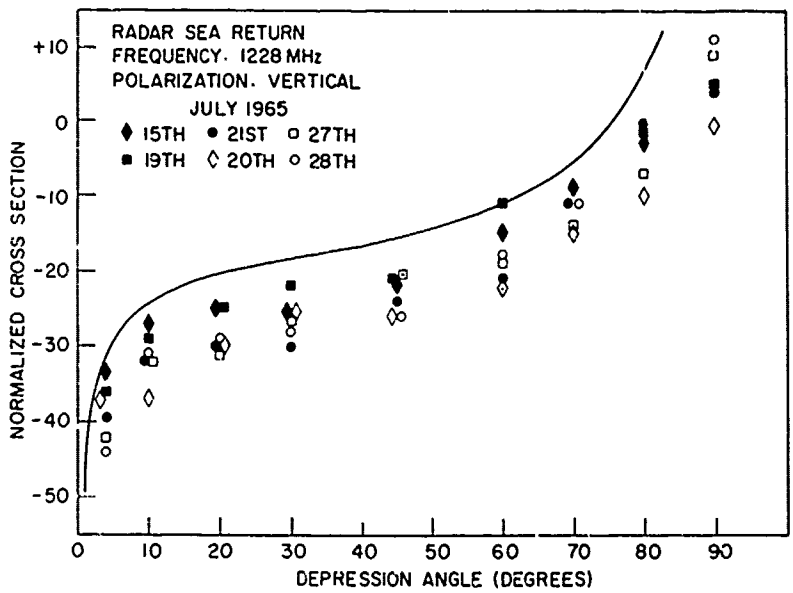

Fig. 2—Variation of RCS with grazing angle; $W(K) = 6 \times 10^{-3} K^{-4}$, $\epsilon = 73\text{-}85i$ [7]

Table 1—Parameters of Four-Frequency Radar System*

Frequency Band	Polarization	Azimuth Beamwidth (deg)	Elevation Beamwidth (deg)	Azimuth Minor Lobe (dB)	Elevation Minor Lobe (dB)	Cross-Polarized (dB)	Antenna Gain (dB)	Peak Power (kW)	Average Power (W)	Pulse-Width (μs)	PRF (pps)
P Band	Horizontal	12.3	40.0	14.5	30.0	25	17.4	25	140	0.25–2.0	100–1463
	Vertical	12.1	41.0	14.5	26.0	28	17.4				
L Band	Horizontal	5.5	13.8	13.4	16.0	25	25.9	25	140	0.25–2.0	100–1463
	Vertical	5.5	13.0	14.0	14.0	25	26.2				
C Band	Horizontal	5.0	5.0	23.2	24.5	>20	31.4	35	100	0.1–2.0	100–1463
	Vertical	5.0	5.0	23.2	24.5	>20	31.4				
X Band	Horizontal	5.0	5.3	23.6	23.5	>20	31.2	25	160	0.1–2.0	100–1463
	Vertical	4.7	5.0	23.6	24.2	>20	31.2				

*From reference [7].

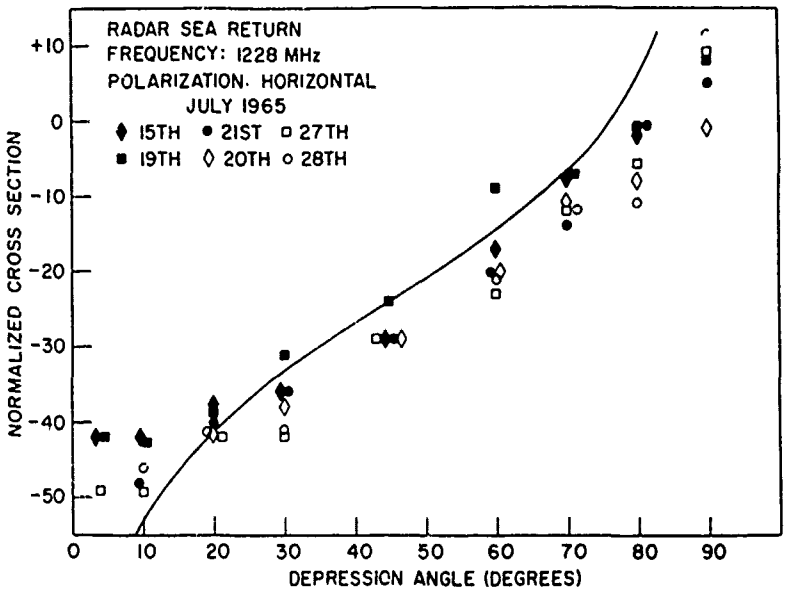

Fig. 3—Variation of RCS with grazing angle· $W(K) = 6 \times 10^{-3} K^{-4}$, $\epsilon = 73\text{-}85i$ [7]

represents the median value of cross section obtained by processing approximately 30 s of data. The pulsewidth selected for all points was 0.25 μs. On July 15, 19, and 21, the seas were 3 to 5 ft high, on July 20 they were 2 to 3 ft high, and on July 27 and 28 they were less than 1 ft high. In Fig. 2 (vertical polarization), one can see that the theoretical bound of Eq. (8) provides a realistic upper bound for sea clutter and exhibits the correct variation with grazing angle.

However, the situation is more complex when the data are compared to the theoretical limit in Fig. 3 (horizontal polarization). While there is good agreement for large grazing angles, there is a wide decrepancy between model and data for small grazing angles. To understand the source of this discrepancy, recall that in the ocean the small waves (i.e., Bragg scatterers) are sitting on the much larger gravity waves and swells. In the composite-surface scattering model (which defines the role of the large and small waves), Wright [3] noted that the only significant effect of the large waves is that they change the angle between the reflecting surface (ocean) and incident radiation. This angular change can be resolved into two components: one a change in the apparent grazing angle; the other, a rotation normal to the plane of incident radiation. Obviously, the first component increases cross sections, and Valenzuela [5] has shown that considerable variation in cross section can be caused by the latter component. Guinard and Daley [7] conclude that to bound the cross section observed with horizontal polarization, it is necessary to use the vertical bound of Eq. (8) for vertical and horizontal polarization.

The purpose of this section was to introduce the slightly rough-surface and composite-surface scattering models. Those with a further interest in the subject should consult Guinard and Daley [7], which provides an overview of the theory and references all the important work.

III. DENSITY FUNCTION OF SEA CLUTTER

In this section, the results of fitting the clutter distribution with the log-normal and contaminated-normal distributions are reviewed. Then, from the composite-surface scattering model, a conditional density $p(x|\sigma_0)$ is introduced, is shown to be Ricean, and is used to explain the non-Rayleigh density $p(x)$ of sea clutter. Finally, the variation of the clutter densities $p(x)$ and $p(x|\sigma_0)$ with parameters such as radar frequency, pulsewidth, polarization, and wind direction is found by analysis of variance techniques.

A. Fitting of Clutter Data

Since 1951 [8], it has been known that the density function of sea clutter was not Rayleigh if the radar pulsewidth was small. While some research was done by laboratories and industry on the non-Rayleigh density (for example, Macdonald [13] and Ballard [14]), nothing appeared in journals until Trunk and George [10]. They considered fitting the log-normal and contaminated-normal distributions to the distribution of envelope-detected sea clutter. (Through the remainder of this report, unless otherwise stated, "distribution of sea clutter" will mean the distribution of the return of envelope-detected sea clutter.) By log-normal clutter, it is meant that the envelope-detected sample x from the sea return has the density function

$$p(x) = \frac{2}{(2\pi\sigma^2 x^2)^{1/2}} \exp\left(\frac{-2[\ln(x/x_m)]^2}{\sigma^2}\right), \tag{9}$$

where x_m is the median value of x and σ is the standard deviation of $[\ln x]^2$. By "contaminated-normal clutter", it is meant that the quadrature components y have a contaminated-normal density

$$p(y) = \frac{(1-\gamma)}{(2\pi\sigma^2)^{1/2}} \exp\left(\frac{-y^2}{2\sigma^2}\right) + \frac{\gamma}{(2\pi K^2\sigma^2)} \exp\left(\frac{-y^2}{2K^2\sigma^2}\right), \tag{10}$$

where γ is the contamination fraction and K is the ratio of the standard deviations of the two Gaussian densities. In a straightforward calculation, it can be shown that the density of the envelope-detected sample is

$$p(x) = (1-\gamma)^2 \frac{x}{\sigma^2} \exp\left(\frac{-x^2}{2\sigma^2}\right) + \frac{\gamma^2 x}{K^2\sigma^2} \exp\left(\frac{-x^2}{2K^2\sigma^2}\right)$$

$$+ \frac{2\gamma(1-\gamma)x}{K\sigma^2} \exp\left(\frac{-x^2(K^2+1)}{4K^2\sigma^2}\right) I_0\left(\frac{x^2(K^2-1)}{4K^2\sigma^2}\right). \tag{11}$$

Trunk and George's data source was a frequency-agile, high-resolution radar (FHR), which is an airborne, noncoherent, pulsed X-band radar capable of frequency diversity on a pulse-to-pulse basis. The radar operates with either a long (100-ns) or short (20-ns) pulse

with vertical or horizontal polarization. The beamwidth is 0.5° and the PRF is 2,560 pps. Standard operating procedure calls for the aircraft to fly at 180 knots sampling the data at a range of 2 n.mi. to obtain a grazing angle of 4.7°.

Some examples of a non-Rayleigh sea clutter distribution taken by NRL in 1967 [15] are plotted in Fig. 4 on probability paper in decibels, with the median of the density arbitrarily set to 0 dB. Each curve represents a 2-min sampling interval. As one can see, the sea clutter distribution is non-Rayleigh; the higher the sea state, the more non-Rayleigh it becomes.

The clutter models were fitted to the data by a minimax method. First the parameters, x_m of the log-normal and σ of the contaminated-normal densities, were used to equate the medians of the theoretical distributions with the median of the actual data. Then the remaining parameters, σ of the log-normal and γ and K of the contaminated-normal densities, were used to minimize the maximum difference in decibels between the theorized curves and the actual data. The best fits for the data in Fig. 4 are shown in Figs. 5 and 6. Because of the recording methods used, data recorded before 1969 could not be thoroughly processed.

On March 11, 1969, the FHR radar was flown 200 mi (320 km) off the Virginia capes. In each run, the aircraft was flown in a given direction with respect to the wind, i.e., upwind (U), downwind (D), or crosswind (C), for about 20 min. After 2 min either the polarization or pulsewidth was varied so that data would reflect a variety of conditions.

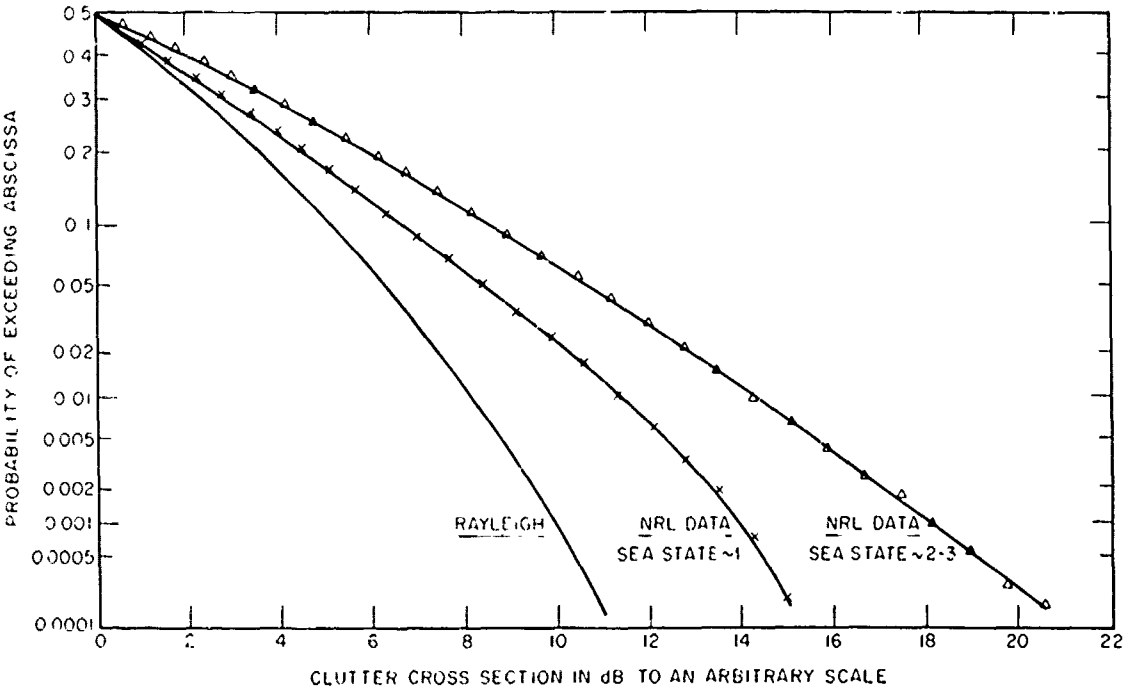

Fig. 4—Experimental sea clutter cross-section data taken by airborne X-band radar; 0.02-μs pulse, vertical polarization, 4.7° grazing angle. Rayleigh distribution included for comparison [10].

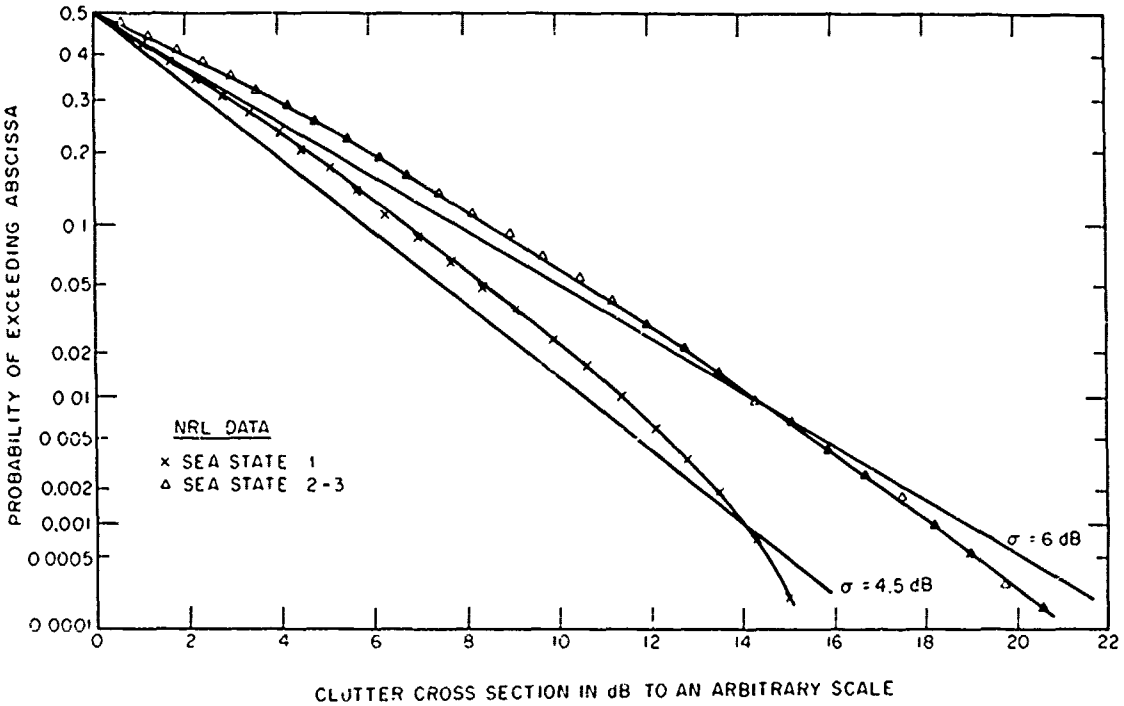

Fig. 5—Log-normal distributions for σ = 4.5 and 6 dB, compared to NRL data [10]

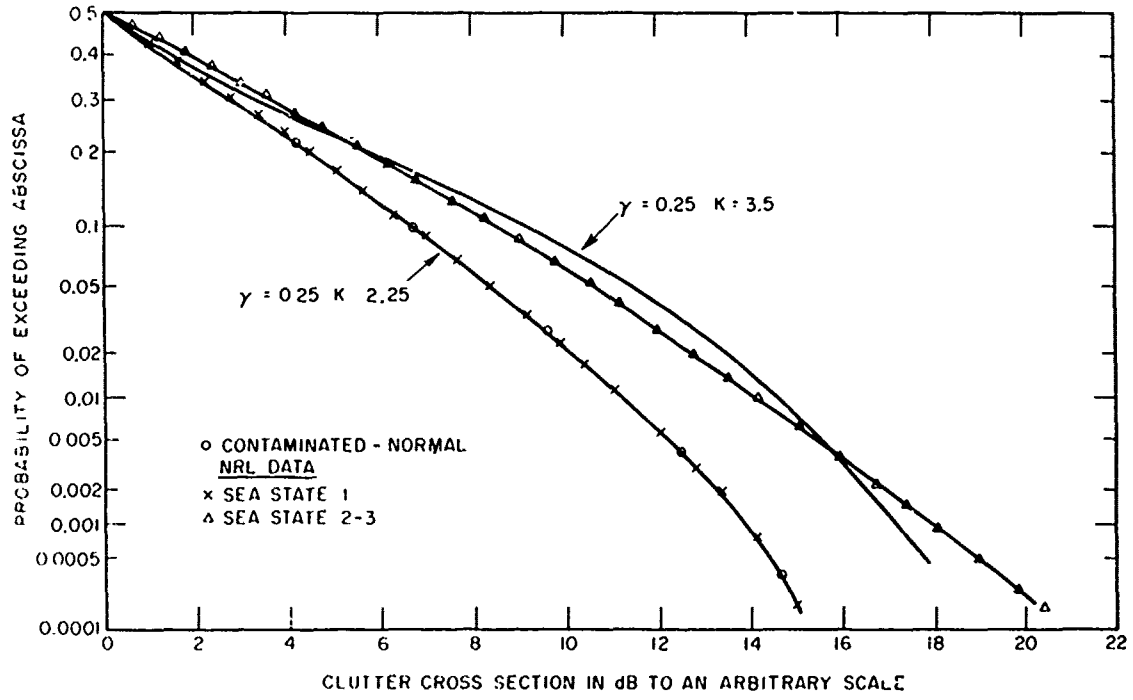

Fig. 6—Contaminated-normal distributions for (γ = 0.25, K = 2.25) and (γ = 0.25, K = 3.5), compared to NRL data [10]

Data on sea conditions were obtained from the Fleet Weather Facility, Naval Reconnaissance and Technical Support Center, Suitland, Md., which reported 25-to-31-knot winds, 8-ft (2.5-m) waves, and a 12-ft (3.7-m) swell.

The best fitting log-normal and contaminated-normal distributions for some short-pulse (20-ns) data are given in Table 2, where "best" is defined by the minimax solution. Columns 1 and 2 are identifiers which distinguish the clutter data runs. Column 3 is the parameter of the log-normal which yields the best fit, and column 4 gives the maximum difference (in decibels) between the data and the best-fitting distribution. Columns 5–7 contain similar information about the contaminated-normal distribution. Both distributions provide essentially the same accuracy of approximation. Also, the previously reported observation [9] that the density function for horizontal polarization has a longer tail than that for vertical polarization seems to be verified.

Since the publication of Trunk and George [10] in 1970, the log-normal density has received considerable attention, and the contaminated-normal density has been neglected. Before we leave this subject, the following cautions are in order:

- Sea clutter is *not* log-normally distributed. (It is shown in the next section to have a spatially varying Ricean density.)

- While the log-normal model of sea clutter can yield useful results, in only one case does it yield the correct probability of detection in clutter. This problem is discussed fully in Sec. V.

Table 2—Parameterization of Clutter Data

Clutter Time	Description Identifier	Log-Normal		Contaminated-Normal		
		σ	Maximum Difference (dB)	γ	K	Maximum Difference (dB)
1145	DH	6.0	1.6	0.025	5.1	1.4
1147	DV	5.2	1.6	0.486	2.7	0.8
1155	DH	6.1	1.3	0.034	5.6	1.5
1151	DV	4.6	1.6	0.426	2.8	0.7
1153	DH	6.0	1.0	0.051	4.9	1.1
1213	CV	4.6	0.4	0.431	2.8	1.4
1215	CH	6.0	1.0	0.051	4.5	1.0
1218	CH	6.1	0.8	0.055	4.5	1.0
1220	CV	4.8	0.8	0.456	3.2	1.7
1248	UV	5.6	1.8	0.065	3.0	1.4
1250	UH	6.3	0.8	0.065	4.6	1.4
1252	UV	5.2	1.2	0.358	2.8	0.8
1254	UH	6.3	0.8	0.104	4.9	1.4

B. Density of Sea Clutter

If the density of sea clutter is not log-normally distributed, what is its density? Some insight can be gained by examining the time records of FHR sea clutter data shown in Figs. 7 and 8. Since the plane is traveling at 180 knots, each record corresponds to the the return from an approximate 2,000-ft swath of ocean. While a structure is apparent in both sets of data, it is much more obvious in Fig. 8. The basic explanation, provided by Trunk [16], of this variation with time is that the width ($c\tau/2$) of the radar's illuminated patch is less than the water wavelength of the sea (over 60 m for sea state 5). Consequently, the density of the envelope return x of clutter is $p[x|\sigma_0(g_\ell)]$. That is, the probability of any value x is conditioned on the average backscatter σ_0, which is a function of the local grazing angle g_ℓ (Eqs. (1) and (2)) at the range cell of interest. If g is the grazing angle for a flat sea and s is the slope of the large wave structure, $g_\ell = g + s$. Then, if clutter is observed over a time period corresponding to several water wavelengths, its density function can be written as

$$p(x) = \int p[x|\sigma_0(g+s)]\, p[\sigma_0(s)]\, d\sigma_0(s)\,, \tag{12}$$

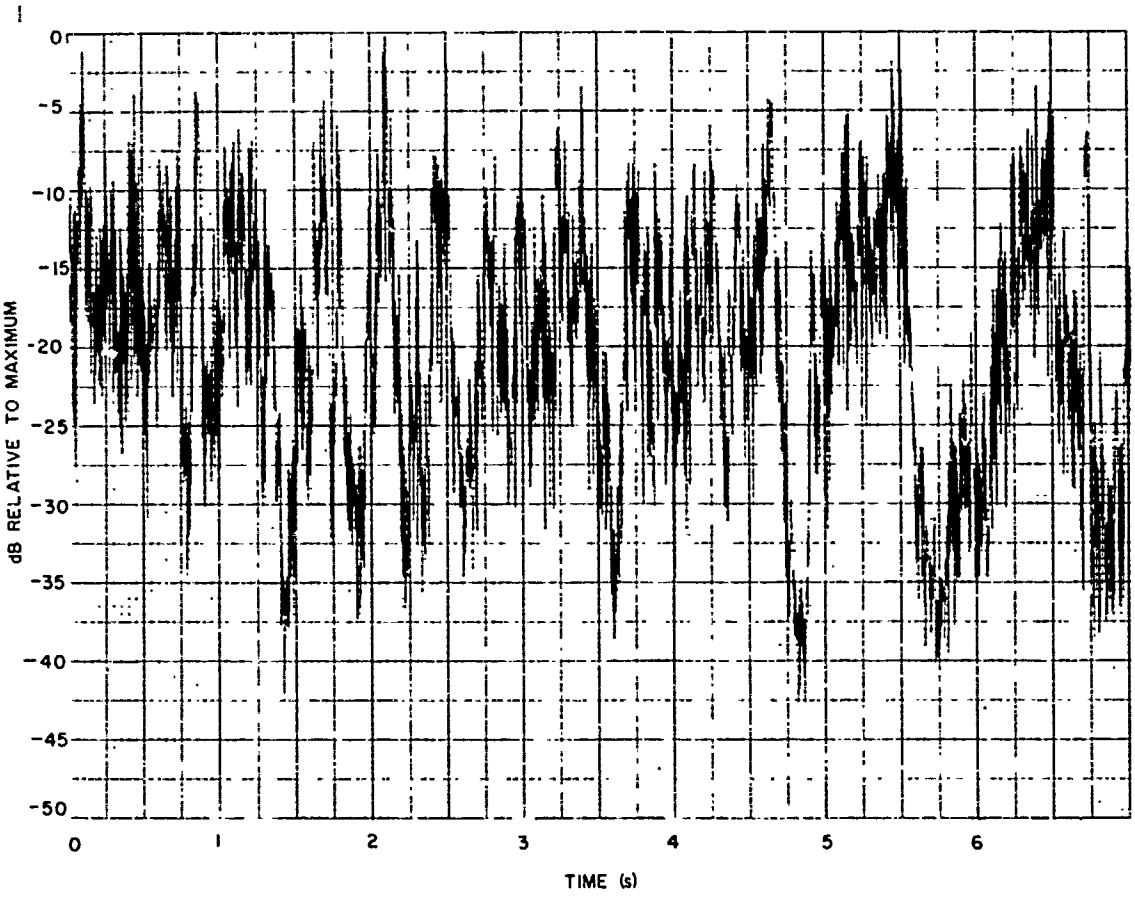

Fig. 7—Sea clutter: short-pulse data taken upwind with horizontal polarization

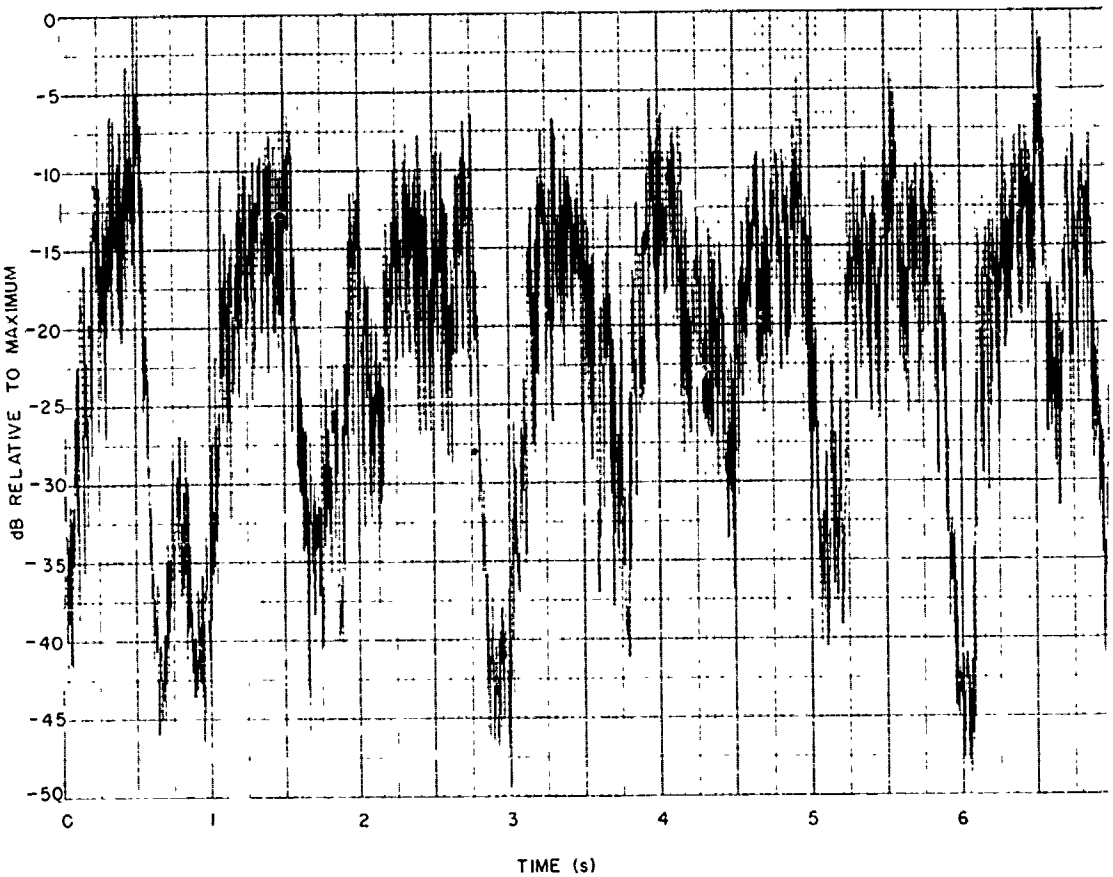

clutter: short-pulse data taken upwind with vertical polarization

where $p[\sigma_0(s)]$ is the probability density of σ_0, which is a function of the slope of the large wave structure (swell and/or wind waves). Equivalently, the density function can be written, as

$$p(x) = \int p[x|\sigma_0(g+s)]p(s)\,ds\,, \tag{13}$$

where $p(s)$ is the slope density.

For simplicity it has been assumed that the large wave structure has constant slope over the illuminated patch area A. To take into account the variation of slope within a range cell, let $S'(A)$ be the variation from the average slope s. Then, since the reflected power from elementary Bragg scattering patches in a range cell add noncoherently, the average cross section in a cell with slope s is given by

$$\sigma_0(g+s) = \frac{1}{A}\oint_A \sigma_0[g+s+S'(A)]\,dA\,, \tag{14}$$

where the integral is a surface integral over the illuminated patch. Thus, since the average slope s is a function of space, the non-Rayleigh density $p(x)$ is seen to be due to a spatially varying density $p(x|\sigma_0)$. (In reality s is a function of time and space. However, since the data are taken from a plane, the major change is spatial and for our purposes the sea may be considered frozen.)

Before verifying these facts, it is worth noting that the formulation yields a Rayleigh density when the illuminated patch (specifically the length along the wave direction) is large with respect to the water wavelength. This is because if the patch encompasses many waves, the density of the average slope s is a delta function; i.e., $p(s) = \delta(s)$. Consequently, $p(x) = p(x|\sigma_0)$; and $p(x|\sigma_0)$ is a Rayleigh density because of the central limit theorem.

1. *Correlation Properties*

For large illuminated patches, independent samples of sea clutter can be obtained either by using pulses separated by about 10 ms (the decorrelation time usually stated for X-band sea clutter return) or by using frequency diversity. However, since the decorrelation is due to phase changes between capillary waves, for a high-resolution radar both methods should yield independent samples from the conditional density $p(x|\sigma_0)$, not from the density $p(x)$.

To verify these conclusions, Trunk [16] calculated the correlation functions using 12.8-s intervals (16,384 data points) of data taken with the FHR system. As can be seen from Figs. 7 and 8, this interval is long enough to represent a sample function from $p(x)$. Decorrelation times are given in Table 3. (Decorrelation time being defined as the time

Table 3—Correlation Values for Data Taken by FHR*

Time	Identifier	Decorrelation Time (ms)	Cross-Correlation Value
1344	VUL	13	0.40
1346	HUL	75	0.57
1411	VDL	19	0.42
1413	HDL	132	0.68
1026	HDS	131	0.83
1028	VDS	168	0.61
1049	VCS	31	0.46
1051	HCS	112	0.64
1125	VCL	12	0.27
1127	HCL	131	0.70
1154	HUS	106	0.74
1156	VUS	193	0.62

*From reference [16].

it takes the correlation function to fall to 1/e.) The decorrelation times vary from 12 to 193 ms; the average is 94 ms, which is much longer than the quoted time of 10 ms.

These particular data were analyzed because the pulse-to-pulse frequency diversity used in each 12.8-s interval equaled the reciprocal of the pulsewidth, and this amount of frequency difference is considered sufficient to decorrelate clutter returns [18]. The cross-correlations for the two frequencies were calculated and are also given in Table 3. It is seen that frequency diversity does not decorrelate sea clutter returns from a high-resolution radar. Next, the above calculations were repeated by dividing each 12.8-s interval into 64 0.2-s intervals (short enough to represent a sample function from $p(x|\sigma_0)$) and averaging the results of the 64 cases. For each of the 12 data records, the decorrelation time was less than 20 ms, and the cross-correlation was less than 0.1. This corresponds favorably to Pidgeon [19], who reports a maximum correlation of 0.2. Thus, time separation of the samples and frequency diversity yield independent samples from $p(x|\sigma_0)$, not from $p(x)$.

2. *Spatially Varying Ricean Density*

What is the density function for the conditional density $p(x|\sigma_0)$? First, although the illuminated patch is rather small (10 ft by 120 ft (3 m by 36.6 m) for FHR data), there are many capillary waves in it. Consequently, from the Central Limit Theorem one would expect $p(x|\sigma_0)$ to be Rayleigh distributed. However, Trunk [16] has shown (the analysis is repeated in Appendix A) that is not. Rather, because of the presence of dominant scatterers, which can be related to scattering from breaking and very peak-crested waves [20,21], $p(x|\sigma_0)$ is a Ricean density.

This is difficult to show because σ_0 changes so rapidly (in airborne systems) that there are too few samples to obtain a good estimate of $p(x|\sigma_0)$ before σ_0 changes. Fortunately, this difficulty can be overcome by analyzing the frequency-diverse FHR data in a special way. For computation ease, a chi density will be used in place of the Ricean density. This approximation is very accurate [22] when the ratio of the dominant scatterer to background noise is in the neighborhood of 0 dB.

Let x_i and y_i be the independent samples from the two frequencies. The conditional densities of the samples are then

$$p(x_i|\sigma_i) = \frac{2x_i^{k-1} \exp\left(-x_i^2/2\sigma^2\right)}{\Gamma(k/2)(2\sigma^2)^{k/2}} \tag{15}$$

and

$$p(y_i|\sigma_i) = \frac{2y_i^{k-1} \exp\left(-y_i^2/2\sigma^2\right)}{\Gamma(k/2)(2\sigma^2)^{k/2}}, \tag{16}$$

where k is the number of degrees of freedom ($k = 2$ is the Rayleigh density) and σ_i is a random variable. The same $\sigma_i = \sigma$ can be used for both frequencies because the time separation, 1/2560 s, is very small and frequency diversity changes σ_0 only slightly.

As mentioned previously, the difficulty in showing that x_i and y_i are chi (or equivalently Ricean) random variables is that σ_i changes too rapidly for good estimate of $p(x_i|\sigma_i)$ to be made. Consequently, a ratio $z_i = x_i/y_i$, whose density is independent of σ_i, is formed. The density of $z = z_i = x_i/y_i$ is found by forming the joint density of x_i and y_i, substituting $z = x_i/y_i$ and $y_i' = y_i$, and integrating over y_i'. This yields*

$$p(z) = \frac{\Gamma(k)}{\Gamma(k/2)\Gamma(k/2)} \frac{2z^{k-1}}{(1+z^2)^k}. \tag{17}$$

Using the FHR data, the sample distribution of independent z_i (constructed from 1,024 samples 12 ms apart, i.e., every 16th z_i) was compared to Eq. (17). The value of k was adjusted to minimize D, which is the maximum difference in probability between the sample and theorized distributions. The fitting results are shown in Table 4, where P_D is the probability that the maximum difference will be less than D when the theorized distribution, given here by Eq. (17), is the true distribution. While the Kolmogorov-Smirnov one-sample test [23], which compares P_D to a threshold α, cannot be run, since k was found by minimizing D (a procedure which biases the test in favor of acceptance), the small

Table 4—Fit of the Chi Density to the FHR Data*

Identifier	Optimum k	D	P_D
VUL	2.7	0.012	0.003
HUL	2.4	0.029	0.663
VDL	2.4	0.016	0.068
HDL	2.6	0.020	0.237
HDS†	4.0	0.035	0.844
VDS	3.4	0.021	0.282
VCS	3.1	0.029	0.681
HCS	3.8	0.019	0.184
VCL	2.4	0.021	0.286
HCL	3.2	0.017	0.078
HUS	3.9	0.014	0.020
VUS	3.2	0.017	0.088

*From reference [16].
†The optimum k for this case is greater than 4.0. The search program employed search in the interval $2 \leq k \leq 4.0$ in 0.1 steps.

*The reason that the Ricean density was not directly analyzed is that the density for z is much more complicated than Eq. (17). Specifically, if x and y are Ricean,

$$p(z) = \frac{2z \exp(-B^2/2)}{(1+Z^2)^2}\left[\left(1+\frac{B}{4}\right) I_0\left(\frac{B^2Z}{Z^2+1}\right) + \frac{B^2Z}{Z^2+1} I_1\left(\frac{B^2Z}{Z^2+1}\right)\right],$$

where B is the ratio of the dominant scatterer to σ.

values of D and P_D indicate that $p(x|\sigma_0)$ is at least nearly a chi, or Ricean, density. For the k's given in Table 4, the ratio of the dominant scatterer to background noise would vary between −3 and +4 dB.

3. *Dominant Scatterers*

In 1974, Lewis and Olin [20] measured the frequency dependence of sea return with a system that transmitted 10-ns simultaneous pulses at 8.6 and 9.2 GHz from the same antenna with horizontal polarization. The measurements were taken at the Chesapeake Bay Division of NRL and at a very short range, which yielded a range cell of about 5 ft by 5 ft (1.5 m by 1.5 m). A typical data record is shown in Fig. 9; the waves were about 4 ft (1.2 m) from peak to trough, with whitecaps forming. Sea return was found to have a large dynamic range, with the largest returns coming from breaking waves. The relationship between sea spikes and breaking waves was recognized and confirmed by a boresight motion picture camera mounted on the radar antenna. The camera was synchronized to the recorded data, viewing a region of the sea containing the range gate responsible for the echoes. It should be noted that white water does not produce sea spikes. Waves must be breaking, a fact which suggests that spray is important.

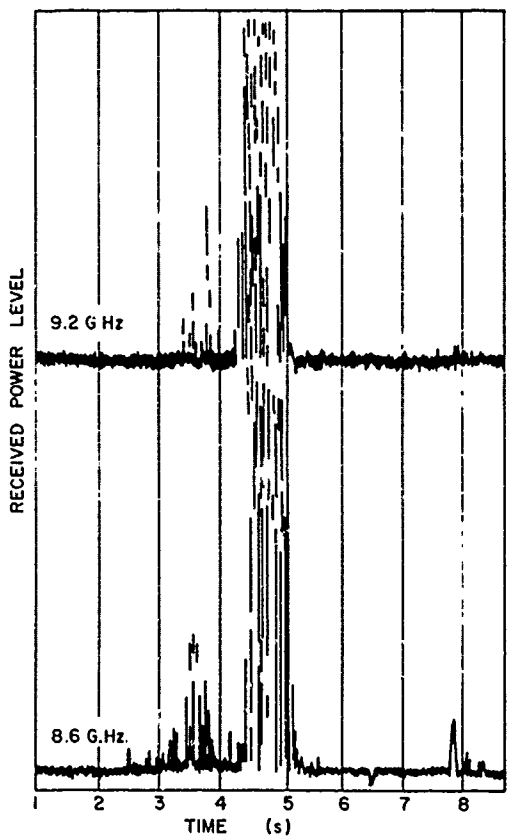

Fig. 9—Typical sea spike

The fine structure in the sea spike was studied and it was noted that the return from the two frequencies appeared to be uncorrelated. Furthermore, it was noted that the decorrelation time within the sea spike was about 10 ms. This time was arrived at by noting times between maximum and minimum values. Lewis noted that these facts could be explained by a fresnel zoning effect produced by the change in size of the whitecap within the range cell. As the whitecap changed its length by a fresnel zone ($\lambda/4$), the signal amplitude would change from a maximum to a minimum or vice versa. The peak return was approximated by assuming that a zone had an effecti.e height of $\lambda/2$ and a width w. Then the scattering cross section of such a zone would be

$$\sigma = \frac{4\pi \left(\frac{\lambda w}{2}\right)^2}{\lambda^2} = \pi w^2 . \tag{18}$$

The cross section predicted by Eq. (18) was compared to the data and reasonable agreement was noted. Research is still being done in this area.

M. Long [21] has also noted the relationship between sea spikes and large wave structure. He reached the following conclusions.

1. For 50% of the sea spikes, a wave breaks (whitecap forms) simultaneously or a fraction of a second thereafter.

2. About 40% of the time, a spike was called when a wave structure had a very peaked crest, as if a whitecap were about to form but did not.

3. No breaking waves were observed in the absence of a sea spike.

Long explains the sea spikes as reflections from facets (smooth areas) of the large wave structure.

While the mechanism producing the sea spikes is still unknown, there is no uncertainty in the fact that sea spikes are associated with breaking waves or waves that almost break.

C. Variation of Clutter Densities

The scanning rate of a search radar is typically 6 to 15 rev/min. Thus, during the scan time, the large-scale sea structure in a range cell changes very little. Consequently, if the illuminated patch is smaller than the water wavelength, the radar return from sea clutter will come from the conditional density $p(x|\sigma_0)$ rather than from $p(x)$. On the other hand, if scan-to-scan processing is performed, it is very likely (depending on scan rates, radar geometry, and sea conditions) that samples are being obtained from $p(x)$. Since the density will determine the behavior of any detector used, the variation of clutter densities $p(x)$ and $p(x|\sigma_0)$ with such parameters as frequency, polarization, pulsewidth, and wind direction will be analyzed.

1. *Variation of* p(x)

To find the variation of $p(x)$ with frequency, the 4FR data taken on February 10, 1969, in the North Atlantic was analyzed. Specifically, the data analyzed by Trunk [16] were taken with a 0.5-μs pulsewidth at L and X bands; the antenna beamwidths were 5° and 5.5°, respectively; horizontal polarization was used for transmission and reception; and the pulse-repetition frequency (PRF) was 683 pps. The aircraft flew at 200 knots, the range was 2,000 yd (1,829 m), the depression angle was 10°, and the azimuthal angle (the angle between the radar beam and the wind direction) was varied from 0° to 45° in 15° increments. Ground truth was provided by Ocean Stations India and Juliet, which reported winds between 30 and 35 mi/h (48 and 56 km/h) a sea of 13.1 ft (4.0 m), and a swell of 18 ft (5.5 m).

The log-normal density (Eq. (9)) was fitted to the data by equating x_m to the sample median and then finding the σ that minimized the maximum difference in decibels between the log-normal distribution and the sample distribution. The log-normal density was used instead of the contaminated-normal one because it is easier to interpret: It has only one parameter (excluding x_m) and a larger value of σ indicates a longer tail associated with the density. A 36-s sample of data was used, the data were fitted between the 50 and 99.95 percentiles, and the results of 16 cases appear in Table 5. The fitting errors ranged from 0.44 to 1.41 dB; the average was 0.78 dB.

From Table 5 it appears that the clutter distribution is a function of the radar frequency but not of the azimuthal squint angle. However, to test whether these factors cause a significant change in the distribution, a statistical procedure called analysis of variance was used. This procedure decides whether differences in experimental results (in our case different values for σ) are true differences or just experimental (sampling) errors. The results of the analysis of variance will appear in this section and further details are given in Appendix B. The analysis of variance procedure was applied to the σ's in Table 5 and the results are summarized in Table 6. The quantity S_F^2 estimates the sum of two effects, the sampling error and the effect of changing frequency; the quantity S_A^2 also estimates the sum of two effects, the sampling error and the effect of changing azimuthal angle; and the quantity S_E^2 is an independent estimate of the sampling error. The quantity S_F^2 is compared to S_E^2. Since their ratio is large,* a frequency effect is present. Next, S_A^2 is compared to S_E^2. Since their ratio is small, an azimuthal effect is not present. That is, changing the azimuthal angle from 0° to 45° does not change the clutter distribution significantly.

P-band data (428 MHz) were fitted to the log-normal density in an identical manner; the results appear in Table 7. The *P*-band distributions have a much larger spread (higher σ) than the *X*-band data but a slightly smaller spread than the *L*-band data. Unfortunately, no definite comparison can be made between these bands since the *P*-band antenna had a 12° beamwidth resulting in an illuminated patch area 140 percent larger than those of L and X bands. However, since a larger patch tends to make a distribution have a

*Under the hypothesis that there is no frequency effect, S_F^2 and S_E^2 are independent estimates of the sampling error, and their ratio has an F-distribution. The threshold value for any significance, which for a significance of 0.1 is 3.2, can be found in either Duncan [24] or Fischer [25], which also provide further information about analysis of variance. All analysis of variance in this section were conducted at a significance level of 0.1.

Table 5—σ in Decibels of the Fitted Log-Normal Distribution*

4FR Radar Parameters	Azimuthal Squint Angle							
	0°		15°		30°		45°	
Frequency								
L band	6.1	6.0	5.4	5.7	5.5	6.3	6.1	5.6
X band	4.8	4.4	4.9	4.3	4.6	4.5	5.0	4.7

*From reference [16].

Table 6—Results of Analysis of Variance: The Effect of Various Parameters on the 4FR Clutter Distributions*

Effect	Mean Square	Variance Ratio	Conclusion
Frequency	$S_F^2 = 5.640$	$S_F^2/S_\epsilon^2 = 55.84$	Frequency effect is present
Azimuthal angle	$S_A^2 = 0.062$	$S_A^2/S_\epsilon^2 = 0.61$	Azimuthal effect not present
Sampling error	$S_\epsilon^2 = 0.101$		

*From reference [16].

Table 7—σ in Decibels of the Fitted Log-Normal Distribution for P Band*

Azimuthal Squint Angle							
0°		15°		30°		45°	
5.8	5.7	5.1	5.8	5.1	5.8	6.0	6.2

*From reference [16].

smaller spread, *P*-band distributions have a larger spread than *X*-band distributions, but the relationship between *P* and *L* bands cannot be determined. Valenzuela and Laing [26] analyzed the 4FR data and concluded that *L*-band data were more Rayleigh than *X*-band data; based on results of *K-S* tests. However, if one studies the results of the individual tests, one sees that the maximum difference in probability (D) between *L*-band data and the Rayleigh distribution is larger than the difference between *X*-band data and the Rayleigh distribution. The reason Valenzuela and Laing concluded that *L*-band data were more Rayleigh than *X*-band data is probably because P_D is smaller for the *L*-band than for the *X*-band. However, since they concluded that neither data are Rayleigh distributed, the only reason P_D is smaller for *L*-band data is that there are fewer independent samples for *L*-band data than for *X*-band data. The result only indicates that the *K-S* test is not a powerful test; i.e., if data do not come from the theorized distribution, many independent samples are needed to reject the hypothesis that the data did come from the theorized distribution.

The FHR data are analyzed again to find the variation of $p(x)$ with polarization, pulsewidth, and wind direction. First, the data were fitted to the log-normal distribution (results appear in Table 8); the fitting errors ranged from 0.4 to 1.4 dB, and the average error was 0.8 dB. An analysis of variance was conducted; the results are summarized in Table 9. The most significant parameter is polarization: the clutter distribution for horizontally polarized data has a much longer tail than that for vertically polarized data. The next most significant parameter is orientation with respect to the wind: upwind or downwind measurements have a longer tail to their distributions than crosswind measurements. While the analysis of variance (Table 9) shows no significant difference between the upwind and downwind measurement, an analysis of variance (Table 10) of the short-pulse data in Table 2 definitely shows a difference between upwind and downwind measurements. (Clutter time 1145 was eliminated to make an equal number of cases in each category.) Finally, while the 20-ns data have a longer tail than the 100-ns data, the

Table 8—Log-Normal Fit of Data Taken by the FHR*

Date	Time	Identifier	σ (dB)	Maximum Difference (dB)
3/11	1344	VUL	4.8	0.45
3/11	1346	HUL	6.0	0.73
3/11	1411	VDL	4.7	0.50
3/11	1413	HDL	7.3	0.81
3/12	1026	HDS	7.5	0.83
3/12	1028	VDS	5.5	1.30
3/12	1049	VCS	4.4	0.52
3/12	1051	HCS	6.1	0.40
3/12	1125	VCL	4.4	0.42
3/12	1127	HCL	5.6	1.40
3/12	1154	HUS	5.9	1.10
3/12	1156	VUS	5.8	1.08

*From reference [16].

Table 9—Results of Analysis of Variance: The Effect of Various Parameters on the FHR Clutter Distributions*

Source	Mean Square	Variance Ratio	Conclusion
Polarization	6.75	26.0	Polarization effect is present
Pulse length	0.56	2.2	Pulse-length effect not present
Upwind vs downwind	0.78	3.0	Effect not present
Upwind and downwind vs crosswind	1.76	6.7	Effect is present
Sampling error	0.26	–	

*From reference [16].

Table 10—Results of Analysis of Variance: The Effect of Various Parameters on the FHR Clutter Distributions in Table 2

Source	Mean Square	Variance Ratio	Conclusion
Polarization	4.32	141.0	Effect is present
Upwind vs downwind	0.15	4.9	Effect is present
Upwind and downwind vs crosswind	0.15	4.9	Effect is present
Sampling error	0.0306	–	

analysis of variance (Table 9) indicates no significant difference. Since it is known that the clutter distribution is Rayleigh for large pulsewidth, there seems to be a threshold effect. That is, small pulse measurements have a larger clutter spread than large pulse measurements; however, once the pulsewidth is smaller than the water wavelength, changes are no longer significant.

2. *Variation of* $p(x|\sigma_0)$

To find the effect of various parameters on the conditional density $p(x|\sigma_0)$, an analysis of variance was run on the data in Table 4 (optimum k are used as data points); the results are summarized in Table 11. The most significant parameter is pulsewidth: the larger the pulsewidth, the more Rayleigh (as oppose to Ricean) the density of clutter backscatter. This can be explained by recalling that the dominant scatterers are breaking waves. If the patch is small, there may be only one breaking wave in it, and the density will be Ricean. However, if the pulsewidth is increased, several breaking waves may be present. Since return from these waves will add noncoherently, the density will tend

Table 11—Analysis of Variance Results: The Effect of Various Parameters on the Conditional Clutter Density*

Effect	Mean Square	Variance Ratio	Conclusion
Polarization	0.606	7.88	Polarization effect is present
Pulse length	2.706	35.21	Pulse-length effect is present
Wind	0.006	0.07	Wind effect not present
Sampling error	0.076	–	

*From reference [16].

toward a Rayleigh density as the pulsewidth and thus the number of breaking waves increases. The other significant parameter is polarization, vertical polarization giving rise to a more Rayleigh-like density than horizontal polarization. This could be explained by the simple fact that the clutter return is higher for vertical polarization. Thus, if the dominant scatterers have the same cross section for both polarizations, the ratio of the dominant scatterer to background clutter will be smaller, and hence the value of k will be nearer to 2. Finally, wind direction has no effect on the conditional density.

D. Empirical Density of $p(\sigma_0)$

In 1972, Trunk [16] showed that the non-Rayleigh density $p(x)$ of envelope-detected sea return could be expressed as

$$p(x) = \int p(x|\sigma_0)p(\sigma_0)\, d\sigma_0 . \tag{12}$$

While Trunk investigated the densities $p(x)$ and $p(x|\sigma_0)$ and concluded that the form of $p(\sigma_0)$ has an important influence on $p(x)$, he did not find the density for $p(\sigma_0)$. This situation was rectified in 1974 when Owens [27] used a nonparametric estimator for the density of 10 log σ_0, which is equivalent to finding $p(\sigma_0)$. Owens' analysis is summarized in the following sections.

1. *Nonparametric Estimation of a Probability Density*

If $\underline{\sigma}_1, \ldots, \underline{\sigma}_N$ are independent random variables with a common density f, a kernel estimator of f at a point y has the form

$$\hat{f}(y) = \frac{1}{N} \sum_{i=1}^{N} K(y, \underline{\sigma}_i) \tag{19}$$

where K is a known kernel. A common form of K is

$$K(y, \sigma) = \frac{1}{h(N)} K[(y - \sigma)/h(N)] \tag{20}$$

where $h(N)$ is a number depending on the number of samples. There are many possible choices for K and $h(N)$. (If the reader is interested in the area of nonparametric density estimation, he should consult Owens [27] who quotes some basic results and references the basic papers.) The choice of Owens was

$$K(Z) = \frac{1}{\pi}\left(\frac{\sin Z}{Z}\right)^2 \tag{21}$$

and

$$h(N) = 20/\sqrt{N}. \tag{22}$$

Thus, if f is the density function of $\underline{\sigma} = 10 \log \sigma$, then

$$\hat{f}(y) = \frac{1}{20\sqrt{N}\,\pi} \sum_{i=1}^{N} \left(\frac{\sin t_i}{t_i}\right)^2 \tag{23}$$

is an estimator of $f(y)$ where

$$t_i = \frac{(y - \underline{\sigma}_i)\sqrt{N}}{20}, \tag{24}$$

and $\underline{\sigma}_1, \ldots, \underline{\sigma}_N$ are independent samples from the density f.

The difficulty in applying Eq. (23) is that the random variables $\underline{\sigma}_i$ are not directly observable. Rather, the data consist of the envelope-detected returns x_i. If the conditional density of $p(x|\sigma_0)$ is known precisely, then empirical Bayes methods [28] could be used to estimate $p(\sigma_0)$. However, while Trunk [16] has shown that $p(x|\sigma_0)$ depends on various parameters such as pulsewidth and polarization, he has also stated that the density of $p(x|\sigma_0)$ has little effect on the density of $p(x)$. Consequently, it is safe to assume that

$$p(x|\sigma_0) = \frac{1}{\sigma_0} g(x/\sigma_0) \tag{25}$$

for some density g. Thus, if

$$b = \int_0^\infty x g(x)\, dx\,, \tag{26}$$

then

$$E(x|\sigma_0) = b\sigma_0\,. \tag{27}$$

Now, consider the following procedure. For each i, $\{i = 1, N\}$, select a sample σ_i from f, and then select k samples, denoted $x_{i1}, \ldots, x_{ik}$ from the conditional density $p(x|\sigma_i)$. Since

$$E\{x_{ij}\} = b\sigma_i \quad \text{for } j = 1, \ldots, k, \tag{28}$$

it follows that an estimate of $b\sigma_i$ is

$$b\hat{\sigma}_i = \frac{1}{k}\sum_{j=1}^{k} x_{ij} . \tag{29}$$

Taking the log yields

$$\underline{\sigma}_i \equiv 10 \log b\hat{\sigma}_i = 10 \log \hat{\sigma}_i + 10 \log b . \tag{30}$$

That is, $\underline{\sigma}_i$ is an estimate of $10 \log \sigma_i$, shifted by a constant that is independent of i. Thus, $\underline{\sigma}_i$ defined by Eqs. (29) and (30) can be used in Eq. (23) to estimate $f(y)$.

2. *Data Analysis*

The data analyzed by Owens were the small-pulse (20-ns) FHR data that appear in Table 8. The nonparametric estimation procedure is applied to these data in the following manner. First the decorrelation times for selected short-pulse data are extracted from Table 3 (presented in column 3 of Table 12). Since 10 ms is the decorrelation time of sea clutter when σ_0 remains constant, the decorrelation times in Table 12 are good estimates of the times required for σ_0 for the illuminated patch to decorrelate. Based on these times, Owens selected a "sampling interval" (approximately one-eighth of the decorrelation time), in which it is assumed that σ remains constant. For each data record, every eighth sample was selected to form a new record, with samples 3 ms apart and adjacent samples recorded at different frequencies. The total number of samples (this corresponds to k in Eq. (29)) in a given sampling interval is given in column 5 and the total number of intervals (corresponding to $N\underline{\sigma}_i$) used in the analysis is given in column 6. Then, using the data sets indicated in Table 12, Owens computed the densities as follows:

Table 12—Decorrelation Times and Sampling Intervals

Time	Identifier	Decorrelation Time (ms)	Sampling Interval (ms)	Number of Samples in Interval	Number of Intervals
1026	HDS	131	39	14	208
1028	VDS	168	51	18	256
1049	VCS	31	9	4	192
1051	HCS	112	33	12	256
1154	HUS	106	33	12	256
1156	HUS	193	63	22	256

1. Use Eq. (29), to obtain average the returns in each sampling interval.

2. Compute the estimates $\underline{a}_i$ of σ_0 (in decibels) for each interval, using Eq. (30).

3. Estimate the probability density of σ_0 (in decibels), using Eq. (23).

The density of each of the six cases is given in Ref. 27, and the density functions for the downwind cases are shown in Figs. 10 and 11.

The density functions for the downwind and upwind cases are quite irregular. This may be the result of shadowing of the patch by large waves. Furthermore, densities for vertical polarization are more peaked than those for horizontal polarization. This supports the conclusion in (Ref. 16) that the density $p(x)$ has a longer tail for horizontal polarization than for vertical polarization. Further information about $p(\sigma_0)$ can be found in Sec. IV.B.

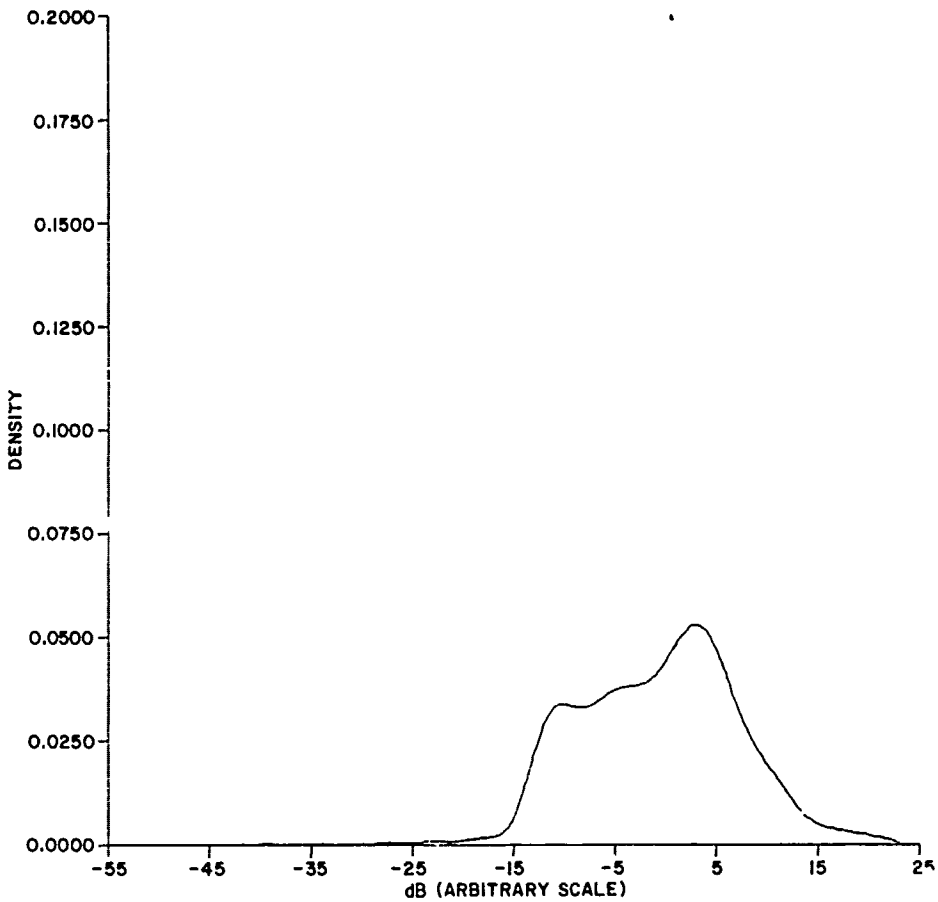

Fig. 10—Estimated probability density of normalized RCS (horizontal polarization, downwind)

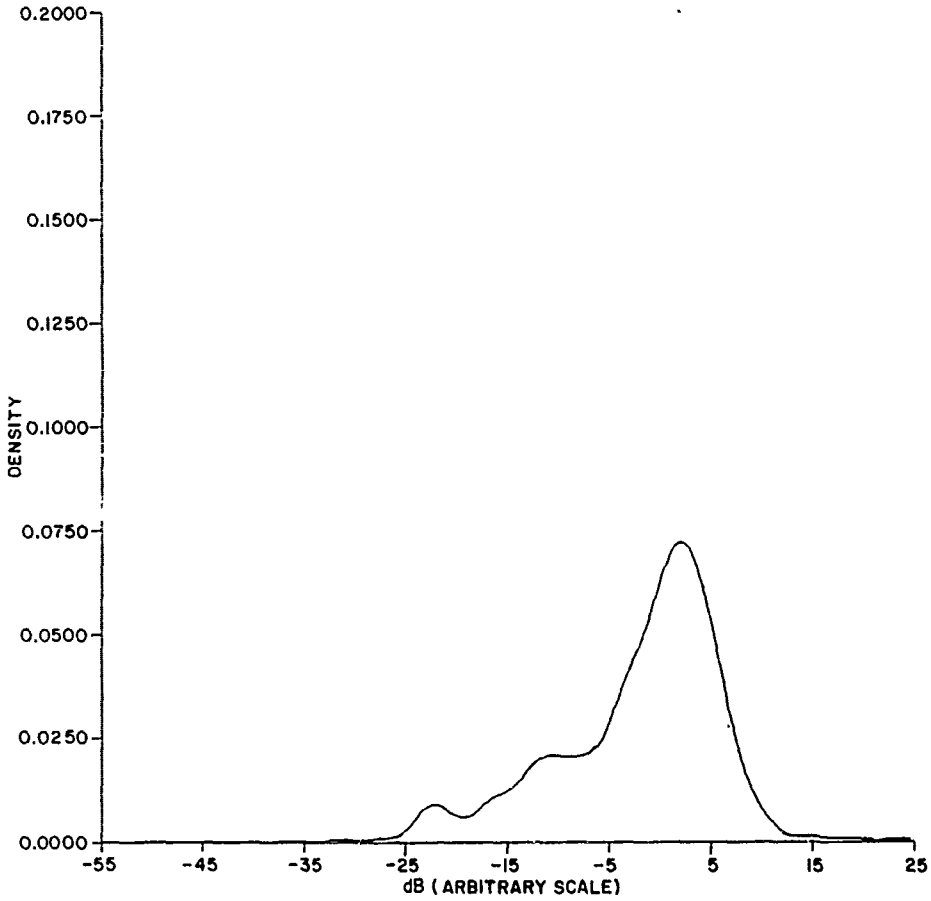

Fig. 11—Estimated probability density of normalized RCS (vertical polarization, downwind)

IV. SEA SURFACE SIMULATION

Trunk [16] and Owens [27,29] have found that a simulation of the sea surface can be extremely useful in certain problems associated with high-resolution radars. In this section, this simulation will be discussed, and two examples of its use will be given.

A. Sea Surface

All investigators [16,27,29] have constructed realizations of the sea surface by using the method suggested by Neumann and Pierson [30]. The realization is obtained by considering the linear solution to the Lagrangian equations of motion for the sea. The long-crested waves are given by the parametric equations in δ,

$$x(t) = \delta - \sin\left[\frac{\omega^2}{g}\,(\delta\cos\theta + y\sin\theta) - \omega_i t\right],$$

$$y(t) = y\,,$$

and

$$z(t) = \cos\left[\frac{\omega^2}{g}\,(\delta\cos\theta + y\sin\theta) - \omega_i t\right], \tag{31}$$

where (x, y, z) are the coordinates of the sea surface and θ is the direction in which the wave crest is moving with respect to the x-axis. The realization is constructed by forming a linear sum of elementary solutions, i.e.,

$$x(t) = \delta - \sum_{i=1}^{N} a_i \sin\left[\frac{\omega_i^2}{g}\,(\delta\cos\theta_i + y\sin\theta_i) - \omega_i t + \gamma_i\right]$$

$$y(t) = y$$

$$z(t) = \sum_{i=1}^{N} a_i \cos\left[\frac{\omega_i^2}{g}\,(\delta\cos\theta_i + y\sin\theta_i) - \omega_i t + \gamma_i\right] \tag{32}$$

where γ_i are independently distributed phases between o and 2π. Given a wave spectrum $S(\omega)$, Trunk [16] suggests setting the N frequencies ω_i by

$$\int_0^{\omega_i} S(\omega)\,d\omega = \frac{2i-1}{2N}\int_0^{\infty} S(\omega)\,d\omega \tag{33}$$

and letting a_i be a Gaussian random variable whose variance is

$$\sigma^2(a_i) = \frac{1}{N}\int_0^{\infty} S(\omega)\,d\omega\,. \tag{34}$$

The wave spectrum that was used was the Kitaigorodskii [31] spectrum for a fully developed sea,

$$S(\omega) = \frac{dg^2}{\omega^5}\exp\left[-b(g/u\omega)^4\right], \tag{35}$$

where $d = 0.0081$, $b = 0.74$, g is the acceleration of gravity, and u is the windspeed.

To see the type of realizations this method yields, let us construct two realizations for a 20-knot wind. First, $N = 100$ values of ω_i were chosen by Eq. (33), and $\sigma^2(a_i)$ was calculated using Eq. (34). Next, the wave directions θ_i were chosen from two Gaussian densities: the first with a standard deviation of 0.2 rad and the second with a standard deviation of 0.5 rad. The surfaces are shown in Figs. 12 and 13. Each surface is about 700 ft (213 m) long and 300 ft (91 m) wide. The 40 y cuts are 7.5 ft (2.3 m) apart and

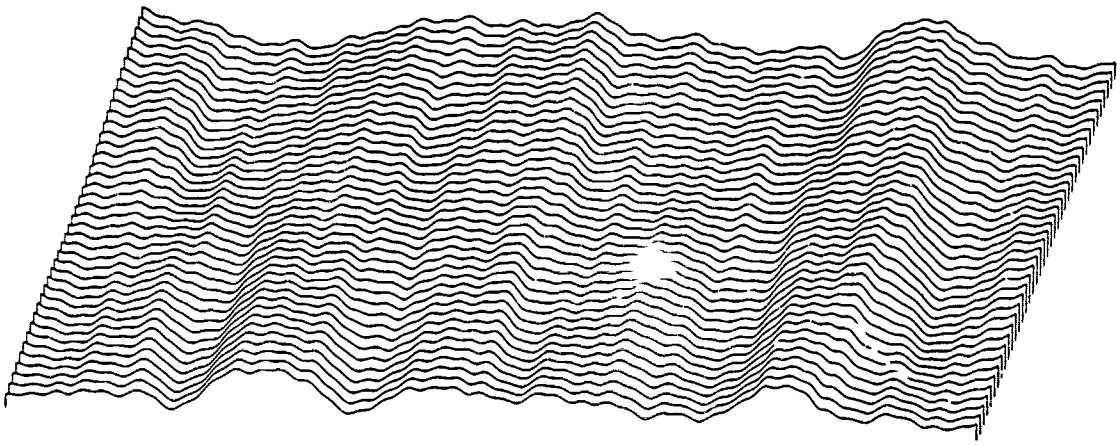

Fig. 12—Simulation of 700-ft by 300-ft (213.4- by 91.4-m) sea surface, with $\sigma(\theta_i) = 0.2$

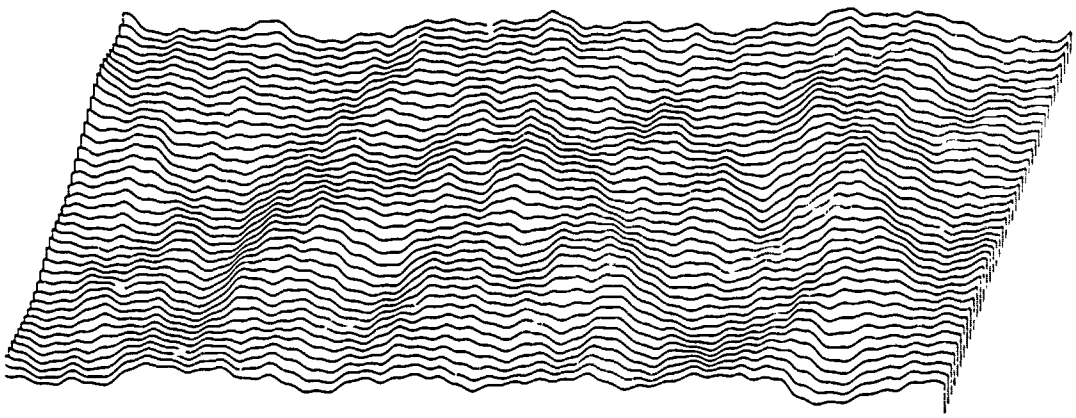

Fig. 13—Simulation of 700-ft by 300-ft (213.4- by 91.4-m) sea surface, with $\sigma(\theta_i) = 0.5$ [16]

the δ values (hence approximate x values) are 1.4 ft (0.4 m) apart. From appearance, Fig. 13, with $\sigma(\theta_i) = 0.5$, is the more realistic sea surface. (Unfortunately, while Trunk [16] used $\sigma(\theta) = 0.5$ he reported $\sigma(\theta) = 0.2$. Consequently, Owens [27,29] later used $\sigma(\theta_i) = 0.2$. It is the author's opinion that this fact will have little effect on upwind and downwind results but could have a larger effect on crosswind results.) While there have been several measurements of directional spectra, the results of one of which is reported in Ref. 30, Phillips [32] states that no simple, realistic model for the direction spectrum, corresponding to the existing one-dimensional wave spectrum, exists.

There are several ways in which the sea surface realization can be used. In Sec. IV.B it is used to estimate the densities for $p(x)$ and $p(\sigma_0)$, and in Sec. IV.C it is used to calculate the probability of detecting a small target on the surface of the ocean.

B. Estimation of the Densities $p(x)$ and $p(\sigma)$

From Sec. II, the cross section for horizontal polarization at a grazing angle θ is

$$\sigma_{HH}(\theta) = 4\pi k^4 \sin^4\theta \left| \frac{(\epsilon - 1)}{\left[\sin\theta + (\epsilon - \cos^2\theta)^{1/2}\right]^2} \right| W(2k\cos\theta) \tag{36}$$

where

ϵ is the complex dielectric constant

$k = 2\pi/\lambda$

$KW(K)\,dK = S(\omega)\,d\omega$

$\omega^2 = Kg$

$K = 2k\cos\theta$

$S(\omega)$ is the wave spectrum of the sea surface.

Since the reflected power from elementary Bragg scattering patches in a range cell add noncoherently, the average cross section in an illuminated patch area A is given by

$$\sigma = \iint_{(x,y,z)\epsilon A} \sigma_{HH}(\alpha) g(x, y, z)\,dx\,dy \tag{37}$$

where

z is the height of the sea surface at the point (x, y),

$\alpha = \alpha(x, y, z)$ is the local grazing angle at the point (x, y, z),

$\sigma(\alpha)$ is the reflected power given by Eq. (36), and

$g(x, y, z)$ is the normalized two-way antenna power gain at the point (x, y, z).

Using Eqs. (12), (36), and (37), Trunk [16] calculated $p(x)$ in the following manner: First, the sea surface shown in Fig. 13 was constructed. Then, σ_i (the average radar cross section for the ith sample) is calculated by approximating the surface integral in Eq. (37) with a double summation involving 210 points: twice the azimuth beamwidth is divided into 21 radials (each with a separation of 0.1 beamwdith) and the range is divided into 10 equally spaced ranges. For each of the 210 unshadowed points the local grazing angle α is calculated, $\sigma_{HH}(\alpha)$ is calculated using Eq. (36), and σ_i is calculated by Eq. (37). Next, σ_{i+1} was calculated by advancing the sea surface 10 ft (3.0 m) and repeating the calculations. This process was repeated until 50 values of σ_i were calculated. Then, $p(x)$, given by

$$p(x) = \int p(x|\sigma)p(\sigma)\,d\sigma \tag{12}$$

was approximated by

$$p(x) = \frac{1}{50} \sum_{i=1}^{50} \frac{x \exp\left[-x^2/2\sigma_i^2\right]}{\sigma_i^2}, \tag{38}$$

where the ergodic theorem has been used to replace the average over $p(\sigma)$ by the time series in σ_i and $p(x|\sigma)$ has been assumed to be a Rayleigh density. The Rayleigh density has been used instead of the Ricean density because it is easier to manipulate and Trunk [16] has shown that it will not affect the results. That is, the variation of $p(x)$ from the Rayleigh is basically due to the density $p(\sigma)$. Several distributions were calculated [33] and are shown in Fig. 14. These calculated distributions indicate the effects of various parameters whose significances have previously been demonstrated (Sec. III.C): (a) the clutter distribution for horizontal polarization HUS has a longer tail than that for vertical polarization VUS; (b) the distribution for the short pulse VUS has a longer tail than that for the long pulse VUL; and (c) the distribution for the upwind case HUS has a longer tail than for the crosswind case HCS. (The computer model does not distinguish between upwind and downwind.) Also, the 20-knot case has a longer tail than the 15-knot case. The Rayleigh curve was obtained for HUS when the windspeed was 2 knots; i.e., when the range cell is greater than the water wavelength, the model yields a Rayleigh density.

Owens [29] calculated $p(\sigma)$ in a similar manner. Using $\sigma(\theta_i) = 0.2$ (Fig. 12), he calculated 200 values of σ_i. Then Eq. (23) was used to calculate the density for 10 log σ_0. The results are shown in Figs. 15 and 16. In comparing the experimental results with the simulation, the following paragraph of Owens [29] is quoted,

> "... one should remember that the observations of log σ_0 are obtained through different mechanisms in the two cases. In the simulation the only errors associated with observations of log σ_0 are caused by the inaccuracies of the model and the mathematical calculations therein. Whereas, in the experiment, σ_0 is observed with an error having essentially two components. The first component of error arises from the fact that on a given sample the only observable variable is the return x, x being related to $\underline{\sigma}$ through the density $p(x|\sigma_0)$. This component of error is further complicated ir that various properties of $p(x|\sigma_0)$, which is not known explicitly, depend on experimental parameters. To reduce this component of error, a number of observed values of x are averaged to obtain an estimate of $\underline{\sigma}$, the average being carried out under the assumption that $\underline{\sigma}$ remains constant over the appropriate time interval. Of course, this assumption is not precisely correct, thus introducing a second component of error in the estimate of $\underline{\sigma}$."

Owens goes on to say that "considering the complexity of the mechanism producing sea clutter at low grazing angles and that the two sets of results are not based on the same set of observables, the authors feels that the agreement is good." It is worth noting that Owens' largest disagreement [29] occurs for the crosswind cases. However, if $\sigma(\theta_i) = 0.5$ is used instead of $\sigma(\theta_i) = 0.2$, the spread of $p(\sigma)$ will increase and better agreement will result.

C. Probability of Detecting Small Surface Targets

Some small, fast ships of tomorrow's Navy, such as surface-effect ships, will probably use collision-avoidance systems to avoid such ocean debris as oil drums and logs. Consequently, Owens [29] investigated the probability of detecting targets at a given height h above the local sea surface. It is important to the debris-detection problem that these

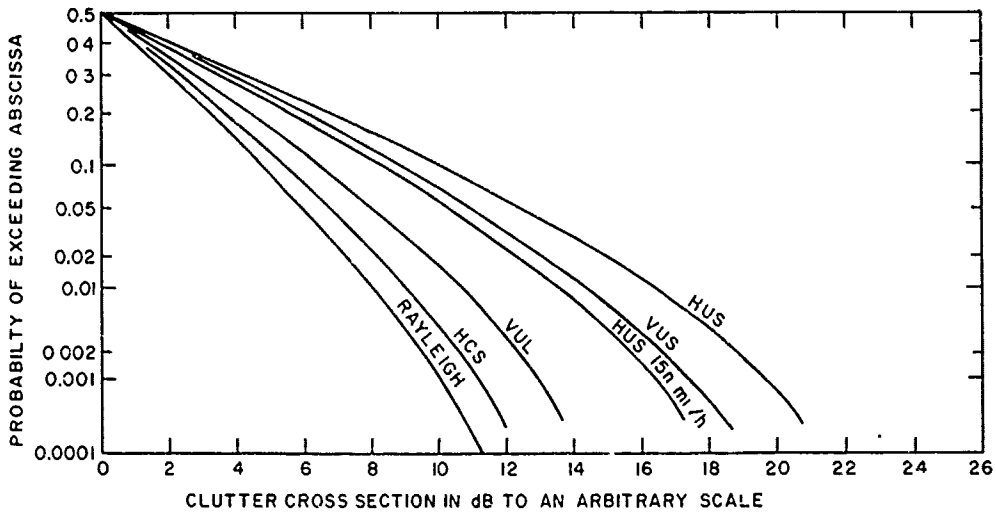

Fig. 14—Distribution functions for various simulations: horizontal (H) or vertical (V) polarization, upwind (U) or downwind (D), short (S) or long (L) pulsewidth. A 15-knot case is marked; all others are for a 20-knot wind [13].

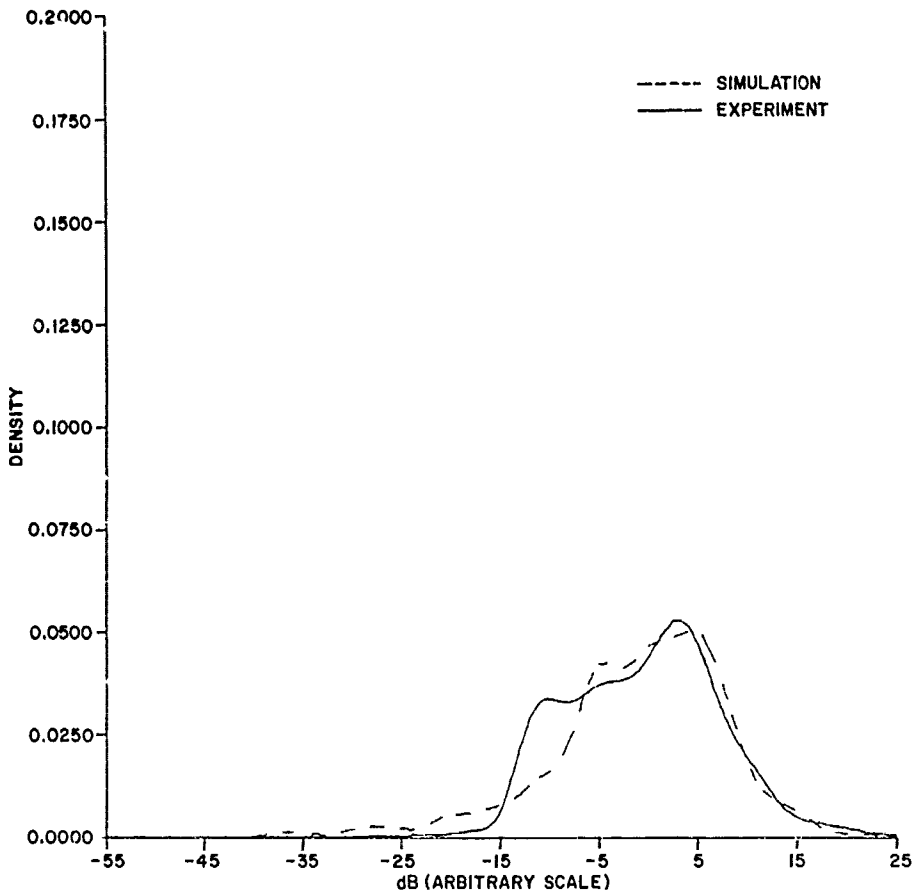

Fig. 15—Estimated probability densities of normalized RCS (horizontal polarization, downwind)

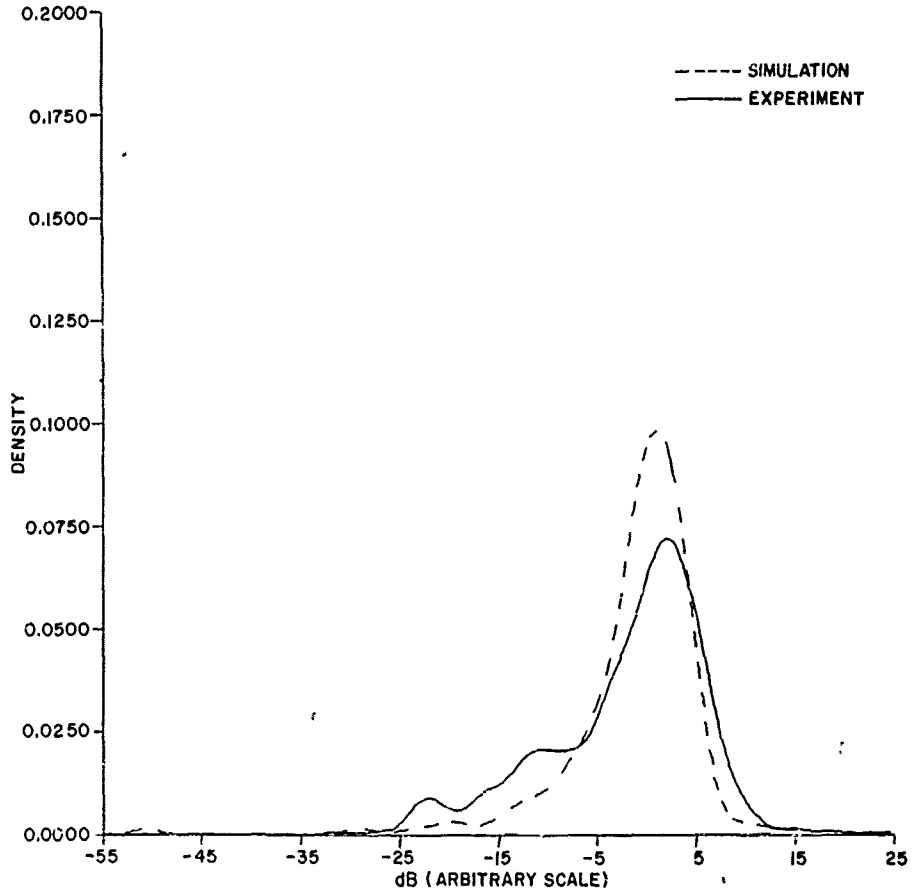

Fig. 16—Estimated probability densities of normalized RCS (vertical polarization, downwind)

targets can be smaller in geometric size than the larger ocean waves, and so the line of sight from antenna to target may be obstructed by surface waves.

This shadowing problem was investigated using the sea surface simulation. At any point (x_0, y_0), the target's height at a time t was $h_0(t) = h + z_0(t)$, where $z_0(t)$ is given by Eq. (32). During periods when the line from the point $[x_0, y_0, h_0(t)]$ to the radar antenna intersects the ocean surface, the target is "shadowed" and cannot be detected. (This ignores refraction effects, which are presently under investigation.) Various cases were computed by Owens and a typical case is given in Fig. 17. For example, if the antenna height is 75 ft (22.9 m), target height h is 1 ft (0.3 m), and the sea state is 3 (wind about 15 knots), the probability of having a clear line of sight at any moment is 0.5 at a range of 2 n.mi.

Owens also calculated the probability of detecting a target by calculating the clutter return in the same range cell as the target. For purposes of illustration, consider the radar to have a beamwidth of 1.5°, a pulsewidth of 20 ns, and a rotation rate of 60 rpm. The radar is 75 ft (22.9 m) above the surface, aboard a ship traveling at 80 knots in sea state 3.

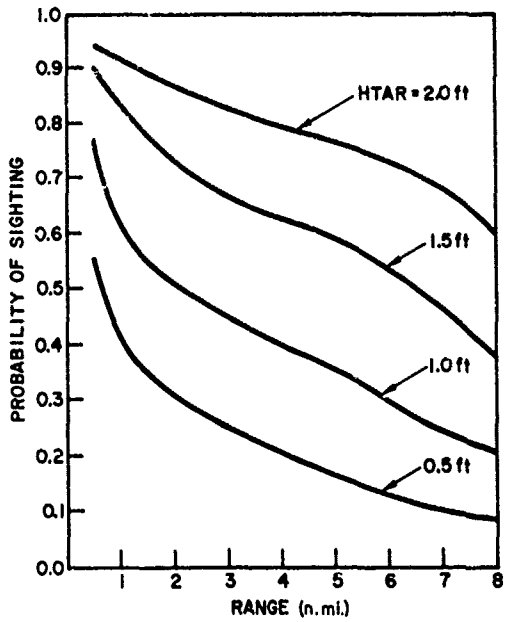

Fig. 17—Probability of sighting vs range for an antenna height of 75 ft (22.9 m) and a sea state of 3

In Fig. 18, the average received signal-plus-noise and average clutter level are graphed as a function of range.

These values are for a particular realization of the sea surface and both curves are referenced to the ambient noise level. First, notice the lower envelope of the clutter return. This represents the clutter received through the sidelobes; when the clutter level falls to this envelope, the entire illuminated patch is obscured by large wave structure. The upper envelope of signal-plus-noise indicates the target return when the target is not obscured. When the curve drops away from the envelope, the target is obscured (zero effective cross section).

Furthermore, the signal and clutter returns are highly correlated. When the target is not obscured, it is likely to be on the front side or top of a large wave; and a large clutter return can be expected. On the other hand, when the target is obscured, the illuminated patch is likely on the back side of a wave, and a relatively small clutter return will result. Owens assumed a square-law detector* and performed scan-to-scan integration. Typical results are shown in Fig. 19. As will be seen in the next section, substantial improvement results from scan-to-scan integration. For specific details of this work, see Ref. 31.

V. DETECTION OF TARGETS IN NON-RAYLEIGH SEA CLUTTER

Since 1947, the classical works of Marcum [35] and Swerling [36] have been used to calculate the probability of detecting targets in sea clutter. Their models, based on a

*Since a target can be shadowed for a number of scans, the detector incurs a loss similar to a collapsing loss: A square-law detector is used, since the collapsing loss is greater for a linear detector than for a square-law detector [34].

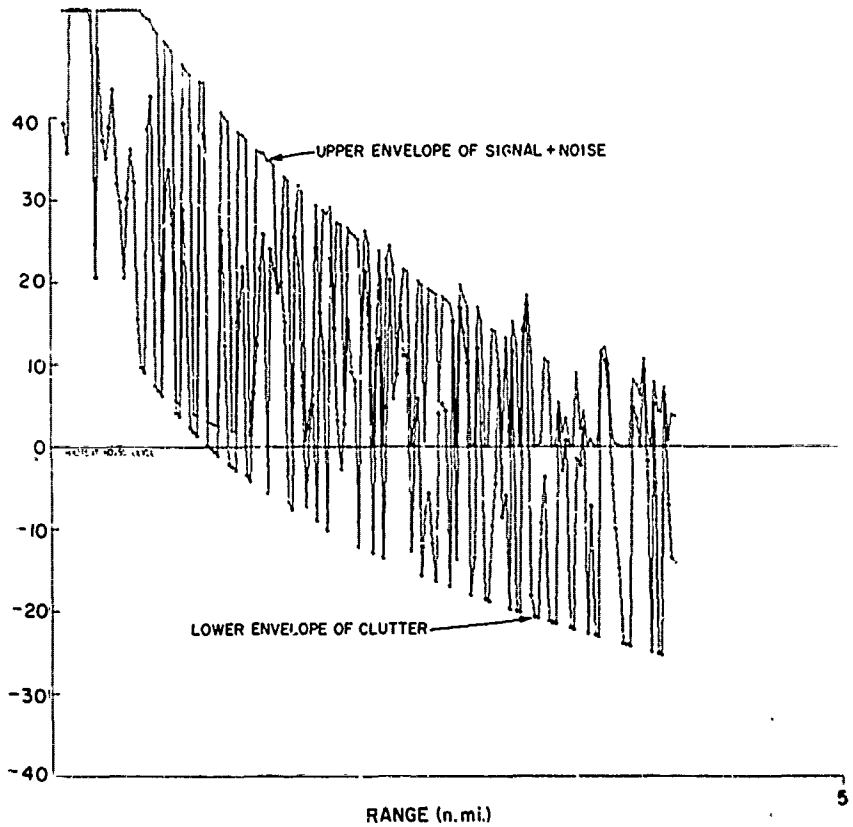

Fig. 18—Received signal strength for a 20-ns radar in sea state 3

Rayleigh density for envelope-detected clutter, usually provide accurate results when pulsewidth is large. (Even for fairly large pulsewidths (0.25 μs), non-Rayleigh densities can occur for high sea states [16,26] or shallow grazing angles [21].) However, as the range-resolution cell decreases in size, the clutter density develops a longer tail than the Rayleigh. Thus, if the Rayleigh theory is used, too many false alarms will occur.

To remedy this situation Trunk and George [10] approximated the clutter return by the log-normal and contaminated-normal densities and calculated probability-of-detection curves for the mean and median detectors. Trunk [37] generated detection curves for fluctuating targets and the trimmed-mean detector. Schleher [38] found a bound for the optimal detector in log-normal clutter and showed that the binary integrator approaches the performance of the optimal detector. Before reviewing the performance of various detectors in the next sections, let us consider the applicability of the various models.

Except for the ratio detector [39] and the work of Owens [29], all investigations have assumed that the available samples are independent samples from $p(x)$. Since it has been shown (Sec. III.B) that frequency diversity produces independent samples from $p(x|\sigma)$, only samples obtained on different scans can be considered independent samples from $p(x)$. (In this section, clutter is restricted to that resembling Figs. 7 and 8, as opposed to Fig. 9.) However, since the range cell is very narrow (this is why the density is

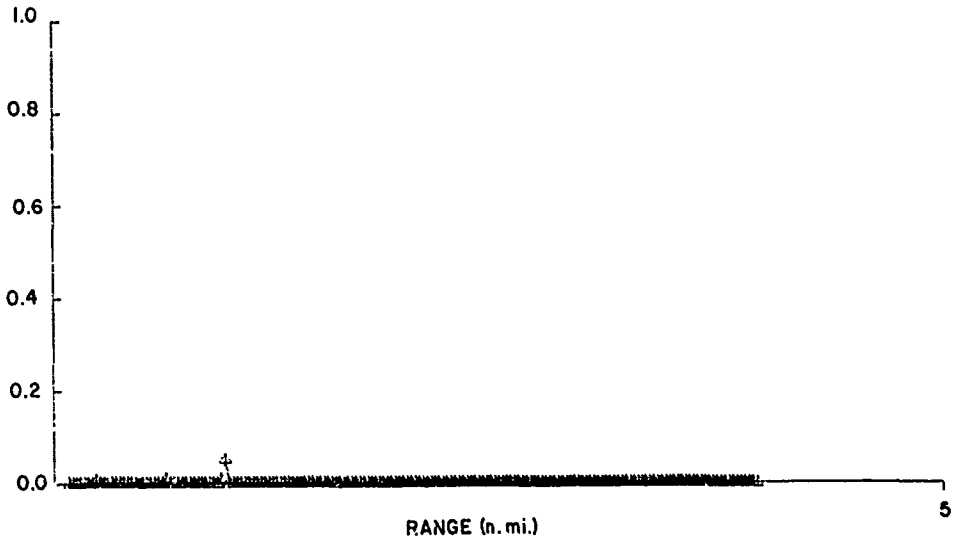

(a) 1 scan

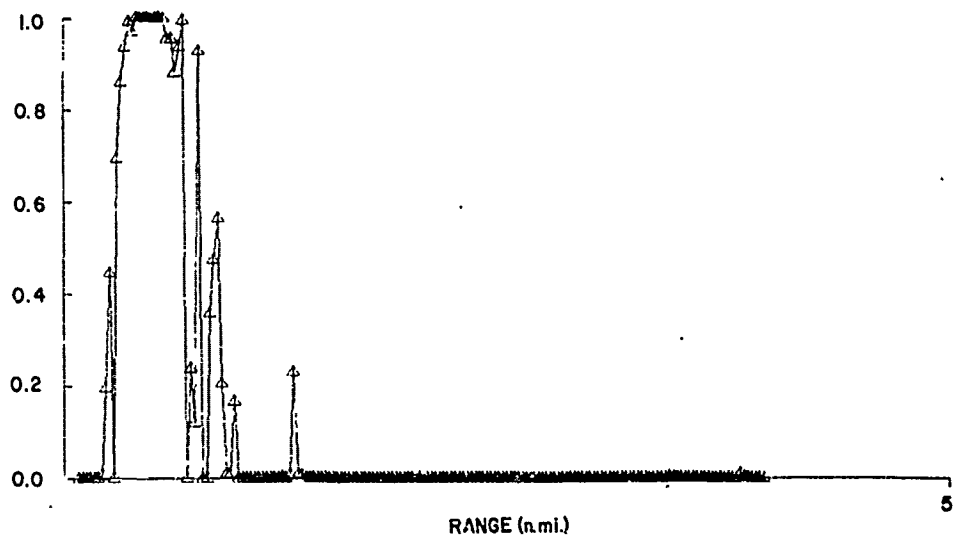

(b) 5 scans

Fig. 19—Probability of detection vs range for a high-resolution radar

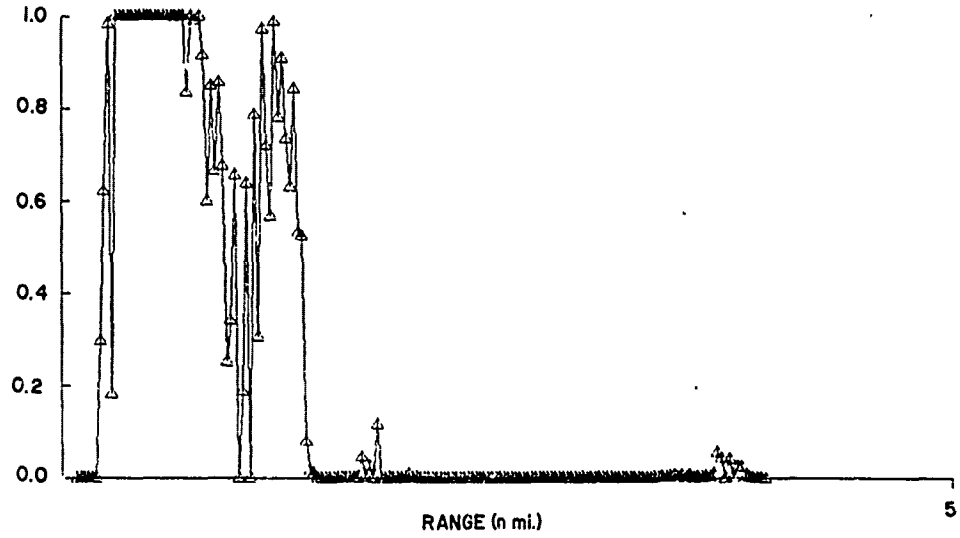

(c) 10 scans

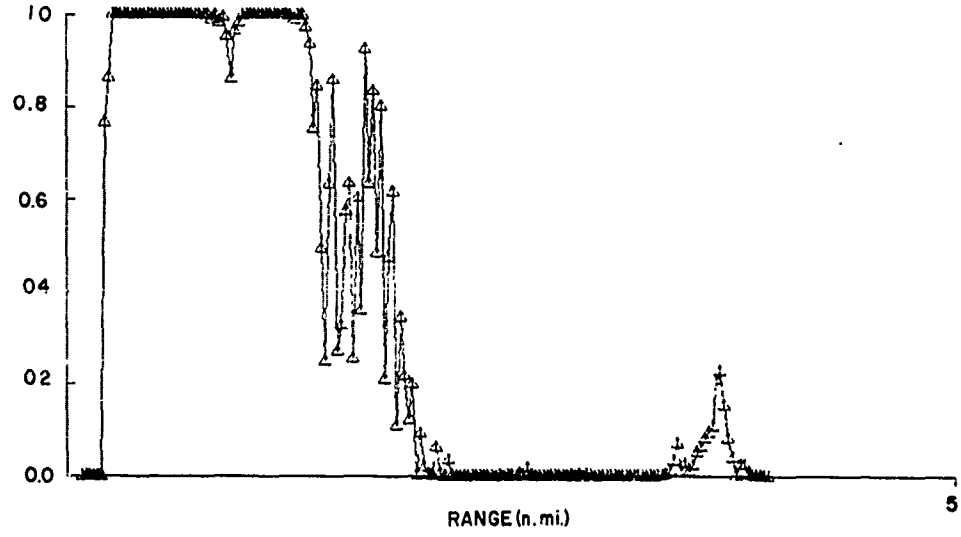

(d) 20 scans

Fig. 19—Probability of detection vs range for a high-resolution radar (Continued)

non-Rayleigh), in order for the target to remain in the same range cell it must either be almost stationary or some kind of range tracking (during detection) or collapsing must be applied.

Besides the problem of independence of the samples, there is the question of the appropriate density for the clutter return. From Fig. 20, it is obvious that the signal required to obtain a particular performance level is very dependent on the distribution assumed for the clutter—a log-normal distribution requires more signal strength than a contaminated-normal one, which requires more than a Rayleigh distribution. Also, the differences are larger for 1 pulse than for 30 pulses. Thus, the choice is extremely critical when only one or a few independent samples are available. It is this author's opinion that for small false alarm rates (i.e., below 10^{-6}), the log-normal density will yield pessimistic results, i.e., performance will actually be better than predicted. This is because $p(x)$ is not really log-normally distributed and has only been used to approximate the density to its 99.99 percentile. As shown in Sec. III.B, $p(x)$ eventually falls off as a Ricean density; i.e., exponentially. Thus, the threshold need not be set quite as high as the log-normal density requires.

Keeping in mind the previous comments, detection results are presented for the log-normal and contaminated-normal densities.

A. Log-Normal Density

For the log-normal model the envelope-detected sample has the density function

$$p(x) = \frac{2}{(2\pi\sigma^2 x^2)^{1/2}} \exp\left(\frac{-2[\ln (x/x_m)]^2}{\sigma^2}\right) \tag{9}$$

where x_m is the median value of x and σ is the standard deviation of $(\ln x)^2$. Following Rice's procedure [40], we can show [41] that the density function of a constant signal A in log-normal noise is

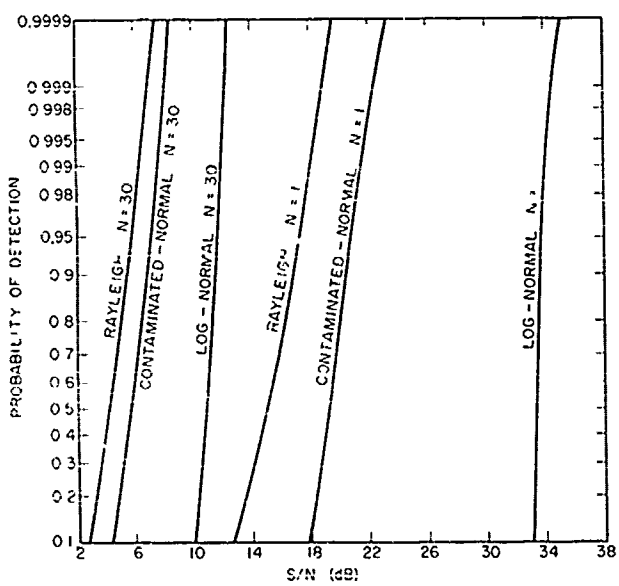

Fig. 20—Comparison of the Rayleigh, contaminated-normal (γ = 0.25, K = 2.25), and log-normal (σ = 6 dB) detection probabilities for N = 1 and 30 pulses and $P_{fa} = 10^{-8}$. For this comparison, S/N is defined in terms of the median value for all the probability distributions [10].

$$p(x, A) = \int_0^{2\pi} \frac{x \exp\left[-2\sigma^{-2} \ln^2 (x^2 - 2xA\cos\theta + A^2)^{1/2}\right] d\theta}{\pi(2\pi\sigma^2)^{1/2}(x^2 - 2xA\cos\theta + A^2)}, \tag{39}$$

where the return has been normalized by median, so that $x_m \equiv 1$.

Various detectors will now be evaluated using the log-normal model.

1. *Mean Detector*

The straightforward method of determining the probability density for the sum of N independent pulses (i.e., the mean detector) is the characteristic function method. If

$$\phi(\omega) \equiv E\{\exp(i\omega x)\} = \int_0^\infty p(x, A) \exp(i\omega x)\, dx \tag{40}$$

is the characteristic function, the probability density of the sum of N statistically independent envelope-detected pulses is

$$p_N(x, A) = \frac{1}{2\pi} \int_{-\infty}^{\infty} [\phi(\omega)]^N \exp(-i\omega x)\, d\omega . \tag{41}$$

The probability of false alarm P_{fa} for a threshold T is given by

$$P_{fa} = \int_T^\infty p_N(x, 0)\, dx , \tag{42}$$

and the probability of detection P_D is

$$P_D = \int_T^\infty p_N(x, A)\, dx , \tag{43}$$

With the fast Fourier transform, it is fairly simple to calculate Eqs. (40) and (41). Then, P_{fa} and P_D are calculated by straightforward numerical integration. Threshold values for N = 1, 3, 10, and 30 for values of P_{fa} ranging from 10^{-2} to 10^{-8} are shown in Fig. 21 for the log-normal density, with σ = 6 dB.* With these thresholds, Eq. (43) is evaluated, yielding P_D vs signal-to-noise ratio S/N per pulse, where S/N is the signal divided by the *median* value of clutter. This is not the usual definition of S/N, in which the noise reference is the rms value of the noise. However, it is an appropriate choice, since it is the median value of clutter that is usually reported [7]. The P_D curves for σ = 6 dB are plotted in Fig. 22. An inspection of these curves shows that the S/N required for

*Additional threshold values and detection probabilities for σ = 3 dB and σ = 9 dB can be found in [41]. It should be denoted that for all detectors σ is not known a priori. Consequently, an adaptive thresholding technique must be used.

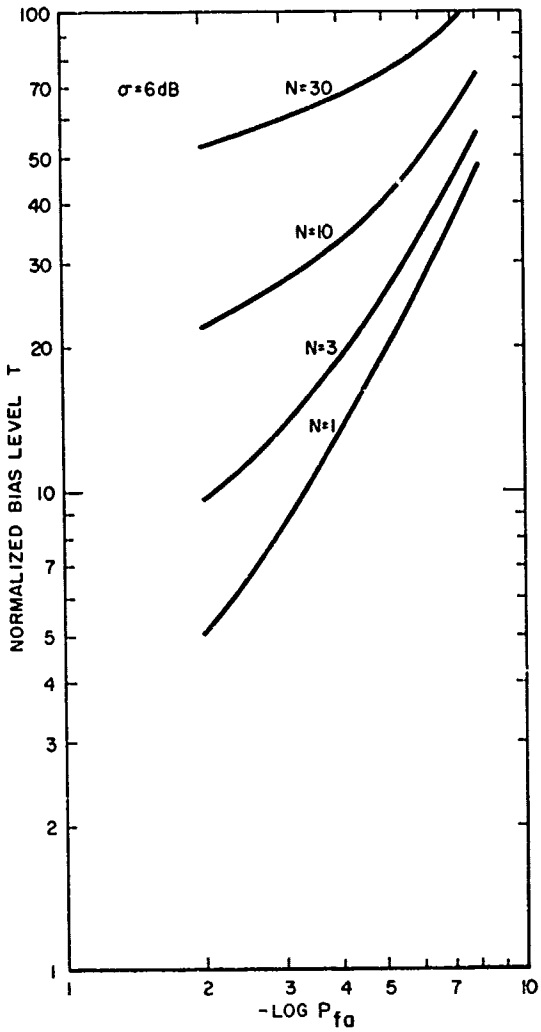

Fig. 21—Normalized bias values for the log-normal distribution with σ = 6 dB [10]

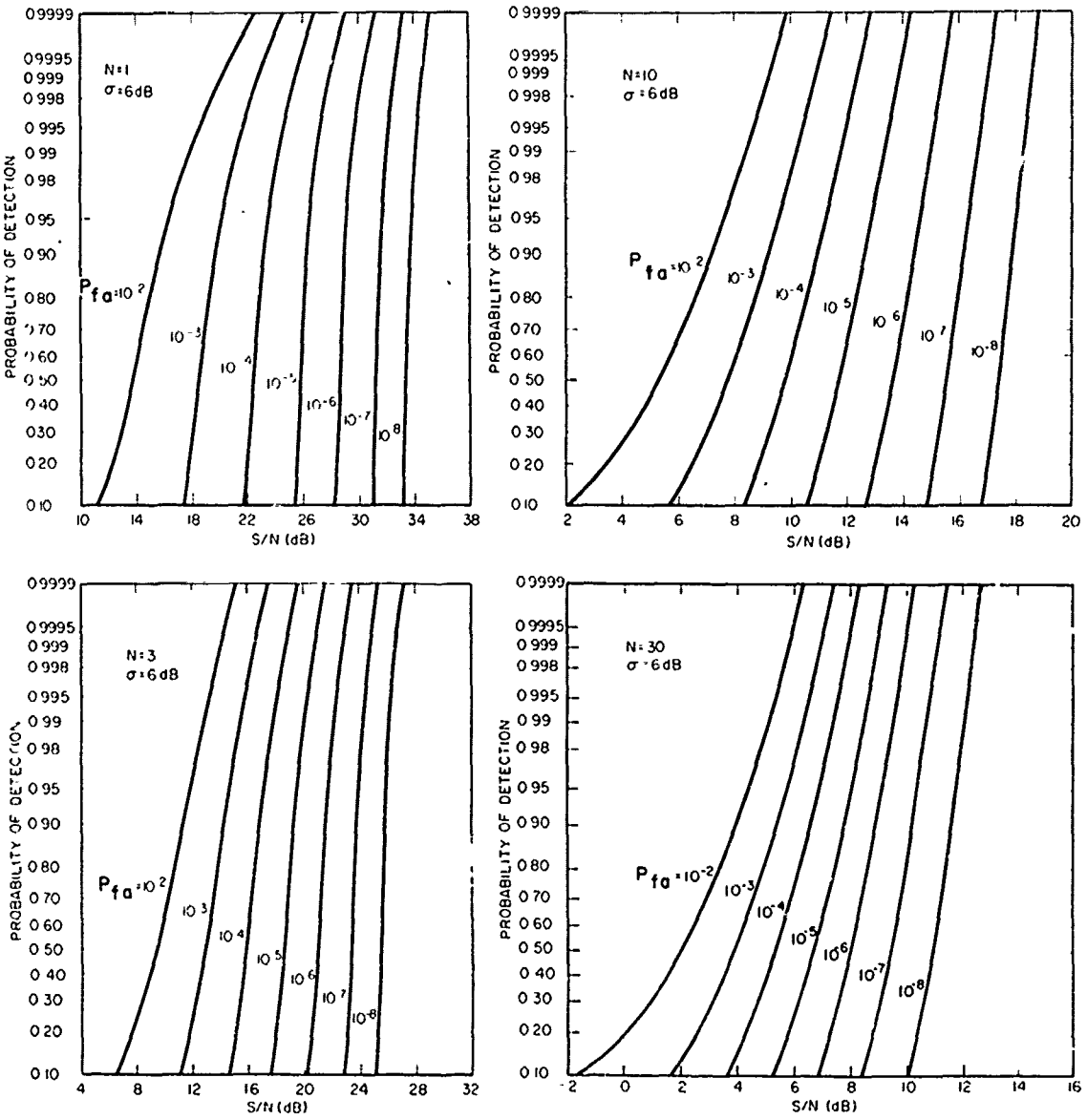

Fig. 22—Probability of detection vs S/N for $P_{fa} = 10^{-2}$ to 10^{-8} [10]

detection decreases rapidly as N increases. In fact, the integration gain I_g is greater than would be obtained for the coherent integration of a Gaussian density, i.e., $I_g > 10 \log N$.

It has been pointed out [37] that this means the optimal beamwidth for a high-resolution scanning radar need not be the smallest. For instance, consider a case in which S/N is 20 dB per pulse, and a three-pulse scan-to-scan integration is being performed. If the clutter has a log-normal distribution with σ = 6 dB, P_D will be 0.1 for a P_{fa} of 10^{-6}. If the beamwidth and scanning rate are both increased by a factor of 10/3, then 10 pulses can be integrated in the same time. In this case, while S/N falls to about 15 dB per pulse, P_D is greater than 0.99. Thus, better performance is obtained with the larger beamwidth.

2. Binary Integrator and Rank Detector

It is well known that the binary integrator (sometimes called a dual-threshold detector or M-out-of-N integrator) is exactly equivalent to a rank detector. Given a set of N ordered samples, $x_1 \leqslant \ldots \leqslant x_k \leqslant \ldots \leqslant x_N$, the kth ordered rank detector involves simply comparing x_k to a threshold. The median detector is the special case where $k = N/2$. However, since the implementation and evaluation of this detector is simpler in the form of the binary integrator, the detector will be discussed in this form. A simple block diagram of the binary integrator (or kth rank) is shown in Fig. 23. The probability $p(A)$ that the returned signal exceeds T is

$$p(A) = \int_T^\infty p(x, A)\, dx \tag{44}$$

where $p(x, A)$ is given by Eq. (39). The probability that more than $m = N - k$ of the N returns exceed T is given by the binomial distribution

$$P(A) = \sum_{\ell=m+1}^{N} \binom{N}{\ell} p^{\ell}(A)[1 - p(A)]^{N-\ell}. \tag{45}$$

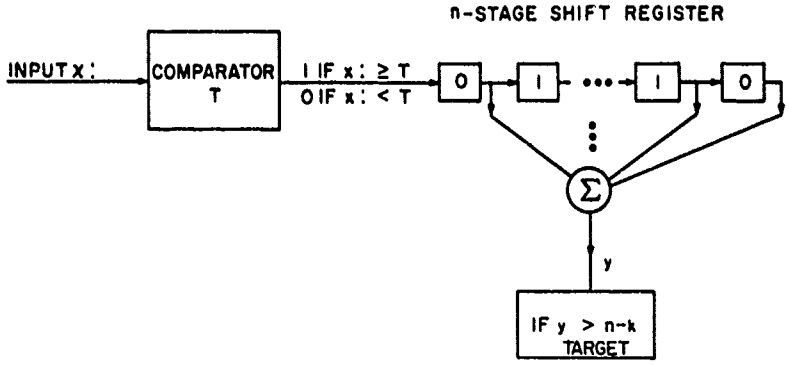

Fig. 23—Implementation of binary integrator or, equivalently, rank detector [10]

The desired probabilities are given by $P_{fa} = P(A = 0)$ and $P_D = P(A)$. In 1970 [10], the median detector for the log-normal distribution with $\sigma = 6$ dB was evaluated. The thresholds are presented in Fig. 24, and the detection results are presented in Fig. 25. Comparing the mean and median detectors in Fig. 26, one concludes that the median requires a smaller S/N than the mean and that the difference increases with increasing N: for $N = 3$, the median is 1.6 dB better than the mean; and for $N = 30$, the median is 2.8 dB better. The performance difference between the two detectors for large sample sizes can be obtained from Pitman's asymptotic relative efficiency (ARE) [42]. This criterion is quite appropriate when the signals are very weak. Specifically, it is the ratio of the number of samples required to maintain a P_{fa} and P_D for the first detector to the number required for the second detector as the S/N approaches zero:

$$\mathrm{ARE}\,(d_1, d_2) = \lim_{S/N \to 0} \frac{N_1(P_{fa}, P_D, S/N)}{N_2(P_{fa}, P_D, S/N)} \tag{46}$$

where N_i is the minimum number of observations required for detector d_i. The simplest way of calculating the ARE is by employing the concept of efficacies, which was also introduced by Pitman. Using a result of Noether [43], Trunk [44] calculated an ARE of 129. (See Appendix C.) Assuming that a noncoherent integration gain of $10 \log\sqrt{N}$ is appropriate for small signals, the median detector is approximately 10.5 dB better than the mean detector for very small signals.

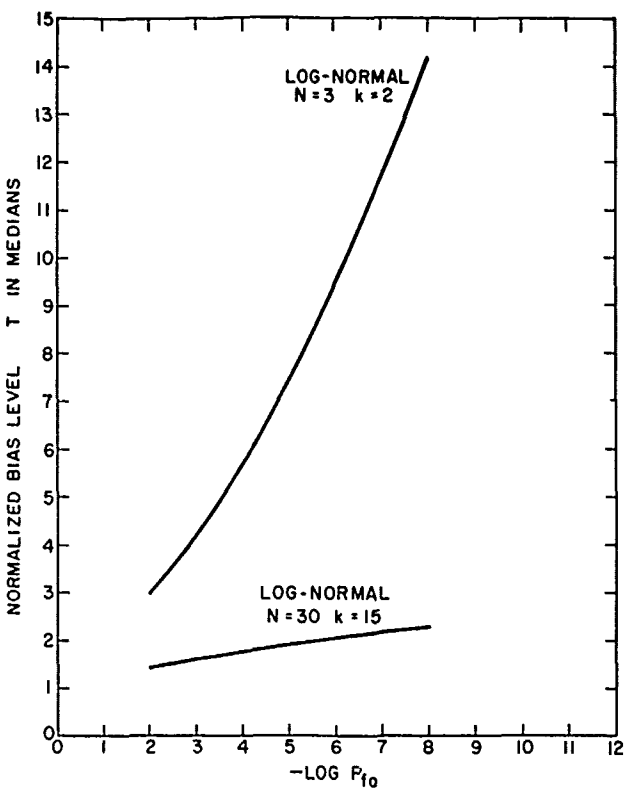

Fig. 24—Normalized bias values for the median detector (log-normal distribution with $\sigma = 6$ dB)

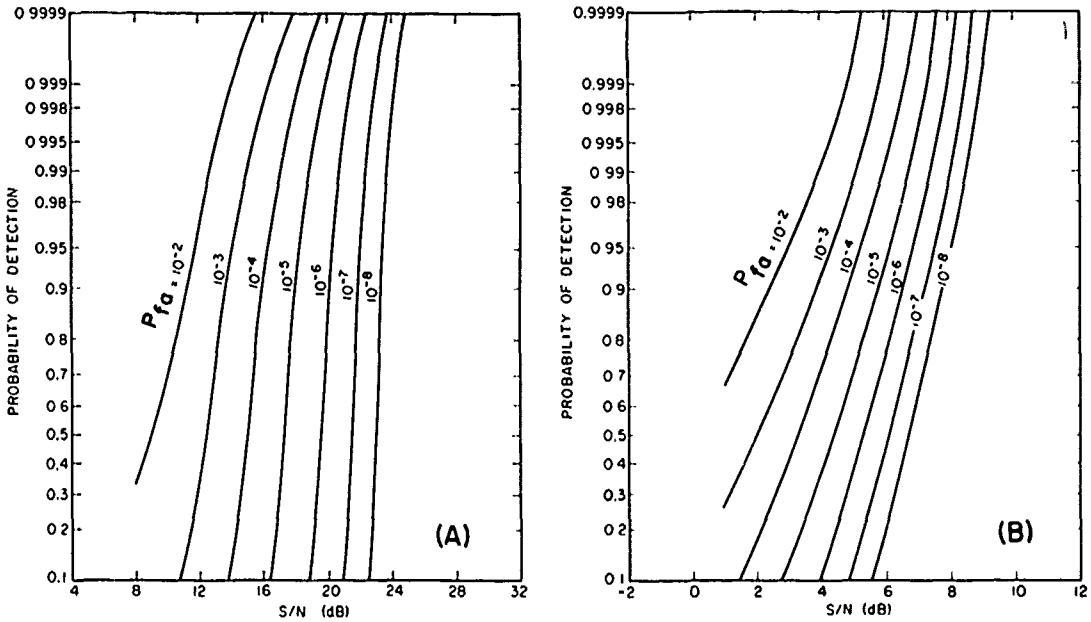

Fig. 25—Probability of detection vs S/N for the median detector and for the log-normal distribution with σ = 6 dB: (a) N = 3 [10]; (b) N = 30 [10]

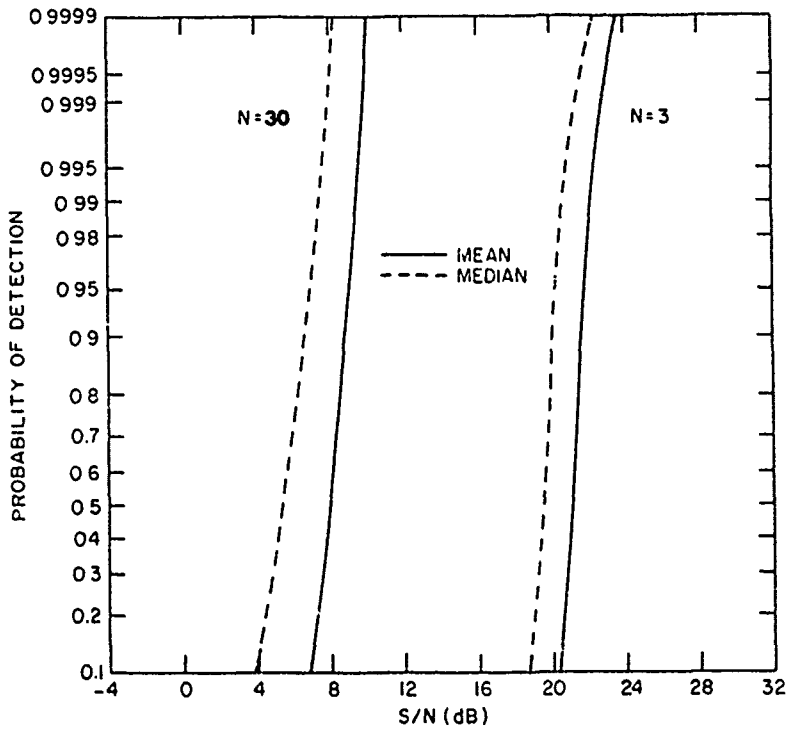

Fig. 26—Probability of detection for the log-normal distribution: S/N = 20 log [A/(median noise value)], probability of false alarm = 10^{-6}, and σ = 6 dB [44]

Since the log-normal density is unsymmetrical about its median value, there is no reason to expect that $k = N/2$ (the median) is the optimal rank. Rather, because of the long tails of the log-normal, one would expect that the smaller ranks ($k < N/2$) would behave better. While Trunk [45] showed that 1 dB could be gained with respect to the median by using $k = N/3$ against the contaminated-normal density, Schleher [38] showed that larger gains were obtained with smaller ranks against the log-normal. Schleher [46] obtained the optimal value of m for different values of N by calculating the detection curves for each possible value of m and choosing the best value. The optimal values of m for $N = 3$, 10, and 30 pulses, for the log-normal density with $\sigma = 6$ dB, are given in Table 13 along with the optimal values for the Rayleigh density, which were determined by Schwartz [47]. Detection curves were generated by Schleher [46] for the log-normal density ($\sigma = 6$ dB) with $N = 3$, 10, and 30 pulses. The detection curves for the optimal m are given in Figs. 27, 28, and 29. Comparing these results with the median detector shows that the largest differential is for smaller N. For $N = 3$, the median is about 4 dB worse (for $P_D \approx 0.9$ and $P_{fa} = 10^{-6}$) than the binary integrator ($m = 2$); for $N = 30$, the median is only about 1 dB worse.

Table 13—Optimal Value of Second Threshold m

n	m (Log-Normal)	m (Rayleigh)
3	2	2
10	7	4
30	24	8

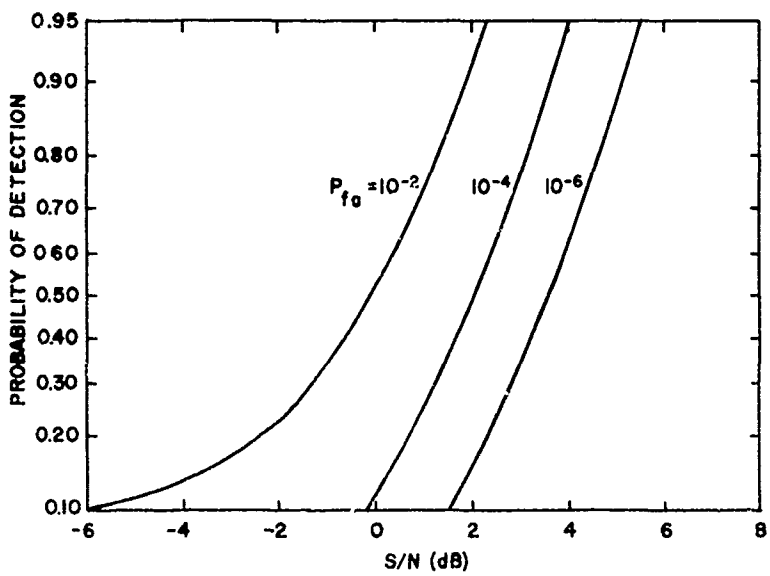

Fig. 27—Probability of detection vs S/N for the log-normal distribution ($\sigma = 6$ dB) and optimal binary integrator: $N = 3$, $m = 2$

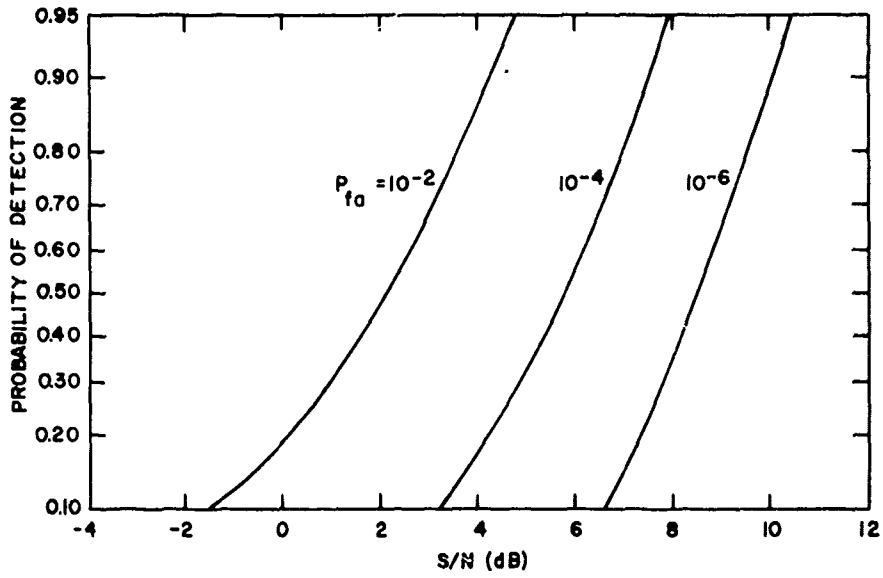

Fig. 28—Probability of detection vs S/N for the log-normal distribution (σ = 6 dB) and optimal binary integrators: N = 10, m = 7

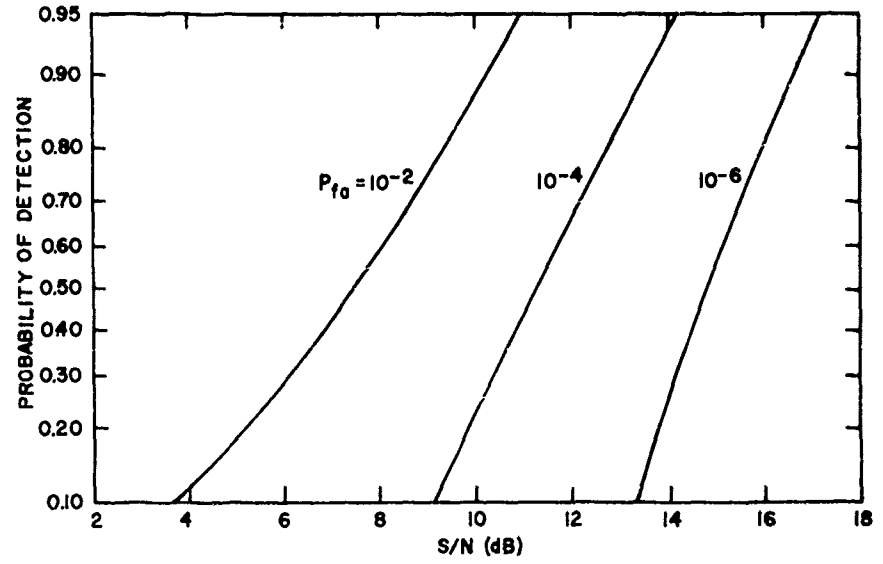

Fig. 29—Probability of detection vs S/N for the log-normal distribution (σ = 6 dB) and optimal binary integrator: N = 30, m = 24

3. *Trimmed-Mean Detector*

Since Tukey [48] has shown that the trimmed-mean detector is effective against contaminated distributions (Tukey only considered symmetrical densities), Trunk [49] conjectured that the trimmed mean would also be effective against long-tailed noncoherent densities, specifically log-normal and contaminated-normal densities.

Given a set of N ordered samples, $x_1 \leqslant x_2 \leqslant \ldots \leqslant x_N$, the trimmed-mean detector is given by

$$S(N_1, N_2) = \sum_{i=N_1}^{N_2} x_i \tag{47}$$

where $1 \leqslant N_1 \leqslant N_2 \leqslant N$. This detector class contains the mean $S(1, N)$ and rank detectors (binary integrators) $S(k, k)$. Unfortunately, when $p(x)$ is a log-normal density, the density of $S(N_1, N_2)$ can only be expressed in terms of an $(N_2 - N_1 + 1)$-order integral to which there exists no known closed-form solution. Since it is impractical to evaluate those densities by numerical integration, a Monte Carlo simulation, involving 10^6 trimmed means,* was performed [49] to estimate the threshold values for desired P_{fa}'s. For $N_1 = 2$ and $N_2 = 5$, the equation

$$-\log P_{fa} = -3.1735 + 1.0685\,T - 0.0070\,T^2\,, \tag{48}$$

relating the threshold T to P_{fa}, was obtained for the log-normal density with $\sigma = 6$ dB. The P_D curves were generated using Monte Carlo techniques and the results are given in Fig. 30. Of the two trimmed-mean detectors, the one using the lower ordered samples yields the higher P_D. This corroborates the previous result [38] that the lower ordered ranks were the better detectors. Comparing the trimmed-mean with the binary integrator shows little or no difference in their performance. However, since the binary integrator is much simpler to implement, it is definitely to be preferred.

4. *Optimal Detector*

It is well known that the optimal detector is specified by the likelihood ratio, or equivalently, the log-likelihood ratio. That is, a decision is obtained by

$$\Lambda(x) \equiv \ell n \frac{p_N(x, A)}{p_N(x, A = 0)} \underset{<}{\geq} T\,, \tag{49}$$

where $p_N(x, A)$ is given by Eq. (41). A decision of "no signal present" is made if $\Lambda(x) < T$, and a decision of "signal present" is made if $\Lambda(x) \geqslant T$. Unfortunately, since the density of $p_N(x, A)$ involves an integral, the likelihood ratio cannot be obtained in closed form. Thus, the optimal detector cannot be found.

*It should be noted that several authors [50,51] using the importance-sampling technique [52] have generated threshold values for the range of $P_{fa} = 10^{-2}$ to 10^{-8} with about 10^4 cases. It is this author's opinion that the technique is very significant. A description of the method is given in Appendix D.

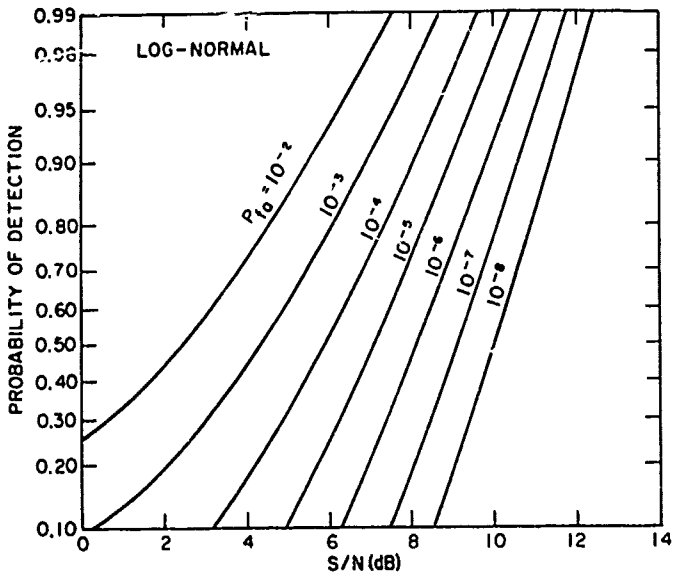

(a) $N = 10$, $N_1 = 2$, $N_2 = 5$

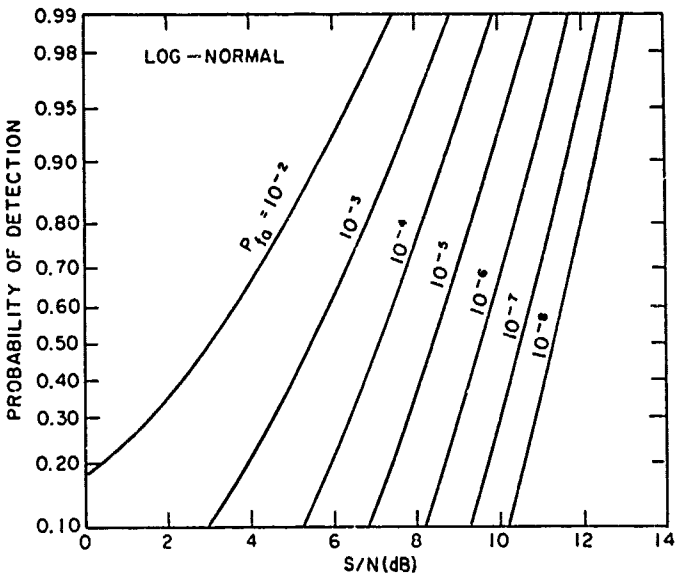

(b) $N = 10$, $N_1 = 4$, $N_2 = 7$

Fig. 30—Probability of detection for the log-normal distribution ($\sigma = 6$ dB) and for the trimmed-mean detector

However, if one can bound the performance of the optimal detector and find a sub-optimal detector that approaches this performance, then there is no reason to specify the optimal detector.

The Chernoff [53] bound,

$$\begin{aligned} P_{fa} &\leqslant \exp[\mu(s) - s\mu(s)] \\ P_D &\geqslant 1 - \exp[\mu(s) + (1-s)\mu(s)], \end{aligned} \qquad 0 \leqslant s \leqslant 1 \tag{50}$$

where the semi-invariant $\mu(s)$ is given by

$$\mu(s) = \ln \int_{-\infty}^{\infty} [p_N(x, A)]^s [p_N(x, A=0)]^{1-s}\, dx\,, \tag{51}$$

provides a rather coarse bound for the desired probabilities. Van Trees [54] tightened the bounds by finding a multiplicative factor for the exponentials, in Ref. 50, using a central-limit-theorem argument. Schleher [38,46] obtained a more accurate result by using an Edgeworth series expansion to approximate the desired probabilities. Schleher [46] shows that P_{fa} is given by

$$\begin{aligned} P_{fa} = {} & \frac{1}{2}\operatorname{erfc}[\alpha(S)] \exp[\alpha^2(S) + B(S)] \\ & - \frac{\dddot{\mu}(S)}{6[\ddot{\mu}(S)]^{3/2}} \exp[B(S)] \left\{ \frac{1}{2}\operatorname{erfc}[\alpha(S)] \left[S\sqrt{\ddot{\mu}(S)} \right]^3 \exp[\alpha^2(S)] \right. \\ & \left. + \frac{1}{\sqrt{2\pi}} [1 - S^2\ddot{\mu}(S)] \right\} \end{aligned} \tag{52}$$

where

$$\alpha(S) = S[\ddot{\mu}(S)/2]^{1/2} \tag{53}$$

$$B(S) = \mu(S) - S\dot{\mu}(S)\,. \tag{54}$$

An expression for $1 - P_D$ can be found [46] by substituting $1 - S$ for S in Eqs. (52), (53), and (54). Evaluation of Eq. (52) for P_{fa} and P_D requires the determination of the first, second, and third derivatives of $\mu(S)$. Schleher calculated these derivatives by evaluating $\mu(\mathcal{S})$ at many points in the interval (0, 1), fitting a cubic spline function to the points, and differentiating the spline function. (The N-degree spline function produces the smoothest curve through the data points while maintaining continuity of the first $N - 1$ derivatives at each data point.) Receiver operating curves were generated and are given in Ref. 46. Curves comparing the mean, median, binary integrator, and trimmed-mean detectors with the optimal detector are given in Figs. 31, 32, and 33, for $N = 3$, $N = 10$, and $N = 30$ pulses, respectively. From these curves it can be seen that the binary integrator and trimmed-mean detector are within 1 dB of the optimal detector. Since the

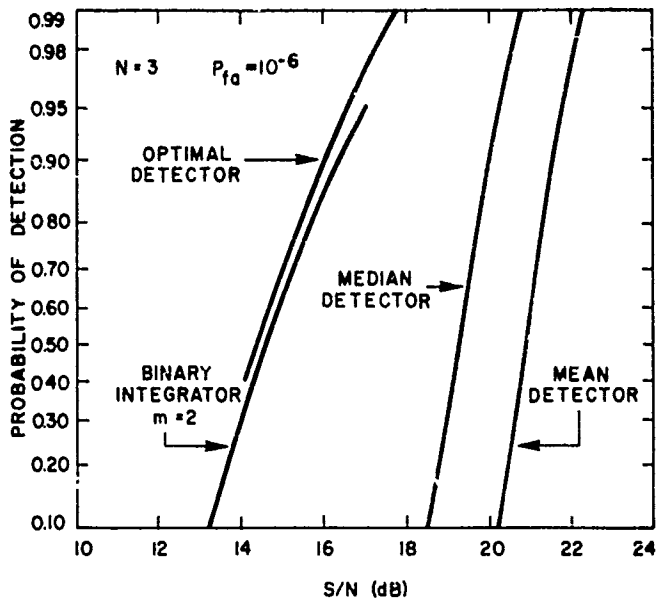

Fig. 31—Comparison of various detectors in log-normal (σ = 6 dB) interference

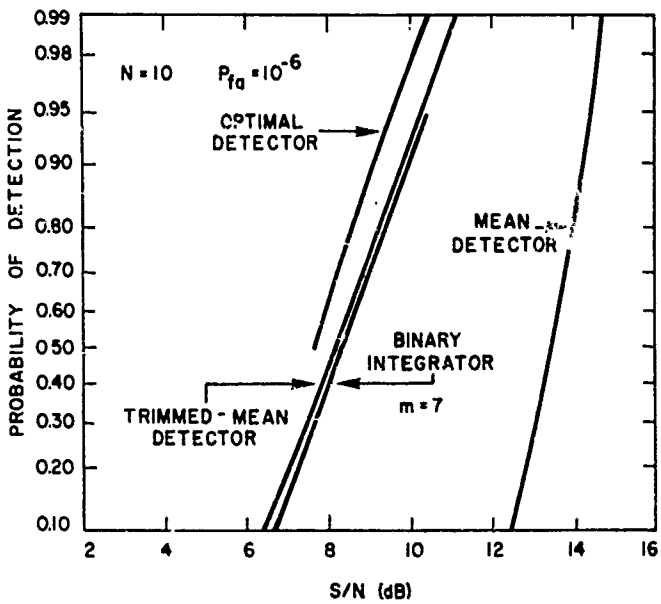

Fig. 32—Comparison of various detectors in log-normal (σ = 6 dB) interference

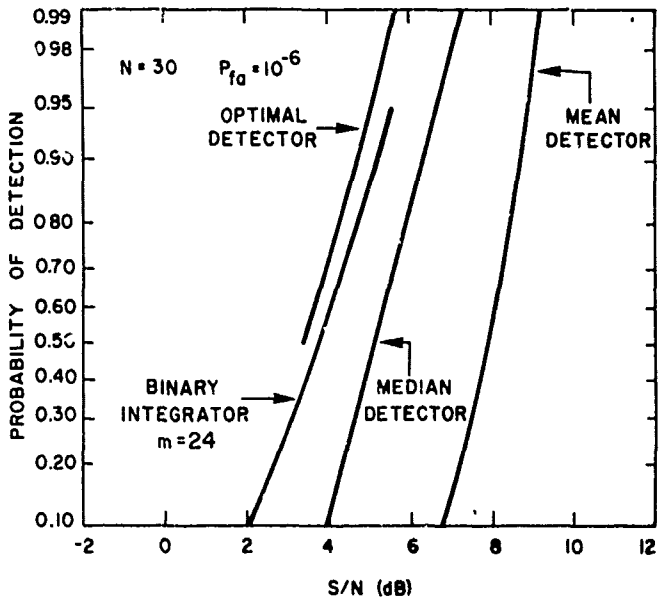

Fig. 33—Comparison of various detectors in log-normal (σ = 6 dB) interference

trimmed-mean detector requires a ranking of the samples, the binary integrator should be used to detect nonfluctuating targets in the presence of log-normal interference.

5. *Fluctuating Targets*

In the previous sections, P_D curves were generated for various detectors. It has been assumed that the target is not fluctuating and that the noise samples are independent. However, to obtain independent samples from sea clutter (whose density is approximated by the log-normal), the returned samples must be from different scans. Since the time separation is probably larger than 1 s, it is quite likely that the target is fluctuating. Consequently, Trunk [55] calculated the performance of the mean, median, and trimmed-mean detectors against the log-normal density, with Swerling II and IV fluctuations assumed [36].

Since the threshold value for any P_{fa} is independent of the target model, they have been already calculated; all that remains is to calculate the P_L for various S/N. Since the interesting range of P_D is from 0.01 to 0.99, Monte Carlo techniques, which require considerably less computer time than the characteristic-function approach, will be used. It is well known that the ith sample x_i of an envelope detector can be generated by

$$x_i = \left(y_i^2 + z_i^2\right)^{1/2}, \tag{55}$$

where y_i and z_i are in-phase and quadrature-phase components. For the generation of log-normal clutter

$$y_i = \exp\{\sigma[-2\,\ell n\,(v_{i1})]^{1/2}\sin(2\pi v_{i2})\}\sin(2\pi v_{i3}) + A\,,$$

$$z_i = \exp\{\sigma[-2\,\ell n\,(v_{i1})]^{1/2}\cos(2\pi v_{i2})\}\cos(2\pi v_{i3})\,, \tag{56}$$

where $\{v_{ij}\}$ are independent and uniformly distributed random numbers on (0, 1) and A is the signal. For the fluctuating signal, the probability densities are

$$p(A) = \frac{2A}{\sigma^2}\,e^{-A^2/\sigma^2} \tag{57}$$

for the Swerling II case and

$$p(A) = \frac{8A^3}{\sigma^4}\,e^{-2A^2/\sigma^2} \tag{58}$$

for the Swerling IV case. The generation of a variable having the density given in Eq. (57) is straightforward. Integrating Eq. (57), one obtains

$$P(u \leqslant A) = 1 - e^{-A^2/\sigma^2}$$

or

$$e^{-A^2/\sigma^2} = 1 - P(u \leqslant A)\,. \tag{59}$$

Now, the quantity $1 - P(u \leqslant A)$ is uniformly distributed between 0 and 1 and so can be replaced by a random number u. If Eq. (59) is solved for A, giving

$$A = \sigma[-\ell n\,(u)]^{1/2} \tag{60}$$

then A is seen to have a Swerling II distribution. The power density for a Swerling IV case is

$$p(Z) = \frac{4Z}{\sigma^2}\,e^{-2Z/\sigma}\,. \tag{61}$$

If $Z = x_1 + x_2$ and if $p(x) = (2/\sigma)\exp(-2x/\sigma)$, Z will have the density given in Eq. (61). Consequently, if

$$A = \left\{-\frac{\sigma}{2}\,[\ell n\,(u_1) + \ell n\,(u_2)]\right\}^{1/2}\,, \tag{62}$$

A will have a Swerling IV distribution. With Eqs. (55), (56), (60), and (62), a Monte Carlo simulation was performed. The results are given in Ref. 55.

In Fig. 34, the fluctuating results are compared with the nonfluctuating results. This figure illustrates the fact that for a given number of samples N, the fewer the samples involved in the detector (i.e., $n_2 - n_1 + 1$) the larger the required increase in S/N to maintain

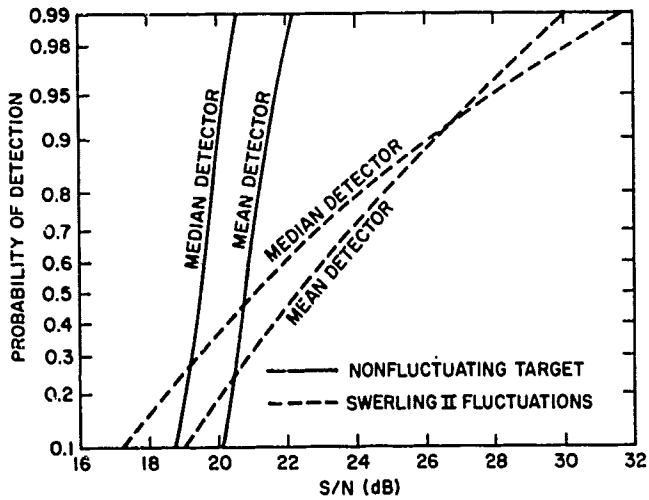

(a) $N = 3$ [37]

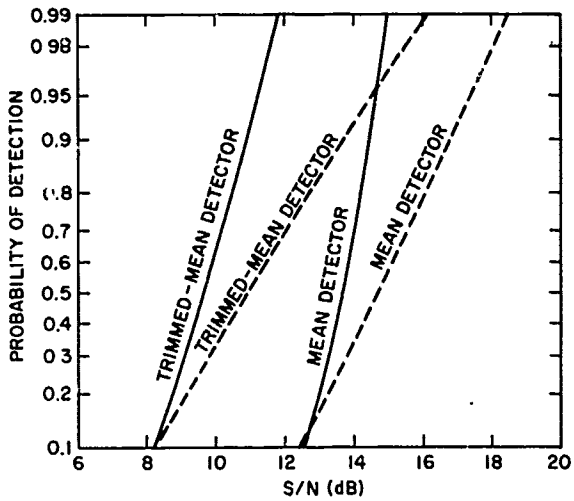

(b) $N = 10$ [37]

Fig. 34—Comparison of various detectors for $P_{fa} = 10^{-6}$, for the log-normal ($\sigma = 6$ dB) distribution and for fluctuating targets

the desired P_D. For instance, to maintain $P_{fa} = 10^{-6}$ and $P_D = 0.9$ for $N = 3$ and a Swerling II target, the mean detector (which uses all three samples) requires a 4.6-dB increase, whereas the median detector (which was only one sample) requires a 6.0-dB increase. Similarly, for $N = 10$, the mean requires a smaller S/N increase than the trimmed mean.

Since the binary integrator uses only one sample, like the median, this author believes it will suffer a "fluctuation loss" similar to that of the median. Thus, for fluctuating targets and log-normal density, the trimmed-mean detector is the most effective one, the binary integrator is next, and the median is third, only slightly better than the mean. Of course, for large samples, the behavior of the detectors for fluctuating targets will approach the nonfluctuating behavior. Consequently, for large sample sizes, the binary integrator and trimmed-mean detector are equivalent, and both are better than the median, which in turn is better than the mean.

B. Contaminated-Normal Density

For the contaminated-normal model, the envelope-detected sample x has the density function

$$p(x) = (1-\gamma)^2 \frac{x}{\sigma^2} \exp\left(\frac{-x^2}{2\sigma^2}\right) + \frac{\gamma^2 x^2}{K^2\sigma^2} \exp\left(\frac{-x^2}{2K^2\sigma^2}\right)$$

$$+ \frac{2\gamma(1-\gamma)x}{K\sigma^2} \exp\left(\frac{-x^2(K^2+1)}{4K^2\sigma^2}\right) I_0\left(\frac{x^2(K^2-1)}{4K^2\sigma^2}\right), \tag{11}$$

where γ is the contamination fraction and K is the ratio of the standard deviations of the two underlying Gaussian densities. Following Rice's procedure [40], we can show [56] that the density function of a constant signal A in contaminated-normal noise is

$$p(x, A) = \int_0^{2\pi} p(x, A, \theta)\, d\theta\,, \tag{63}$$

where

$$p(x, A, \theta) = \frac{x}{2\pi\sigma^2} \left\{ (1-\gamma)^2 \exp\left[-(x^2 - 2xA\cos\theta + A^2)/2\sigma^2\right] \right.$$

$$+ \frac{\gamma^2}{K^2} \exp\left[-(x^2 - 2xA\cos\theta + A^2)/2K^2\sigma^2\right]$$

$$\left. + \frac{\gamma(1-\gamma)}{K} \exp\left[-(x^2\sin^2\theta - 2xAK^2\cos\theta + A^2K^2\right.\right. \tag{64}$$

Continued

$$+K^2x^2\cos^2\theta)/2K^2\sigma^2]$$

$$+\frac{\gamma(1-\gamma)}{K}\exp[-(x^2\cos\theta - 2xA\cos\theta + A^2$$

$$+K^2x^2\sin^2\theta)/2K^2\sigma^2]\Big\}. \tag{64}$$

Various detectors will now be evaluated using the contaminated-normal model.

1. *Mean Detector*

The threshold T for a desired P_{fa} and the P_D have been calculated using the characteristic function approach given by Eqs. (40) through (43). The thresholds for $\gamma = 0.25$ and $K = 2.25$ can be found in Ref. 10, and the detection curves for $N = 1$, 3, 10, and 30 pulses are given in Fig. 35, where S/N is still the signal divided by the median clutter, which for this case is 1.41σ. Two points should be noted: (a) the integration gain for the contaminated-normal density is greater than for the Rayleigh density, but less than for the log-normal density; (b) comparing Figs. 22 and 35 shows that the contaminated-normal model requires considerable less signal strength then the log-normal model to obtain the same probabilities. The curves for $N = 1$ and 30 and $P_{fa} = 10^{-6}$ are shown in Fig. 20.

2. *Binary Integrator and Rank Detector*

The threshold values and the P_D can be found with Eqs. (44) and (45), by using Eqs. (63) and (64) for $p(x, A)$. The threshold values are given in Ref. 45, and the detection curves for $N = 3$ and 30 for the median ($k = N/2$) and 33d percentile ($k = N/3$) are shown in Fig. 36. The following observations can be made.

1. Whether the 33d-percentile value or the 50th-percentile value (median) is better depends on P_{fa} and P_D. For the values of P_{fa} and P_D investigated, there is only a 1-dB difference between the two. Furthermore, since the difference is so small, only a minor improvement can be made by finding the optimal rank.

2. For a fixed P_D, as P_{fa} becomes smaller, the 33d percentile becomes the better detector.

3. For a fixed P_{fa}, as P_D becomes larger, the 50th percentile becomes the better detector.

Comparing the mean and median detectors in Fig. 37, one concludes that the mean requires a smaller S/N than the median. However, the difference decreases with increasing N. For $N = 3$, the mean is about 1 dB better than the median; for $N = 30$, the mean is less than 0.2 dB better than the median. The performance difference between the two detectors for large sample sizes can be obtained from the ARE. In Appendix C, it is shown that the ARE of the mean with respect to the median is 1.76. If a noncoherent

*U.S GOVERNMENT PRINTING OFFICE: 1976 211-264/591 1-3

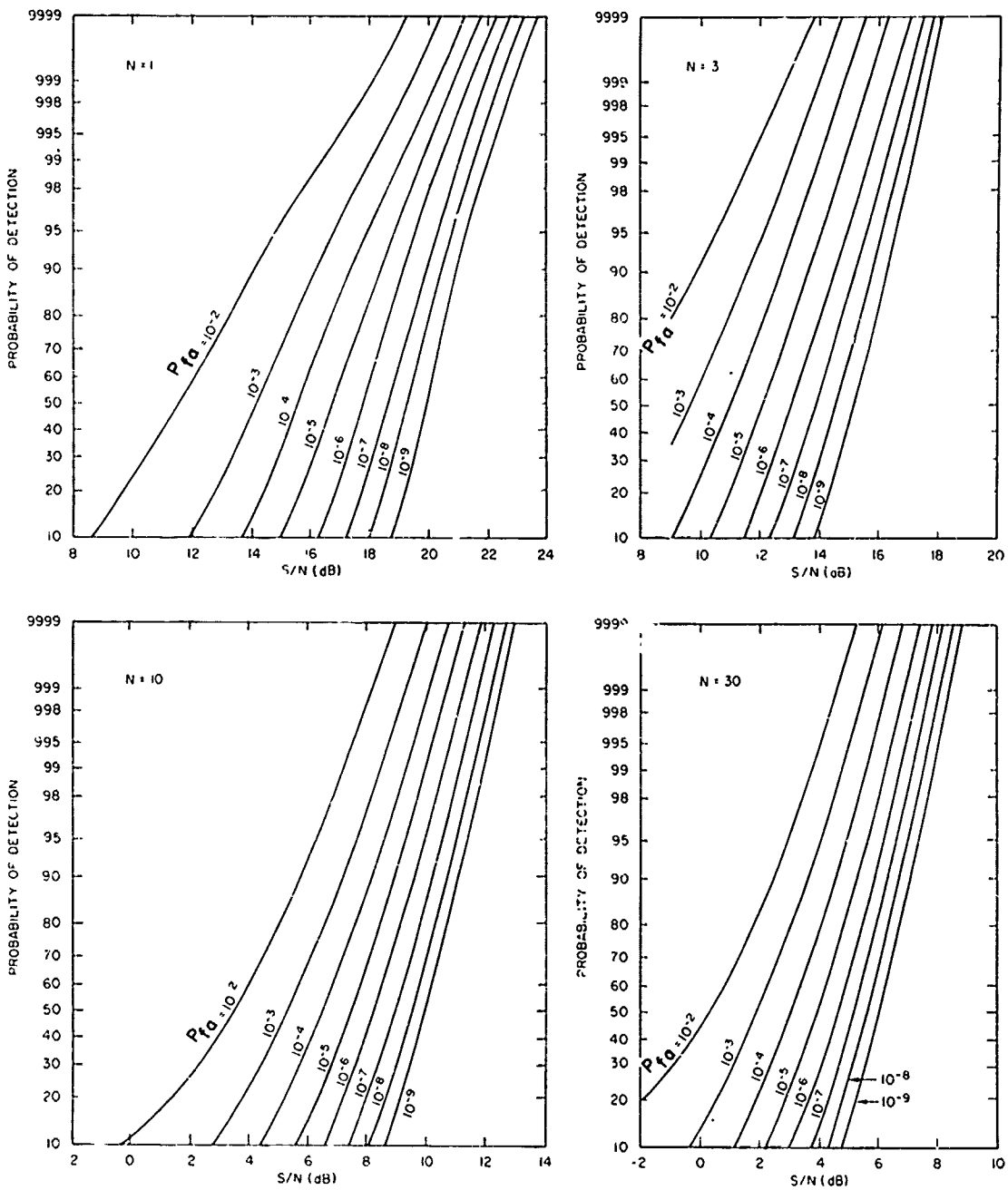

Fig. 35—Probability of detection vs S/N for the mean detector against the contaminated-normal distribution; $\gamma = 0.25$, $K = 2.25$ [10]

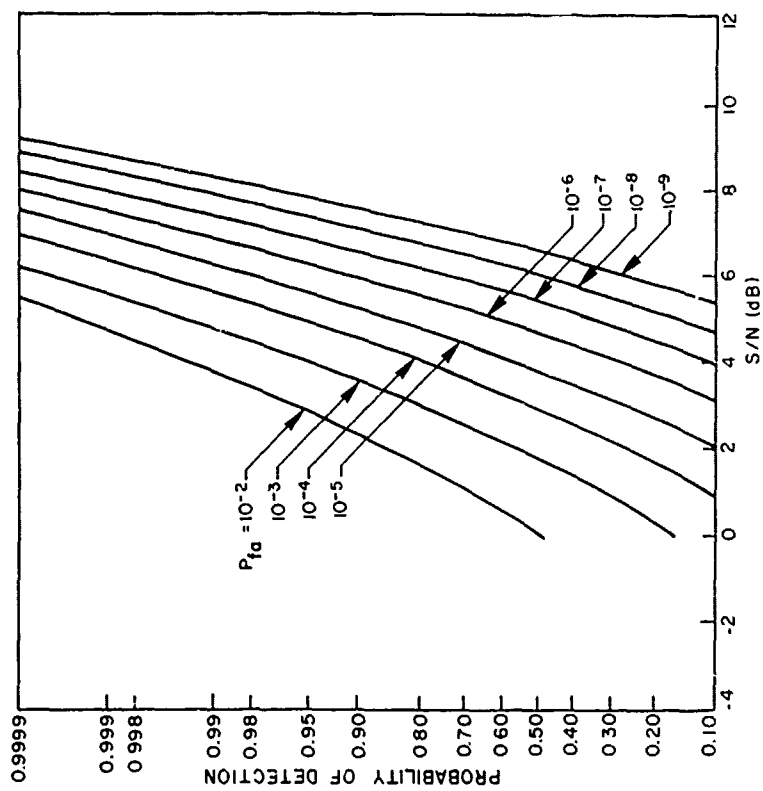
PROBABILITY OF DETECTION
0.9999
0.999
0.998
0.99
0.98
0.95
0.90
0.80
0.70
0.60
0.50
0.40
0.30
0.20
0.10
S/N (dB)
-4
-2
0
2
4
6
8
10
12
$P_{fa}=10^{-2}$
10^{-3}
10^{-4}
10^{-5}
10^{-6}
10^{-7}
10^{-8}
10^{-9}

(b) $N = 3, k = 1$

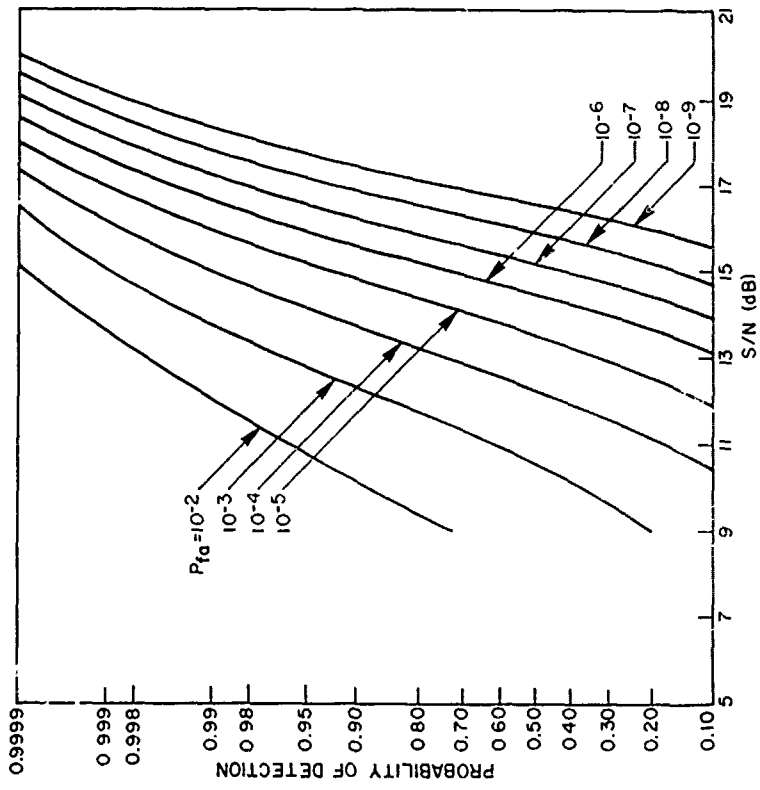
PROBABILITY OF DETECTION
0.9999
0.999
0.998
0.99
0.98
0.95
0.90
0.80
0.70
0.60
0.50
0.40
0.30
0.20
0.10
S/N (dB)
5
7
9
11
13
15
17
19
21
$P_{fa}=10^{-2}$
10^{-3}
10^{-4}
10^{-5}
10^{-6}
10^{-7}
10^{-8}
10^{-9}

(a) $N = 3, k = 2$

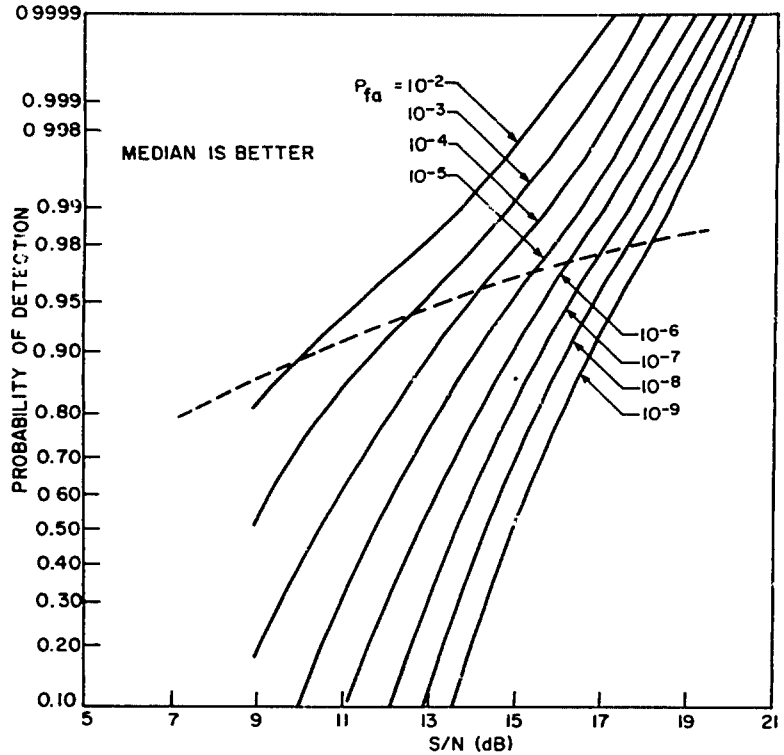

(c) $N = 30$, $k = 15$

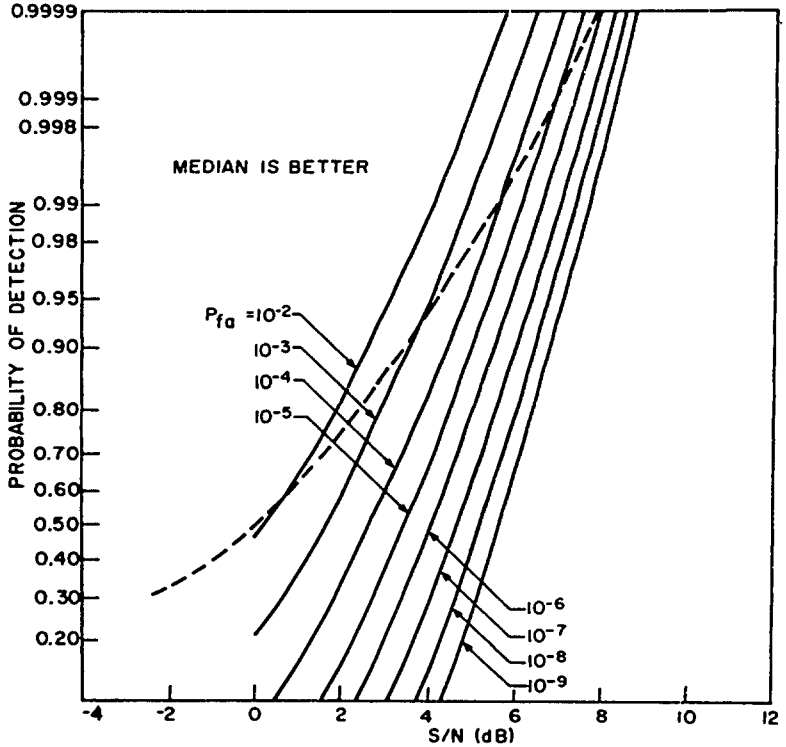

(d) $N = 30$, $k = 10$

Fig. 36—Probability of detection for rank detectors against the contaminated-normal distribution; $\gamma = 0.25$, $K = 2.25$

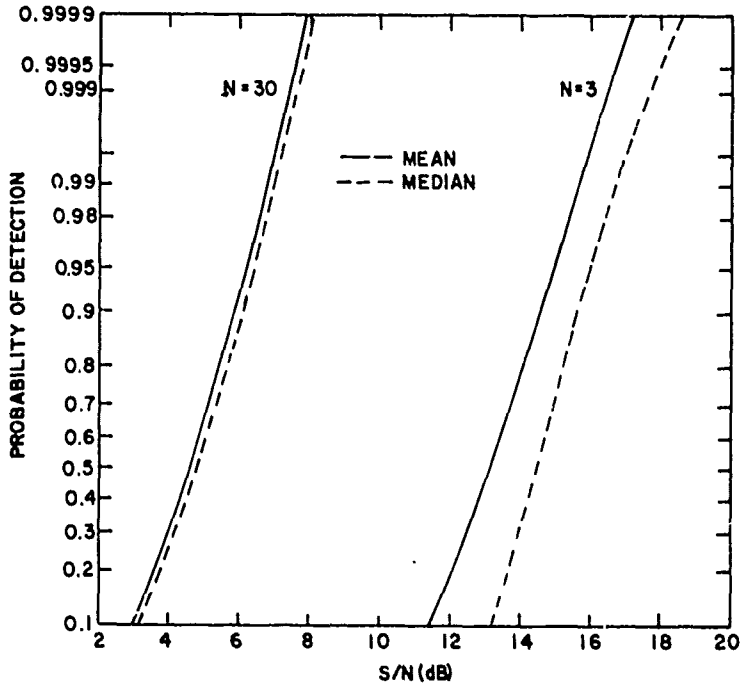

Fig. 37—Probability of detection vs S/N for the contaminated-normal distribution with $\gamma = 0.25$ and $K = 2.25$ [44]

integration gain of $10 \log \sqrt{N}$ is appropriate for small signals, the median is approximately 1.2 dB better than the mean for very small signals.

3. *Trimmed-Mean Detector*

With the previously outlined procedure of Ref. 49, a Monte Carlo simulation was performed. For $N_1 = 2$ and $N_2 = 5$, the equation

$$-\log P_{fa} = -1.691 + 0.3123T + 0.0308T^2 , \tag{65}$$

relating the threshold T to P_{fa}, was obtained for the contaminated-normal model, with $\gamma = 0.25$ and $K = 2.25$. The P_D curves were generated using Monte Carlo techniques; the results are given in Fig. 38. Again, the detector with the smaller ranks ($N_1 = 2$ and $N_2 = 5$) is the better detector. Comparing the trimmed-mean detector's performance with that of the mean (Fig. 35) indicates that the trimmed-mean is the better detector, requiring 0.5 to 1 dB less S/N than the mean.

4. *Fluctuating Targets*

The P_D curves for fluctuating targets are generated by the Monte Carlo method discussed in the previous section on the log-normal method. For the contaminated-normal model with parameters K and γ, the in-phase and quadrature-phase components are

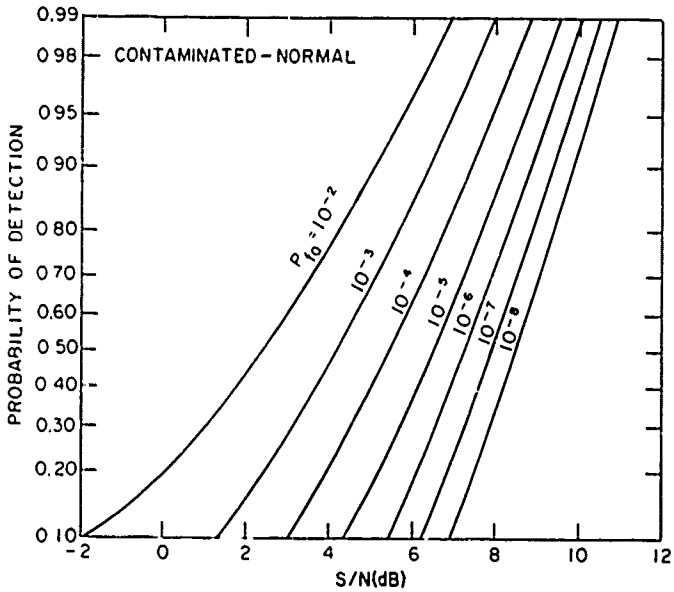

(a) $N = 10$, $N_1 = 2$, $N_2 = 5$

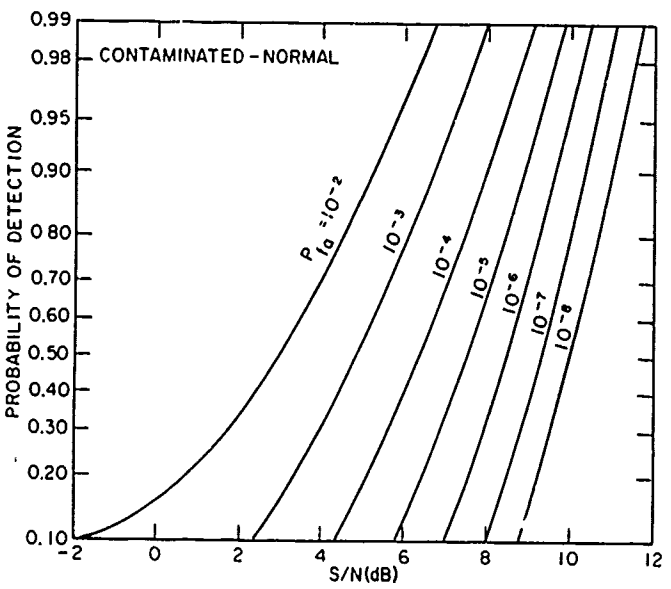

(b) $N = 10$, $N_1 = 4$, $N_2 = 7$

Fig. 38—Probability of detection for the trimmed-mean detection for the trimmed-mean detector and contaminated-normal distribution with $\gamma = 0.25$ and $K = 2.25$

$$y_i = [-2 \ln (u_{i1})]^{1/2} \sin (2\pi u_{i2}) S(u_{i3}) + A$$

$$z_i = [-2 \ln (u_{i1})]^{1/2} \cos (2\pi u_{i2}) S(u_{i4}) \qquad (66)$$

$$S(u_{ij}) = \begin{cases} K\sigma, & u_{ij} \leq \gamma \\ \sigma, & u_{ij} > \gamma, \end{cases}$$

where $\{u_{ij}\}$ are independent, uniformly distributed, random numbers on (0, 1). Using Eqs. (55), (66) in place of (56), (60), and (62), a Monte Carlo simulation was performed; the results are given in Ref. 55. In Fig. 39, the fluctuating results are compared with the nonfluctuating results. This figure illustrates the fact that for a given number of samples N, the smaller the number of ranked samples involved in the sum $(n_2 - n_1 + 1)$, the larger the required increase in S/N to maintain the desired P_D. That is, the median suffers the largest "fluctuation loss," the trimmed mean the next largest, and the mean the smallest. Thus, for fluctuating targets and contaminated-normal

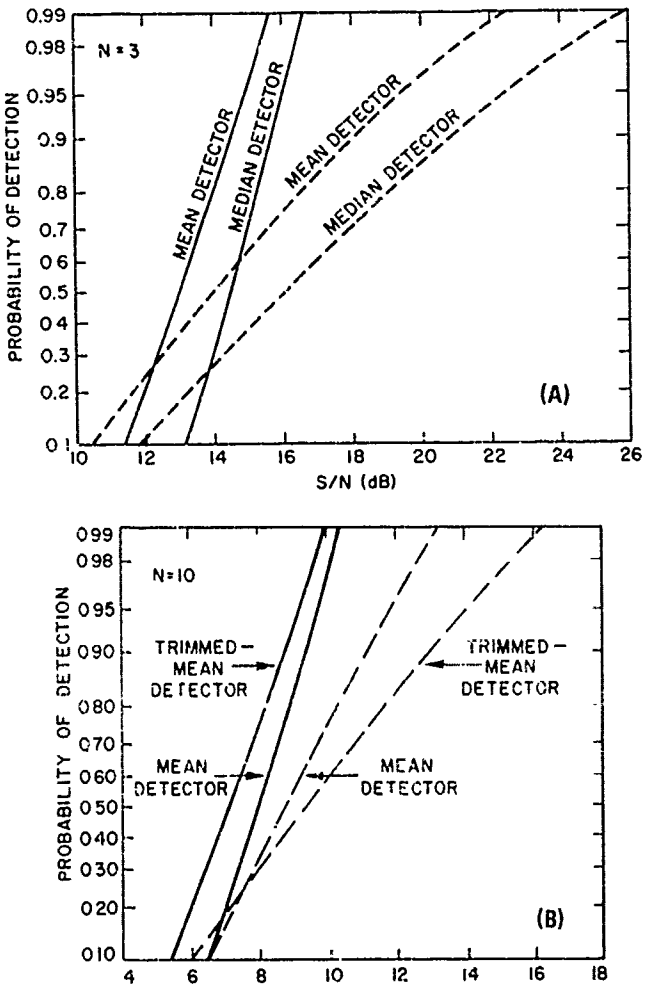

Fig. 39—Comparison of various detectors for $P_{fa} = 10^{-6}$, for the contaminated-normal distribution ($\gamma = 0.25$, $K = 2.25$), and for fluctuating and nonfluctuating targets [37]

densities, the mean is the most effective detector, the trimmed mean is the next best, and the median the least effective.

C. Pulse-to-Pulse Processing

Trunk [39] investigated the problems associated with pulse-to-pulse processing of data taken with a high-resolution radar. His results are summarized in this section. It should be noted that if integration takes place during a single scan, the detection curves (given in Secs. V.A and V.B) cannot be used, because the integrated samples are not independent samples from $p(x)$. If they are used, a higher number of false alarms than predicted will occur. To illustrate this, the threshold values for $N = 3$ and $P_{fa} = 10^{-2}$, and 10^{-3} were taken from Ref. 10. Letting S_j be the sum of three samples taken 12.5 ms apart, we calculated 3,000 values for S_j from the FHR data (run 1153, HUS [10]). The sums were compared to the thresholds and P_{fa} values of 0.15, 0.016, and 0.0032 were obtained. Thus, the P_{fa} is higher than predicted; the relative error becomes larger for smaller P_{fa}. The only way of calculating the correct thresholds for a detector summing N pulses per scan is to calculate (approximate, as in Sec. III.A) the density of S_j rather than that of x_j. While Trunk approximated a density of S_j for the HUS case, he noted that adaptive thresholding was a more fruitful method.

A common adaptive thresholding technique is the cell-averaging constant-false-alarm-rate (CFAR) method considered by Finn and Johnson [57]. Their detector for the jth range cell can be written as a ratio,

$$R_j = \frac{\frac{1}{N}\sum_{i=1}^{N} x_{ij}^2}{\frac{1}{2MN}\sum_{\ell=1}^{M}\sum_{i=1}^{N}\left(x_{i,j+\ell+1}^2 + x_{i,j-\ell-1}^2\right)}, \tag{67}$$

where x_{ij} is the ith envelope-detected sample in the jth range cell. (The samples on either side of the test cell are not used because when a target is present, the Gaussian pulse shape causes target returns in the adjacent cells.) A decision is made by comparing R_j to a threshold T(CFAR). This detector provides CFAR when the noise samples are Rayleigh distributed. The threshold T(CFAR) is a function of the number of reference cells and approaches the threshold T (which is the threshold if the σ of the Rayleigh density is known a priori) as the product MN approaches infinite. The difference in S/N caused by T(CFAR) being larger than T is called the "CFAR loss." It can be found in Mitchell and Walker [58] and it is given in Table 14 for $N = 3$. Thus, to minimize the "CFAR loss," one wants M as large as possible.

Unfortunately, if one views the clutter in Fig. 40, which was generated by assuming the sea to be frozen and converting time data in Fig. 8 to spatial data, one sees that the return goes from a minimum to a maximum in 30 or 40 ft (9.1-12.2 m). Therefore, Trunk [39] suggested setting M small to detect in the nulls of the sea clutter (for targets that are not shadowed, i.e., low-flying targets) and evaluating the detector with $M = 1$ and actual clutter data. First, if x_{ij} are independent samples from the conditional density

$p(x|\sigma)$, which is Rayleigh, then the density of R_j, under the assumption of no signal present, is the F-distribution with $2N$ and $4N$ degrees of freedom. The thresholds can be found in Ref. 24. Since it has been assumed that $p(x|\sigma)$ is a Rayleigh density, x_{ij}^2 has a chi-squared density with two degrees of freedom. If the chi-densities obtained in Table 4 were used, the degrees of freedom for the F-distribution would be greater than $2N$ and $4N$. Consequently, the threshold obtained from Ref. 24 would be lower. Thus, we see that the Rayleigh assumption is a conservative approach: the actual P_{fa} will be lower than desired.

To calculate the P_D of the detector, a Monte Carlo simulation that used actual clutter data (run 1153, HUS [10]) was performed. The output of the cell containing signal was generated by

$$Z_{ij}^2 = \left(x_{ij}^2 \cos\theta_i + A\right)^2 + \left(x_{ij}^2 \sin\theta_i\right)^2 \tag{68}$$

where x_{ij} is the actual FHR data sample, A is the nonfluctuating target amplitude, and θ_i is a random number uniformly distributed on $(0, 2\pi)$. The detection curve for $N = 3$ and $P_{fa} = 10^{-6}$ (which was derived from 512 cases) is shown in Fig. 41. The ratio detector is compared to the one-pulse detector (i.e., x_i is compared to an appropriate threshold) and the three-pulse integrator

$$S_j = \sum_{i=1}^{3} x_{ij}^2$$

is compared to a threshold, assuming that $p(S_j)$ is known a priori. (This is equivalent to a ratio detector with $M = \infty$). The ratio detector is better than the three-pulse integrator except for $P_D > 0.96$, in which case the integrator can be 1.2 dB better.

The explanation for this is that when signal strength is fairly low, the ratio detector can detect signals in the null of the clutter. On the other hand, when signal strength is high, resulting in high P_D, signals must be detected in all regions, including the high-clutter region. However, in the high-clutter regions the three-pulse integrator is better, since no CFAR loss is suffered in estimating the threshold. While the P_D is fairly low for low S/N, it should be noted that this P_D is for a single scan. It can be improved by using scan-to-scan integration or a binary integrator. It should be noted from Table 14 that the

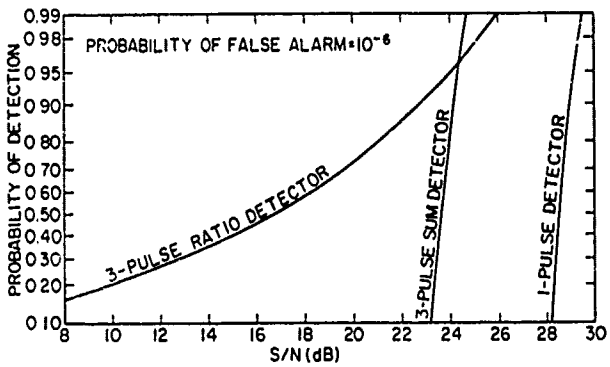

Fig. 41—Comparison of the ratio detector with the one- and three-pulse integrators using sea clutter data [39]

ratio detector with $M = 1$ incurs a CFAR loss of 7.8 dB. If the geometry of the situation (the range resolution with respect to the water wavelength) permits M to equal 2, the CFAR loss can be reduced to about 4.0 dB.

VI. SUMMARY

When the range resolution of a radar becomes less than the water wavelength, the probability density of the radar echoes from the sea has a longer tail than the Rayleigh density. This non-Rayleigh density $p(x)$ has been approximated by the log-normal and contaminated-normal densities. However, $p(x)$ is neither of these densities. Rather, the non-Rayleigh nature of $p(x)$ is due to a spatially varying density $p(x|\sigma)$. The density of $p(x)$ can be expressed as

$$p(x) = \int p(x|\sigma_0)p(\sigma_0)\, d\sigma$$

where $p(\sigma_0)$ is the probability density of σ_0 and is related to the low-frequency sea spectrum (i.e., large wave structure). The conditional density $p(x|\sigma_0)$ is a Ricean density and the dominant scatterers are associated with return from breaking, or near-breaking, waves. From the analysis of variance, the following conclusions were drawn about the effect of various parameters on the density $p(x)$:

1. Data taken with horizontal polarization have a large clutter spread than those taken with vertical polarization.

2. L-band data have a larger clutter spread than X-band data. This is true for very high sea states and may be true for lesser sea states.

3. Upwind and downwind data have a larger clutter spread than crosswind data.

4. Small-pulse data have a larger clutter spread than large-pulse data. However, if the pulsewidth is smaller than the water wavelength, changes are no longer significant. (This ignores the extremely small (5 ft by 5 ft; 1.5 m by 1.5 m) resolution cells.)

Analysis of variance was also applied to the conditional density $p(x|\sigma_0)$, and the following conclusions were reached:

1. Data taken with vertical polarization follow more closely the Rayleigh distribution than horizontal-polarization data, which are more Ricean.

2. Large-pulse data are more Rayleigh, while short-pulse data are more Ricean.

3. Wind direction has no effect on $p(x|\sigma_0)$.

A simulation of the sea surface has been developed. It has been used to predict the variation of $p(x)$ and $p(\sigma_0)$ with various radar parameters. The simulation has also been used to calculate the probability that a small surface target is being shadowed and to

show that the times that the target is not shadowed are correlated with large clutter returns.

Various problems associated with detection of targets have been investigated. Using samples separated by about 10 ms (the decorrelation time usually stated for X-band sea clutter return) or employing frequency diversity produced independent samples from $p(x|\sigma_0)$, not from $p(x)$. Independent samples from $p(x)$ can be obtained only by collecting samples from different scans. Since $p(x)$ has been modeled by log-normal and contaminated-normal densities, detection curves for these two densities have been generated for the mean, median, binary integrator, and trimmed-mean detectors for fluctuating and nonfluctuating targets using independent samples (scan-to-scan processing). Overall, the trimmed mean detector is the best. However, because of implementation problems, the appropriate binary integrator should be used. If pulse-to-pulse processing is used, it is recommended that if the target is above the surface a small number of reference cells be used, so that the target can be detected in the clutter nulls. On the other hand, if the target is a small target on the surface, it can be shadowed and the sea surface simulation must be used to evaluate detector performance.

The question of what polarization should be used remains. Croney and Woroncow [59] recommend vertical polarization, and Trunk and George [10] recommend horizontal polarization. This author believes the question is now open; no generalization can be made. Depending on radar parameters, data-processing constraints, and environmental requirements, either horizontal or vertical polarization could be used. However, in general this author favors vertical polarization because of the false-alarm problem associated with the sea spikes attributed mainly to horizontal polarization.

ACKNOWLEDGMENTS

I wish to thank S. F. George, who sparked my interest in the sea-clutter problem, and J. D. Wilson, who helped with various programing problems. I am indebted to P. Thiebaud and M. Laing, who provided me with the FHR and 4 FR data, respectively. Special thanks are due B. Suits, who typed the manuscript and provided many references while the author was on sabbatical. Thanks also are due K. Ivan, who typed the final version.

REFERENCES

1. S.O. Rice, "Reflection of Electromagnetic Waves from Slightly Rough Surfaces," *Commun. Pure Appl. Math.* 4, 351-378 (Aug. 1951).

2. J.W. Wright, "Backscattering from Capillary Waves with Applications to Sea Clutter," *IEEE Trans. Antennas Propog.* AP-14, 749-754 (Nov. 1966).

3. _____, "A New Model for Sea Clutter," *IEEE Trans. Antennas Propag.* AP-16, 217-223 (Mar. 1968).

4. G.R. Valenzuela, "Depolarization of EM Waves by Slightly Rough Surfaces," *IEEE Trans. Antennas Propag.* AP-15, 552-557 (July 1967).

5. _____, "Scattering of Electromagnetic Waves from a Tilted Slightly Rough Surface," *Radio Sci.* 3, (new series), 1057-1066 (Nov. 1968).

6. _____and M.B. Laing, "Study of Doppler Spectra of Radar Sea Echo," *J. Geophys. Res.* 75, 551-563 (Jan. 1970).

7. N.W. Guinard and J.C. Daley, "An Experimental Study of a Sea Clutter Model," *Proc. IEEE*, 58, 543-550 (Apr. 1970).

8. D.E. Kerr, ed., *Propagation of Short Radio Waves*, MIT Radiation Laboratory Series New York McGraw-Hill, 1951), vol. 13, Secs. 6.6-6.12.

9. F.E. Nathanson, *Radar Design Principles*, McGraw-Hill, New York, 1969.

10. G.V. Trunk and S.F. George, "Detection of Targets in Non-Gaussian Sea Clutter," *IEEE Trans. Aerosp. Electron. Syst.* AES-6, 620-628 (Sept. 1970).

11. O.M. Phillips, *The Dynamics of the Upper Ocean* Cambridge University Press, London, 1966, pp 109-119.

12. N.W. Guinard, "The NRL Four-Frequency Radar System," Report of NRL Progress, May 1969, pp. 1-10.

13. F.C. Maddonald, "Cnaracteristics of Radar Sea Clutter. Part 1 — Persistent Target-Like Echoes in Sea Clutter," NRL Report 4902, Feb. 1957.

14. A.H. Ballard, "Detection of Radar Signals in Log-Normal Sea Clutter," TRW Systems Doc. 7425-8509-TO-000, May 31, 1966.

15. A.M. Findlay, "Sea Clutter Measurements by Radar-Return Sampling," NRL Report 6661, Feb. 12, 1968.

16. G.V. Trunk, "Radar Properties of Non-Rayleigh Sea Clutter," *IEEE Trans Aerosp. Electron. Syst.* AES-8(2), 196-204 (Mar. 1972).

17. M.I. Skolnik, *Introduction to Radar System* McGraw-Hill, New York, 1962.

18. M.I. Skolnik, *Radar Handbook*, McGraw-Hill, New York, 1970, chap. 26.

19. V.W. Pidgeon, "The Frequency and Spatial Correlation of Radar Sea Return," Proc. Amer. Astronaut. Soc. Symp. (Boston, May 25-27, 1967), *in Use of Space Systems for Planetary Geology and Geophysics* The Society, Tarzana, Calif., 1968, pp. 455-458.

20 B.L. Lewis and I.D. Olin, "Measurement and Theory of Spiky Sea Return in a Horizontally Polarized High Resolution Radar".

21. M.W. Long, "On a Two-Scatterer Theory of Sea Echo," *IEEE Trans. Antennas Propag.* AP-22(5), 667-672 (Sept. 1974).

22. P. Swerling, "Lecture Notes on Radar Target Signatures: Measurements, Statistical Models, and System Analysis," Aug. 1968.

23. S.S. Wilks, *Mathematical Statistics* Wiley, New York, 1962.

24. A.J. Duncan, *Quality Control and Industrial Statistics* (Homewood, Ill.: Irwin, 1959).

25. R.A. Fisher, *Statistical Methods for Research Workers* Oliver and Boyd, Edinburgh, 1941.

26. G.R. Valenzuela and M.B. Laing, "On the Statistics of Sea Clutter," NRL Report 7349, Dec. 30, 1971.

27. M.E.B. Owens, "Empirical Bayes Estimation of the Probability Density of the Radar Cross Section of the Sea Surface," NRL Report 7741, June 13, 1974.

28. J.S. Maritz, *Empirical Bayes Estimation* Methuen and Co., Ltd., London, 1970.

29. M.E.B. Owens," Detection of Small Surface Targets in Sea Clutter," RAS Technical Memorandum 45, Radar Analysis Staff, Radar Division, NRL, Jan. 27, 1976.

30. G. Neumann and W.J. Peierson, Jr., *Principles of Physical Oceanography*, Ch. 12, Prentice-Hall, Englewood Cliffs, N.J., 1966.

31. S.A. Kitaigorodskii, "Application of the Theory of Similarity to the Analysis of Wind Generated Wave Motion as a Stochastic Process," *Izv. Akad. Nauk SSR, Ser Geofiz.* 1, 105-117. (English translation in vol. 1, pp. 73-80 (1961).

32. O.M. Phillips, Johns Hopkins University private communication, June 10, 1975.

33. G.V. Trunk, "Modification of Radar Properties of Non-Rayleigh Sea Clutter," *IEEE Trans. Aerosp. Electron. Syst.* AES-9(1), 110 (Jan. 1973).

34. G.V. Trunk, "Comparison of the Collapsing Losses in Linear and Square-Law Detectors, *Proc. IEEE* 60(6), 743-744 (June 1972).

35. J.I. Marcum, "A Statistical Theory of Target Detection by Pulsed Radar," *IRE Trans. Inform. Theor.* IT-6, 59-144 (Apr. 1960).

36. P. Swerling, "Probability of Detection for Fluctuating Targets," *IRE Trans. Inform. Theor.* IT-6, 269-308 (Apr. 1960).

37. G.V. Trunk, "Further Results on the Detection of Targets in Non-Gaussian Sea Clutter," *IEEE Trans. Aerosp. Electron. Syst.* AES-7(3), 553-556 (May 1971).

38. D.C. Schleher, "Radar Detection in Clutter," *Proc. IEEE Int. Radar Conf.*, April 1965, pp. 262-267.

39. G.V. Trunk, "Detection of Targets in Non-Rayleigh Sea Clutter," *Eascon Conference Proceedings* 1971, pp. 239-245.

40. S.O. Rice, "Mathematical Analysis of Random Noise," in *Selected Papers on Noise and Stochastic Processes*, N. Wax, ed. Dover, New York, 1954.

41. S.F. George, "The Detection of Nonfluctuating Targets in Log-Normal Clutter," NRL Report 6796, Oct. 4, 1968.

42. E.J.G. Pitman, "Lecture Notes on nonparametric statistical interference," Columbia University, Spring 1948.

43. G.E. Noether, "On a Theorem of Pitman," *Ann. Math. Statist.* 26, 64-68 (1955).

44. G.V. Trunk, "Small- and Large-Sample Behavior of Two Detectors Against Envelope-Detected Sea Clutter," *IEEE Trans. Inform. Theor.* IT-16, 95-99 (Jan. 1970).

45. G.V. Trunk, "Median Detector for Noncoherent Distributions," NRL Report 6898, May 9, 1969.

46. D. Schleher, "Radar Detection in Log-Normal Clutter," Ph.D. Dissertation, Polytechnical Institute, June 1975.

47. M. Schwartz, "A Coincidence Procedure for Signal Detection," *IEEE Trans. Inform. Theor.* IT-2(4), 135-139 (1956).

48. J.W. Tukey, "A Survey of Sampling from Contaminated Distributions," in *Contributions to Probability and Statistics*, J. Olkin, ed. Stanford University Press, Standford, Calif., 1960.

49. G.V. Trunk, "Trimmed-Mean Detector for Noncoherent Distributions," NRL Report 6997, Dec. 11, 1969.

50. V.G. Hansen, "Detection Performance of Some Nonparametric Rank Tests and an Application to Radar," *IEEE Trans. Inform. Theor.* IT-16(3), 309-318 (May 1970).

51. G.V. Trunk, B.H. Cantrell, and F.D. Queen, "Modified Generalized Sign Test Processor for 2-D Radar," *IEEE Trans. Aerosp. Electron. Syst.* AES-10(5), 574-582 (Sept. 1974).

52. F.S. Hillier and G.J. Lieberman, *Introduction to Operation Research* Holden-Day, San Francisco, 1967, pp. 457-459.

53. H. Chernoff, "A Measure of Asymptotic Efficiency for Tests of a Hypothesis Based on the Sum of Observations," *Ann. Math. Stat.* 23, 493-507 (1952).

54. H.L. Van Trees, *Detection, Estimation and Modulation Theory*, Part I, Wiley, New York, 1968.

55. G.V. Trunk, "Detection Results for Fluctuating Targets," NRL Report 7039, Feb. 24, 1970.

56. G.V. Trunk, "Noncoherent Detection of Nonfluctuating Targets in Contaminated Normal Clutter," NRL Report 6858, Mar. 21, 1969.

57. H.M. Finn and R.S. Johnson, "Adaptive Detection Made With Threshold Control as a Function of Spatially Sampled Clutter-Level Estimates," *RCA Review* 29(3) 414-464 (Sept. 1968).

58. R.L. Mitchell and J.F. Walker, "Recursive Methods for Computing Detection Probabilities," *IEEE Trans. Aerosp. and Electron. Syst.* AES-7(4), 671-676 (July 1971).

59. J. Croney and A. Woroncow, "Radar Polarization Comparisons in Sea-Clutter Suppression by Decorrelation and Constant False Alarm Rate Receivers," *Radio Electron. Eng.* 38(4), 187-197 (Oct. 1969).

Appendix A
ANALYSIS OF SPATIALLY VARYING RAYLEIGH MODEL

It can be shown from the frequency-diverse FHR data that the conditional density $p(x|\sigma_i)$ is not a Rayleigh density. If x_i and y_i are the independent backscatter samples from the two frequencies, the conditional densities of the samples are

$$p(x_i|\sigma_i) = \frac{x_i}{\sigma_i^2} \exp(-x_i^2/2\sigma_i^2) \tag{A1}$$

and

$$p(y_i|\sigma_i) = \frac{y_i}{\sigma_i^2} \exp(-y_i^2/2\sigma_i^2), \tag{A2}$$

where σ_i is a random variable. The same σ_i can be used for both frequencies, since the time separation (1/2560 s) is very small and the frequency difference, of the order of the reciprocal of the pulsewidth, changes σ_0 only slightly.

Since σ_i changes rapidly with time, only a few samples of x_i and y_i are available for a fixed σ_i. Consequently, a ratio $z_i = x_i/y_i$, whose density is easily shown to be

$$p(z_i) = 2z_i/(z_i^2 + 1)^2, \tag{A3}$$

is formed. The ratio $p(z_i)$ is independent of σ_i. Thus, even though σ_i changes, all the samples can be used to test whether Eq. (A3) gives the correct density for the ratio. From the FHR data, the sample distribution of independent z_i (constructed from 1,024 samples taken 12 ms apart) was compared to Eq. (A3) using the Kolmogorov-Smirnov (*K-S*) one-sample test.* The results of the test are shown in Table A1; D is the maximum difference between the sample and theorized distributions and P_D is the probability that the difference will be less than D when the theorized distribution is the true distribution. All 12 cases are rejected at the $\alpha = 0.002$ level (i.e., $P_D \geqslant 0.998$), indicating that x_i and y_i are not independent random variables of a conditional Rayleigh density. However, the surprising thing is that the sample density is more peaked (has a narrower spread) than Eq. (A3). This indicates that either x_i and y_i are correlated, or the density of x_i and y_i is more peaked than a Rayleigh density, like a chi or Ricean density.

However, it can be shown that the first of these explanations is not possible. To test whether correlation between x_i and y_i can account for the observed peaked sample density of z, one must calculate the density of z when x and y are correlated Rayleigh

*S.S. Wilks, *Mathematical Statistics*, Wiley, New York, 1962.

Table A1 — Test of FHR Data for a Conditional Rayleigh Distribution

Identifier	D	P_D
VUL	0.081	0.999
HUL	0.080	0.999
VDL	0.059	0.998
HDL	0.093	0.999
HDS	0.224	0.999
VDS	0.161	0.999
VCS	0.152	0.999
HCS	0.166	0.999
VCL	0.059	0.998
HCL	0.133	0.999
HUS	0.192	0.999
VUS	0.136	0.999

random variables. Let the in-phase and quadrature components of x and y be x_s, x_c, y_s, and y_c; let the in-phase components be independent of the quadrature components and let both have correlation ρ. The joint density of the components, then, is

$$p(x_s, x_c, y_s, y_c) = \frac{1}{(2\pi)^2(1-\rho^2)} \exp[-(x_c^2 - 2\rho x_c y_c + y_c^2 + x_s^2 - 2\rho x_s y_s + y_s)/2(1-\rho^2)]. \quad \text{(A4)}$$

Using transforms $x_s = x \sin\theta$, $x_c = x\cos\theta$, $y_s = y\sin\gamma$, and $y_c = y\cos\gamma$, one obtains

$$p(x, y, \theta, \gamma) = \frac{1}{(2\pi)^2(1-\rho^2)} \exp\{-[x^2 + y^2 - 2\rho xy(\cos\theta\cos\gamma + \sin\theta\sin\gamma)]/2(1-\rho^2)\}. \quad \text{(A5)}$$

Letting $\alpha = \theta - \gamma$ and $\beta = \theta$ and integrating reveal that

$$\int_0^{2\pi}\int \exp[2\rho xy\cos(\theta-\gamma)/2(1-\rho^2)]\, d\alpha\, d\gamma = \int_0^{2\pi}\int \exp[2\rho xy\cos\alpha/2(1-\rho^2)]\, d\alpha\, d\beta = (2\pi)^2 I_0\left(\frac{\rho xy}{1-\rho^2}\right). \quad \text{(A6)}$$

Consequently, the joint density of x and y is

$$p(x, y) = \frac{xy}{(1-\rho^2)} \exp\left[-(x^2+y^2)/2(1-\rho^2)\right] I_0\left(\frac{\rho xy}{1-\rho^2}\right). \tag{A7}$$

Letting $z = x/y$ and $R = y$ and integrating over R produces

$$p(z) = \int_0^\infty \frac{R^2 z}{(1-\rho^2)} \exp\left[-R^2(1+z^2)/2(1-\rho^2)\right] I_0\left(\frac{\rho z R^2}{1-\rho^2}\right) dR. \tag{A8}$$

To, evaluate Eq. (A8), we use the series expansion of I_0.

$$I_0(x) = \sum_{R=0}^{\infty} \frac{\left(\frac{x^2}{4}\right)^k}{(k!)^2}. \tag{A9}$$

By substituting Eq. (A9) into Eq. (A8) and letting $A = (1+z^2)/(1-\rho^2)$ and $B = \rho z/(1-\rho^2)$, we find the kth term in the series to be

$$\frac{z}{1-\rho^2} \frac{B^{2k}}{2^{2k}(k!)^2} \int_0^\infty R^{4k+3} \exp\left[-AR^2/2\right] dR. \tag{A10}$$

Integrating by parts $2k+2$ times yields

$$\frac{z}{(1-\rho^2)} \frac{B^{2k}}{2^{2k}(k!)^2} \left[\frac{2^{2k+1}(2k+1)!}{A^{2k+2}}\right]. \tag{A11}$$

Substituting for A and B gives the density of z as

$$p(z) = \sum_{k=0}^{\infty} \frac{2(2k+1)!}{(k!)^2} \frac{\rho^{2k}(1-\rho^2)z^{2k+1}}{(1+z^2)^{2k+2}}. \tag{A12}$$

The FHR data were used again. This time they were compared to Eq. (A12). The K-S results are presented in Table A2, where "Opt ρ^2" is the value of ρ^2 at which the minimum D is obtained. (The only values of ρ^2 used were 0.0 to 0.4, in steps of 0.1.) Since (a) only 4 of the 12 cases are accepted at the $\alpha = 0.1$ level, (b) the maximum cross-correlation calculated for this data is 0.1, (c) Pidgeon reports a maximum correlation of

Table A2 — Test of FHR Data for a Correlated TVR Distribution

Identifier	Optimum ρ^2	D	P_D
VUL	0.4	0.015	0.037
HUL	0.3	0.042	0.951
VDL	0.3	0.027	0.558
HDL	0.4	0.037	0.879
HDS	0.4	0.138	0.999
VDS	0.4	0.077	0.999
VCS	0.4	0.069	0.999
HCS	0.4	0.088	0.[illegible]
VCL	0.3	0.031	0.749
HCL	0.4	0.046	0.974
HUS	0.4	0.104	0.999
VUS	0.4	0.060	0.998

0.2 when the frequency difference is the reciprocal of the pulsewidth,* and (d) the smallest "Opt ξ^2" was 0.3, the hypothesis that x and y are correlated, Rayleigh-distributed, random variables must be rejected. It is worth noting that the value of ρ^2 was set by minimizing D; a procedure which biased the test in favor of acceptance.

*V.W. Pidgeon, "Time Frequency and Spatial Correlation of Radar Sea Return," Proc. Amer. Astronaut. Soc. Symp. (Boston, May 25-27, 1967), in *Use of Space Systems for Planetary Geology and Geophysics* The Society, Tarzana, Calif., 1968, pp. 455-458.

Appendix B
BRIEF DESCRIPTION OF ANALYSIS OF VARIANCE

The analysis of variance (ANOVA) procedure will be demonstrated by finding the variation of the clutter distribution with changing frequency and azimuthal squint angle. As shown in Table B1, the distribution can be represented by a single number σ. In analysis of variance, the data σ_{ijk} are represented by a linear model which consists of a mean μ, a frequency effect F_i, an azimuthal angle effect A_j, and a random error ϵ_{ijk}, such that

$$\sigma_{ijk} = \mu + F_i + A_j + \epsilon_{ijk} \qquad \begin{matrix} i = 1, \ldots, N_F \\ j = 1, \ldots, N_A \\ k = 1, \ldots, N_R \end{matrix}$$

where N_F is the number of frequencies, N_A is the number of azimuthal angles, N_R is the number of repetitions of each frequency azimuth case,

$$\sum_{i=1}^{N_F} F_i = 0, \quad \sum_{j=1}^{N_A} A_j = 0,$$

and ϵ_{ijk} are independent Gaussian random variables with mean 0 and unknown variance λ^2.

The significance of a change in frequency is checked by testing the hypotheses,

$H_0: F_i = 0$, for all i (no frequency effect present)

$H_1: F_i \neq 0$, for some i (frequency effect present),

using an F-test (an optimal test for the equality of unknown variances). The test is performed by taking the ratio R of two statistics; S_F^2, an unbiased estimator of $\lambda^2 + 4(F_1 - F_2)^2$, and S_ϵ^2, an unbiased estimator of λ^2. Under H_0, the ratio has an F-distribution, and under H_1 the ratio has a noncentral F-distribution. For a type-I error of 0.1, the threshold value is found in Duncan to be 3.2.* In Table B2, R = 55.8; consequently, the null hypothesis is rejected. That is, a frequency effect is present. The procedure is repeated for the azimuthal angle, and the effect is not significant. Interactions† were found not to be significant at the 0.1 level in this or any other data used in this paper. Consequently, to avoid unnecessary complications, the results of interactions were not mentioned in the report. Further details about analysis of variance can be found in either Duncan* or Fisher.†.

*A.J. Duncan, *Quality Control and Industrial Statistics*, Irwin, Homewood, Ill., 1959.
†R.A. Fisher, *Statistical Methods for Research Workers* Oliver and Boyd, Edinburgh, 1941.

Table B1—σ in Decibels of the Fitted Log-Normal Distribution*

4 FR Radar Parameters	Azimuthal Squint Angle							
	0°		15°		30°		45°	
Frequency								
L band	6.1	6.0	5.4	5.7	5.5	6.3	6.1	5.6
X band	4.8	4.4	4.9	4.3	4.6	4.5	5.0	4.7

*From reference [16].

Table B2—Results of Analysis of Variance: The Effect of Various Parameters on the 4FR Clutter Distributions*

Effect	Mean Square	Variance Ratio	Conclusion
Frequency	$S_F^2 = 5.640$	$S_F^2/S_\epsilon^2 = 55.84$	Frequency effect is present
Azimuthal angle	$S_A^2 = 0.062$	$S_A^2/S_\epsilon^2 = 0.61$	Azimuthal effect not present
Sampling error	$S_\epsilon^2 = 0.101$		

*From reference [16].

Appendix C
ASYMPTOTIC RELATIVE EFFICIENCY OF MEAN AND MEDIAN DETECTORS

The asymptotic relative efficiency (ARE) can usually be calculated rather easily by employing a concept known as efficacy.* That is, the ARE of two detectors d_1 and d_2 is

$$\text{ARE}\,(d_2, d_1) = \frac{\mathcal{E}_2}{\mathcal{E}_1}, \tag{C1}$$

where $\mathcal{E}_i$ is the efficacy of detector d_i. Specifically, given a binary hypothesis-testing problem (H_0:$A = A_0$ vs H_1:$A > A_0$), if the detector d_i is based on a statistic $T_{in} = T_i(x_1, x_2, \ldots, x_n)$ and if $E\{T_{in}\} = \psi_{in}(A)$ and $\text{Var}\{T_{in}\} = \sigma_{in}^2(A)$ and m and δ are defined by

$$\psi_{in}(A_0) = \ldots = \psi_{in}^{(m-1)}(A_0) = 0,\ \psi_{in}^{(m)}(A_0) > 0 \tag{C2}$$

where

$$\psi_{in}^{(m)}(A_0) \equiv \left.\frac{\partial^m \psi_{in}(A)}{\partial A^m}\right|_{A = A_0}$$

and

$$\lim_{n\to\infty} n^{-m\delta}\,\frac{\psi_{in}^{(m)}(A_0)}{\sigma_{in}(A_0)} = C > 0, \tag{C3}$$

then the efficacy of detector d_i is

$$\mathcal{E} = \left[\frac{\psi_{in}^{(m)}(A_0)}{\sigma_{in}(A_0)}\right]^{1/m\delta}, \tag{C4}$$

subject to certain regularity conditions.† When dealing with the class of translation alternatives, the following conditions generally apply: $m = 1$, $\delta = 1/2$, and the evaluation of Eq. (C4) is very simple. However, when dealing with other alternative classes (e.g., noncoherent detection), generally $m = 2$, $\delta = 1/4$, and the evaluation of Eq. (C4) is not always simple.

*E.J.G. Pitman, "Lecture Notes on Nonparametric Statistical Interference," Columbia University, Spring 1948.

†G.E. Noether, "On a Theorem of Pitman," *Ann. Math. Statist.* 26, 64-68 (1955).

An expression for the efficacy of the mean against the log-normal density is derived from

$$\left[\sigma^{-1}\,\frac{\partial^2}{\partial A^2}\int_0^\infty xp(x, A)\,dx\right]_{A=0} \tag{C5}$$

by taking the second derivative inside the integral and dropping terms that when evaluated at zero signal strength are zero. The efficacy of the mean can be written as

$$\mathcal{E}_i = \left[\int_0^{T_i} F_i(x)\left[\frac{4(\sigma^2-1)}{\sigma^2 x^3} + \frac{16(\sigma^2 \ln x + (\ln x^2)}{\sigma^4 x^3}\right] \times (2\pi\sigma^2)^{-1/2}\exp\left[-2(\ln x)^2/\sigma^2\right]dx\right]^2, \tag{C6}$$

where, for the efficacy of the sample mean, $F_1(x) = nx$, $T_1 = \infty$, and $\sigma_1 = [ne^{\sigma^2}(e^{\sigma^2} - 1)]^{1/2}$.

The expression for the efficacy of the median is derived by first noting that making a decision when the median is greater than a threshold value T is entirely equivalent to making the decision by counting the number of samples greater than T. Thus, as the number of samples approaches infinity, T approaches the median value of the distribution, since the median detector is consistent. Hence, if

$$E\{T_n\} = np = n\int_0^{x_m} p(x, A)\,dx, \tag{C7}$$

the efficacy of the median is

$$\mathcal{E}_2 = n\left[\frac{(\partial^2 p/\partial A^2)}{0.5\sqrt{n}}\right]^2, \tag{C8}$$

which reduces to Eq. (C6) with $F_2(R) = 1$, $T_2 = 1$, and $\sigma^2 = 0.5/\sqrt{n}$.

Now, if one repeats the previous procedure, one obtains for the efficacy of the mean against the contaminated-normal density

$$\mathcal{E}_i = \left(\int_0^{T_i} F_i(x)\left\{\frac{(1-\gamma)^2}{\sigma^4}\left(-1 + \frac{x^2}{2\sigma^2}\right)\exp\left(\frac{-x^2}{2\sigma^2}\right)\right.\right.$$

$$\left.\left. + \frac{\gamma^2}{K^4\sigma^4}\left(-1 + \frac{x^2}{2K^2\sigma^2}\right)\exp\left(\frac{-x^2}{2K^2\sigma^2}\right)\right. \tag{C9}$$

(Continued)

$$+ \frac{2\gamma(1-\gamma)}{K\pi\sigma^4} \int_0^{\pi/2} \left[\left(-1 + \frac{x^2 \cos^2\theta}{\sigma^2} \right) \right.$$

$$\times \exp\left(\frac{-[x^2 + (K^2-1)x^2\cos^2\theta]}{2K^2\sigma^2} \right)$$

$$+ K^{-1}\left(-1 + \frac{x^2\cos^2\theta}{K^2\sigma^2} \right)$$

$$\left. \times \exp\left(\frac{-(x^2K^2 - (K^2-1)x^2\cos^2\theta)}{2K^2\sigma^2} \right) \right] d\theta \Bigg\} \frac{dx}{\sigma_i}^2 \Bigg) \qquad \text{(C9)}$$

where $F_1(x) = nx$, $T_1 = \infty$, and σ_1 is the standard deviation of the sample mean for the noncoherent contaminated-normal distribution with $A = 0$, which is $(12 - \pi/2)^{1/2}\,\sigma\sqrt{n}$ for $\gamma = 0$ and is $1.11\,\sigma\sqrt{n}$ for $\gamma = 0.25$ and $K = 2.25$. The latter value for σ_1 was found by numerical integration.

The efficacy of the median against the contaminated-normal density reduces to Eq. (C9) with $F_2(x) = nx$, T_2 = the median value of the noncoherent contaminated normal distribution (which is $(2\,\ell n\,2)^{1/2}\,\sigma$ for $\gamma = 0$ and is 1.41σ for $\gamma = 0.25$ and $K = 2.25$), and $\sigma_2 = 0.5\sqrt{n}$.

For the Rayleigh case ($\gamma = 0$), the integral in Eq. (C9) can be performed. It yields

$$\mathcal{E}_1 = \frac{\frac{1}{8}\pi n}{2(1-\pi/4)} = 0.915n$$

and

$$\mathcal{E}_2 = (\ell n\,2)^2 n = 0.48n$$

for the efficacies of the mean and median, respectively. The ARE is

$$\text{ARE (median, mean)} = \frac{\mathcal{E}_2}{\mathcal{E}_1} = 0.525.$$

This implies that in the limit as $A \to 0$, in order to maintain the same probabilities of false alarm and detection, the mean requires only 52.5 percent as many samples as the median. Thus, the mean is the better large-sample detector for the Rayleigh distribution.

For the noncoherent contaminated-normal ($\gamma \neq 0$) and the log-normal densities, Eqs. (C6) and (C9) have been evaluated numerically; the results obtained are given in Table C1. These show that, in all cases, the median is the better large-sample detector.

Table C1 — Asymptotic Relative Efficency of the Mean and Median Detectors

Distribution	Efficacy of Sampled Mean	Efficacy of Median	ARE
Log-normal ($\sigma = 3$)	$0.286n$	$5.334n$	18.6
Log-normal ($\sigma = 6$)	$0.0103n$	$1.333n$	129
Contaminated-normal ($\gamma = 0.25$ and $K = 2.25$)	$0.0137n$	$0.0238n$	1.76

E. K. AL Hussein* has solved the integral in Eq. (C9) for $\mathcal{E}_2$ and has obtained

$$\mathcal{E}_2 = 8n/\pi\sigma^2. \tag{C10}$$

Substituting $\sigma = 0.2303\sigma(\text{dB})$ into Eq. (C10) with $\sigma = 3$ dB and $\sigma = 6$ dB, one obtains $5.334n$ and $1.333n$, respectively.

*E.K. AL Hussein, Cairo University, Giza, Egypt, in a letter received April 8, 1976.

Appendix D
IMPORTANCE SAMPLING

A straightforward method of determining the required threshold for a given P_{fa} is to perform a Monte Carlo simulation. Unfortunately, for $P_{fa} = 10^{-6}$, more than one million repetitions would need to be run, and the computation time on any computer would be large. However, a simulation that uses importance sampling can be used.* The main purpose of importance sampling is to modify the probabilities that govern the outcome of the basic experiment of the simulation so that the event of interest (i.e., a false alarm) occurs more frequently. This distortion is then compensated for by weighting each event by the ratio of its probability if the true probabilities had been used to its probability with the distorted probabilities. Consequently, by proper choice of distorted probabilities, the number of repetitions can be reduced greatly. For instance, in estimating the mean of a function $Q(x)$

$$E[Q(x)] = \int Q(x)\, dP(x), \tag{D1}$$

where $P(x)$ is the distribution of x; the mean can be estimated by selecting m independent samples x_i from $P(x)$ and associating the probability $1/M$ with each event. Then, $E[Q(x)]$ can be estimated by

$$\frac{1}{M} \sum_{i=1}^{M} Q(x_i). \tag{D2}$$

The importance-sampling technique used the Radon-Nikodyn derivative to express the mean value of $Q(x)$ by

$$E[Q(x)] = \int Q(x) \frac{dP(x)}{dG(x)}\, dG(x), \tag{D3}$$

where $G(x)$ is a distribution function. Now, $E[Q(x)]$ can be estimated by selecting M independent samples from $G(x)$ and associating the probability $dP(x_i)/MdG(x_i)$ with event $Q(x_i)$. Thus, $E[Q(x)]$ is estimated by

$$\frac{1}{M} \sum_{i=1}^{M} Q_i(x) \frac{dP(x_i)}{dG(x_i)} . \tag{D4}$$

*F.S. Hillier and G.J. Lieberman, *Introduction to Operation Research* Holden-Day, San Francisco, 1967, pp. 457-459.

Since Eqs. (D3) and (D4) are both unbiased estimates of $Q(x)$, it is possible to select $G(x)$ so that the variance of Eq. (D4) is less than the variance of Eq. (D2).

To illustrate, let us generate the distribution function (and hence curve of threshold T vs P_{fa}) for the trimmed-mean detector against the log-normal density with σ = 6 dB. If $\{u_{ij}\}$ are independent and uniformly distributed on (0, 1), then the variables $\{x_i\}$, such that

$$x_i = \exp\{\sigma[-2\,\ell n(u_{i1})]^{1/2} \sin(2\pi u_{i2})\}, \tag{D5}$$

have a log-normal density, with $x_m = 1$. Recalling* that the σ in Eq. (D5) is in natural units ($\sigma = 0.2303\sigma$ (dB)), choose σ_H, which is greater than σ. To simulate the trimmed mean for $n_1 = 2$, $n_2 = 5$, and $N = 10$, generate 10 samples x_i, using Eq. (D5) with σ replaced by σ_H. Order the $\{x_i\}$ and form the sum

$$\sum_{i=n_1}^{n_2} x_i.$$

Since this procedure is repeated M times, denote log-normal samples by x_{ij} and trimmed-mean samples by S_j. The estimated cumulative distribution of S_j for the log-normal model with parameter σ is

$$\hat{p}(S_j \leqslant T) = \frac{1}{M} \sum_{j=1}^{M} \delta_j p_j \tag{D6}$$

where

$$\delta_j = \begin{cases} 1 & S_j \leqslant T \\ 0 & S_j > T \end{cases} \tag{D7}$$

$$p_j = \prod_{i=1}^{N} \frac{2\exp\{-2[\ell n(x_{ij})]^2/\sigma^2\}/(2\pi\sigma^2 x_{ij})^{1/2}}{2\exp\{-2[\ell n(x_{ij})]^2/\sigma_H^2\}/(2\pi\sigma_H^2 x_{ij})^{1/2}}$$

This reduces to

$$p_j = \left(\frac{\sigma_H}{\sigma}\right)^N \exp\left\{\left(\frac{2}{\sigma_H^2} - \frac{2}{\sigma^2}\right) \sum_{i=1}^{N} [\ell n\,(x_{ij})]^2\right\}. \tag{D8}$$

While, a priori, the desired value of σ_H is unknown, an appropriate value can easily be found since the variance of the estimate $\hat{p}(T)$ is given by

*S.F. George, "The Detection of Nonfluctuating Targets in Log-normal Clutter," NRL Report 6796, Oct. 4, 1968.

$$\frac{1}{M^2} \sum_{j=1}^{M} (\delta_j P_j - \hat{p}(T)^2). \tag{D9}$$

That is, every value of σ_H allows us to calculate the density accurately in a particular interval. Equation (D9) is used to find the accurate interval. A much simplier heuristic method is to plot $\hat{p}(s_j \leqslant T)$. In the regions where the function is smooth, the estimate is accurate.